EFFECTS OF TEMPERATURE ON THE PERFORMANCE OF A SMALL INTERNAL COMBUSTION ENGINE AT ALTITUDE

THESIS

Travis Don Husaboe, Captain, USAF

AFIT-ENY-13-M-17

DEPARTMENT OF THE AIR FORCE
AIR UNIVERSITY

AIR FORCE INSTITUTE OF TECHNOLOGY

Wright-Patterson Air Force Base, Ohio

AFIT-ENY-13-M-17

EFFECTS OF TEMPERATURE ON THE PERFORMANCE OF A SMALL INTERNAL COMBUSTION ENGINE AT ALTITUDE

THESIS

Presented to the Faculty

Department of Aeronautics and Astronautics

Graduate School of Engineering and Management

Air Force Institute of Technology

Air University

Air Education and Training Command

In Partial Fulfillment of the Requirements for the

Degree of Master of Science in Aeronautical Engineering

Travis Don Husaboe

Captain, USAF

March 2013

AFIT-ENY-13-M-17

EFFECTS OF TEMPERATURE ON THE PERFORMANCE OF A SMALL INTERNAL COMBUSTION ENGINE AT ALTITUDE

Travis Don Husaboe

Captain, USAF

Approved:

_____	_____
Marc D. Polanka, Ph.D. (Chairman)	Date
_____	_____
Paul I. King, Ph.D. (Member)	Date
_____	_____
Jeremy S. Agte, Lt Col, USAF (Member)	Date

Abstract

The effects of atmospheric pressure and temperature variations on the performance of small internal combustion (IC) engines operating at altitudes significantly above sea level are not widely documented. A test stand with the capability to control atmospheric conditions was utilized for characterizing the performance of a representative small IC engine. During previous research, data were recorded to identify the impact of varying engine intake pressure on engine performance both with a carburetor and with a throttle body fuel injection system delivering a gasoline-oil mixture. Using the stand and fuel-injected two-stroke engine, data were collected while varying air temperature along with pressure. Quantifying temperature and pressure effects is vital for establishing the capability of operating spark ignition engines at altitudes well above those for which they were designed. The peak engine power was 4.1 kW at roughly sea level standard conditions and dropped to 3.5 kW at the standard conditions for an altitude of 1.5 km. At a combination of pressure and temperature corresponding to an altitude of 3 km, peak power fell further to 2.5 kW. The combined effects of standard atmospheric conditions showed pressure dominated temperature and resulted in around a 3.5% loss of power and brake mean effective pressure (BMEP) along with a 3% increase in brake specific fuel consumption (BSFC) per 300 m increase in altitude. The engine's thermal efficiency fell by about 0.4 percentage points per 300 m of increased altitude.

Acknowledgments

"Praise God from Whom all blessings flow." Thanks to my wonderful parents for raising me to love the Lord Jesus Christ. My niece is a tremendous gift who has brought me great joy, and I fondly recall my outstanding Christian grandparents. Thanks to my thesis advisor, Dr. Marc Polanka, for all the help. Thanks to Dr. Fred Schauer, Paul Litke, Dr. John Hoke, Dave Burris, J.R. Groenewegen, Ben Naguy, Rich Ryman, Curtis Rice, Justin Goffena, Dave Courson, Keith Grinstead, LCDR Brandon Smith, Lt Joe Ausserer, Lt Josh Rittenhouse, Jacob Baranski, Adam Brown, Renate Hannaford, Dr. Eric Anderson, Dr. Chris Stevens, Andy Naples, Capt Justin Carl, Capt Colin Engebretsen, and Drew Cole. Thanks to the many AFIT students and faculty members who have shown me kindness and patience. Thanks to Dr. Paul King and Lt Col Jeremy Agte for serving on my thesis committee. Thanks to Capt Pete Schmick for his work in the development of the altitude rig. Thanks to Capt Steve Crosbie for his improvement of the rig and help. Praise the Name of the Lord: Father, Son, Holy Spirit.

Travis Don Husaboe

Table of Contents

Page

List of Figures

Page

List of Tables

Page

EFFECTS OF TEMPERATURE ON THE PERFORMANCE OF A SMALL INTERNAL COMBUSTION ENGINE AT ALTITUDE

I. Introduction

I.1 Background

Efforts have been undertaken in recent years to quantify combustion performance in small internal combustion (IC) engines in order to develop scaling relationships and design higher-performance, higher-efficiency engines. Although small IC engines have powered model airplanes for many years, these aircraft have generally remained near ground level during flight. There is a current need for small, lightweight, high-performance engines capable of reliable operation at altitudes of 4.5 km or more in Remotely Piloted Aircraft (RPA).

For simplified logistics and lower brake specific fuel consumption (BSFC), the Department of Defense desires the ability to operate all its aircraft on heavy fuels such as Jet Propellant 8 (JP-8). Research of temperature effects, complementing previous efforts in fuel injection and reduced chamber pressure, will yield results more consistent with operations at altitude than pressure control alone can provide. Additionally, a temperature control capability would allow study of cold-soak effects and starting engines at altitude, which are particularly relevant problems for heavy fuel engines.

Small RPA in most cases require a compact, lightweight powerplant with high power density. Such requirements have led to the adoption of spark ignition (SI) engines of both the two- and four-stroke varieties in many small drone airframes, but SI engines are designed to run on some form of gasoline. Therefore, military units operating RPA

frequently require a special logistics chain to supply the required gasoline and, in the case of two-stroke engines, oil. Although the IC engines with the greatest fuel conversion efficiency are of the two-stroke type (Heywood [1]), such engines are also gigantic with bores approaching a meter and strokes near three meters, compression ignition (CI), and run on heavy fuel oil. Small two-stroke engines also impose unique labor requirements for mixing the fuel and oil and offer relatively high power density but also low BSFC.

Because of the time and cost involved in developing new and innovative engines specifically for small RPA, it is common for these aircraft to use commercial off the shelf (COTS) engines. Converting COTS SI engines to operate on heavy fuels is no trivial task, as a fuel like JP-8 has both low volatility and low resistance to detonation (knock), meaning starting an engine with JP-8 and then preventing knock present challenges. It is necessary to vaporize a liquid fuel in order to burn it, so the low volatility of JP-8, with low vapor pressure and tendency to vaporize, translates to hard-starting characteristics. Starting difficulties become even more acute at low temperatures, and operating at altitude in most cases involves low temperatures along with low air pressures. Once the engine has started, though, avoiding the severe vibrations, forces, and stresses attendant with knock may require air-fuel mixtures and spark timing that also limit the engine's power and efficiency.

Although the gasoline-based fuels commonly used in RPA have more energy per unit mass than the heavy fuels used in jet engines, their lower density results in a lower volumetric energy density. Thus, heavy fuels typically offer greater potential for minimizing BSFC. Because the heavy fuels known as JP-8 and JP-5 are the preferred fuels of the United States Air Force and Navy, respectively, and have safer storage

characteristics by virtue of much higher flash points than aviation gasoline (Avgas), it is desirable to find ways to operate small RPA engines with heavy fuel.

Historically, CI engines have been extremely rare in aircraft operations, but the high cost of avgas and concerns about its future availability have spurred recent development of aircraft CI engines designed for use with Diesel fuel. Diesel fuel has much more in common with JP-8 than with gasoline, and it is much simpler to convert a Diesel engine to run on JP-8 than it is to do so with a SI engine. However, CI engines are still virtually unknown with the sizes and power densities demanded for small RPA.

I.2 Research Objectives

The primary objective of this research is to investigate and characterize the combined effect of temperature and pressure on a small Avgas-fueled two-stroke SI IC engine. The long-term objective, beyond this experiment, is to research the viability of converting a gasoline engine to start and run on JP-8 at altitude. These objectives are consistent with the US DoD's desires to procure RPA engines with greater reliability, lower specific fuel consumption, and a single-fuel concept for deployed operations.

The initial research focused on collecting performance and fuel consumption data for simulated altitude conditions. This required the development of an altitude chamber with control of both pressure and temperature. The test facility used for prior research was capable of controlling pressure with an automotive supercharger, but the potential for temperature control had yet to be exploited. Previous research with this rig was successful in producing enhanced understanding of the power and efficiency penalties

imposed by reduced air pressure, but a more thorough simulation of altitude demands reduced temperatures, as well.

A suitable heat exchanger was used to transfer heat from atmospheric air to liquid nitrogen in order to reach the reduced standard air temperatures associated with altitudes of approximately 1.5 and 3 km. Humidity and fuel temperature control were not included in this research. A representative small reciprocating aircraft engine modified with electronic fuel injection was already in place to provide control of the fuel-air mixture.

Data for power production, brake mean effective pressure (BMEP), and BSFC at various engine speeds and air pressures and temperatures were obtained, and in the future, the test facility will be utilized by researchers for discovering altitude effects on other small engines. These data will be of use to RPA manufacturers as they design or modify small drones to operate reliably at altitudes previously not encountered by the small SI engines used in such airframes. In addition, the capability to collect relevant engine performance and efficiency data for higher-altitude operations without the extensive coordination, planning, risk mitigation, and on-board data acquisition systems required for flight-testing RPA will be a great asset to the DoD.

In conjunction with DoD researchers, RPA designers will be able to more accurately anticipate the performance of engines at altitude without expending extensive amounts of time and money in flight testing. Given the understanding gained from this line of research, manufacturers will be able to eliminate unreliable or poor-performing candidate engines. Instead of wasting resources on less promising candidates, RPA development can be tailored to the most promising power plants and technologies.

With data regarding the BMEP and BSFC for a small IC engine running on gasoline at various combinations of pressure and temperature, a fuller understanding of small engines' dependence on altitude can be gleaned. Later, converting engines with 1 to 8 kW of peak power to run on JP-8 and JP-5 with varied spark timing at various simulated altitude test points will demonstrate the viability of starting and running small engines on a fuel logistically supported by the DoD in its current deployed locations. The successful use of direct fuel injection for heavy fuel will facilitate the improvement of specific fuel consumption for small engines while decreasing the cost and inconvenience of supporting them in the field. Accomplishment of these goals would be of great benefit to the US military as it increasingly relies upon small RPA in its operations.

I.3 Research Methodology

In order to accomplish the goal of characterizing the combined effect of pressure and temperature on a small IC engine, the test engine was operated at a throttle opening of 100% at standard atmospheric conditions corresponding to altitudes of about 213 m, 1.5 km, and 3 km. These studies were conducted over the range of 3,000 to 8,000 RPM at 500 RPM increments. The test fuel is a consistent mixture of 100 octane low lead Avgas mixed 80:1 with two-stroke oil.

To expand the usefulness of the temperature effect data gathered in this research, a temperature sweep was conducted at constant pressure along with a pressure sweep at constant temperature. Accordingly, the performance of the engine was examined for the 213 m, 1.5 km, and 3 km pressure altitudes at temperatures of 268, 278, and 295 K, respectively. The 295 K value was chosen because it was the nominal room temperature

in the test cell and required no additional temperature control capability. The two temperature-controlled values of 268 and 278 K represent the temperatures at 3 and 1.5 km operational altitudes, respectively, for the standard atmosphere.

In addition, the pressure altitude was varied from approximately 213 m to 4.5 km in increments of about 1.5 km at a temperature of 295 K. The 213 m altitude represents the elevation of the test cell and required no pressure control. At the other end of the range of altitudes involved in this experiment, 4.5 km is approximately the elevation of the high peaks in central Afghanistan or the continental United States. Power and BMEP were calculated from dynamometer measurements of torque and engine speed, and a fuel flow meter enabled fuel consumption measurement.

Pressure reduction was provided via the partial evacuation of air from an altitude chamber in which the engine is resident. The pressure difference was created through the operation of a compressor with its inlet at the exit of the chamber. Temperature reduction was by heat transfer from air to liquid nitrogen, either directly from atmospheric air for the cooling air stream or from dry shop air in a heat exchanger for the engine air stream.

II. Literature Review

Investigation of the effects of altitude on a small engine's performance calls for a basic understanding of the theory and practice of operating such an engine. In addition, the usefulness of research can be improved by thoroughly reviewing previous work in and related to the field of study at hand. Accordingly, it is wise to learn from the successes of others as well as problems encountered during similar studies. Additional literature review information is located in Appendix A.

Air pressure and temperature can be expected to vary with altitude as a small aircraft ascends and descends during a sortie, and air density will vary as a result. With a fixed volume available for the combustion process, the variation in air density affects the mass of air that may oxidize the fuel mass and therefore convert the fuel's energy into power. Also, temperature affects the vaporization of the liquid fuel used in this experiment, and it is the vapor that combusts and favorably affects power and efficiency.

II.1 Internal Combustion Engines

The majority of internal combustion (IC) engines in use are of the reciprocating type, although some rotary engines of the type credited to Felix Wankel have made their way into a variety of vehicles. Jet, gas turbine, and rocket engines may be categorized as IC engines with continuous combustion, but IC engines are most commonly considered to be reciprocating or rotary ones with discontinuous combustion. Combustion in an engine requires an oxidizer, fuel, and ignition. The two common IC engine ignition types are spark ignition (SI), involving one or more spark plugs to provide the necessary energy

for igniting an air-fuel mixture, and compression ignition (CI), involving energy imparted to the air during compression causing a temperature rise sufficient for autoignition.

The majority of IC engines operate on a two-stroke or four-stroke cycle, and SI or CI can be used for either cycle. For a two-stroke engine, the cycle is completed in a single revolution of the engine, while a four-stroke engine requires two revolutions per cycle. Regardless of the number of strokes, a cycle includes four basic processes: intake, compression, power or expansion, and exhaust.

The simplest reciprocating engine may have only three core moving parts, including the piston, connecting rod, and crankshaft. It must be noted that a simple Wankel engine, with its continuous rotary motion and thus no need for a piston to reciprocate between two linear extreme positions in connection with a crankshaft, contains just two core moving parts, a rotor and an eccentric shaft. An explanation of the four-stroke cycle is found in Appendix A.1.

II.2 Reciprocating Engine Cycles

This research effort involves a reciprocating SI IC engine operating with a two-stroke cycle that allows power production during each revolution, whereas a four-stroke cycle features a power stroke only every other revolution. The number of strokes per cycle does not imply a method of ignition, as either SI or CI may be used for either a two- or four-stroke cycle. The cycle for any of these IC engines is open rather than closed, because the working fluids are replaced with each cycle rather than continuously returning to the first stroke after the final stroke is complete.

The fundamental design features of a two-stroke engine are credited to Dugald Clerk (also known as Clark) and Joseph Day, whose assistant, Frederick Cock, introduced piston-controlled ports. The two-stroke cycle combines the four processes of intake, compression, power or expansion, and exhaust into a single revolution consisting of an up-stroke and a down-stroke. Figure 1 shows how a SI two-stroke engine accomplishes this feat in an application such as a small RPA.

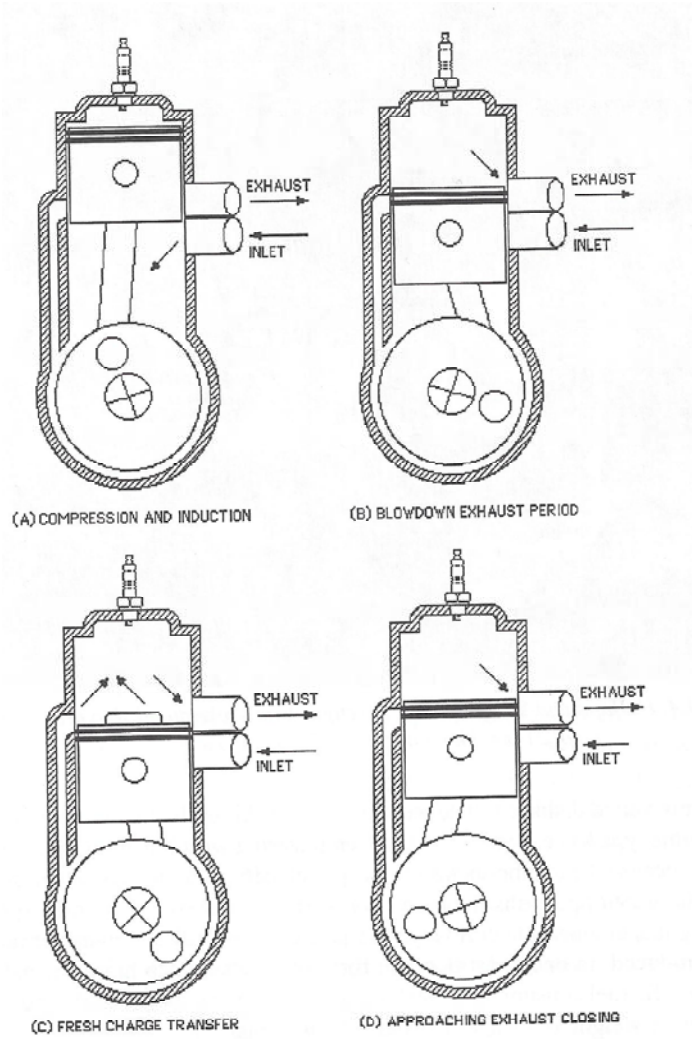

Figure 1. Processes for a two-stroke engine (from Blair [2])

The spark plug is visible at the top of the figure, and piston begins near the point (Top Dead Center, or TDC) where it yields minimum volume in the combustion chamber. The crankshaft is at the bottom of the figure, and the piston and crankshaft are joined by the connecting rod between them. The top end of the connecting rod moves in a straight line between two points, just as the piston does, while its bottom end rides on a crankpin and rotates with the crankshaft. In this way, the connecting rod allows the reciprocating motion of the piston to be translated into rotary motion, first for the crankshaft, and eventually for the propeller or other drive mechanism.

Figure 1 depicts a crankcase-compression two-stroke engine similar to the one used for this research, where three types of piston-controlled ports are visible: exhaust, inlet, and transfer. In part (A) of the figure, induction occurs as the inlet port is uncovered and a fresh fuel-air mixture flows into the crankcase beneath the piston. Also around this time in the cycle, electricity is supplied to the spark plug to cause ignition and a sharp rise in pressure and temperature of the fuel-air mixture above the piston. Following ignition, the burned mixture expands and drives the piston down, leading to the production of power as the crankshaft rotates. The transfer port, on the left side of the cylinder, and the exhaust port are both covered by the piston. Compression of the fuel-air mixture occurs as the piston descends toward the point (Bottom Dead Center, or BDC) where it yields maximum volume in the combustion chamber.

In part (B) of Figure 1, the power process is largely complete for the cycle, as the high pressure of the combustion products acting on the top surface area of the piston has created a downward force. Now, the piston has begun uncovering the exhaust port during the down-stroke, and this allows the blowdown exhaust period to commence. Thus, the

burned gases flow out of the combustion chamber through the exhaust port because they have higher pressure than the gases in the exhaust system or atmosphere.

In part (C) of Figure 1, the transfer port has opened to allow the fresh charge transfer. The fresh and compressed fuel-air mixture flows from the crankcase into the combustion chamber due to its greater pressure than that of the gases remaining above the piston. However, because the exhaust port is almost fully uncovered, a portion of the fresh mixture may flow out through the exhaust port before it has had a chance to burn. The phenomenon in which known fresh gases flow out of the cylinder before burning is known as short-circuiting. Additionally, pressure waves may cause backflow of exhaust gases into the cylinder.

In part (D) of Figure 1, the piston is now on its up-stroke, has closed the transfer port, and is approaching exhaust closing. Until the exhaust port closes, short-circuiting is still a possibility. After the exhaust port closes, further compression of the fresh charge will occur while the piston approaches TDC and returns to the portion of the cycle depicted in part (A).

II.3 Small Cylinders

Small cylinders, such as those with a bore under five cm, normally have very poor brake thermal efficiency. Relatively high heat transfer rates, a lack of focus on fuel economy, the use of carburetors, and the installation of short intake manifolds that allow only a very brief time for the air and fuel to mix all contribute to the low efficiency of typical small cylinders (Taylor [3]). Although the Brison 95 cc for this research has a

bore of 5.5 cm and is fuel-injected, the test cylinder suffers from some of the same efficiency issues as smaller cylinders.

Menon, Moulton, and Cadou [4] examined the performance of two identical 2.45 cm^3 engines to aid in understanding how engine performance varies between examples of a given design. They found the variation in performance between small engines of the exact same design may not be negligible, and even the performance of one engine may vary significantly when subjected to the same test multiple times. This indicates the importance of studying repeatability in experimental research.

Park, Fernandez-Pello, Pisano, and Walther [5] found in their rotary engine research that small engines require very fine fuel droplets for reducing evaporation time at high engine speeds. Operating at greater than 7,000 RPM, these small two-stroke cycle engines suffer from fuel-rich regions in which large droplets of fuel may quench the flame. Unless the equivalence ratio is adjusted according to altitude conditions, small engines realize additional performance losses when operating at higher altitudes than the one for which the carburetor was adjusted. Electronic fuel injection systems, with their capability of optimizing fuel-air ratios at a wide variety of operating conditions, thus offer particular value for increasing small IC engine reliability at altitude.

II.4 Pressure Effects

Inlet air pressure has a very significant effect on the performance of an engine because of its influence on the mass of oxidizer available for a combustion event. With all other independent parameters held constant, a decreasing pressure leads to reductions in the density and mass of the air in the cylinder for a given cycle. On the other hand,

increasing pressure tends to allow more fuel to be burned, and this effect is the primary reason supercharging or turbocharging is desirable for IC engines. For an ideal gas, the density ρ is:

$$\rho = \frac{P}{RT} \tag{1}$$

where P is the absolute pressure, R is the gas constant, and T is the temperature.

Noting that air pressure tends to fall with increasing altitude, we expect air density to decrease for a fixed temperature and increasing altitude. Knowing the density of air, we may calculate its mass flow rate $\dot{m}$:

$$\dot{m} = \rho A V \tag{2}$$

where A is the cross-sectional flow area and V is the velocity. The local speed of sound a may also be calculated:

$$a = \sqrt{\gamma R T} = \sqrt{\frac{\gamma P}{\rho}} \tag{3}$$

where γ is the ratio of specific heats for air, commonly taken to be equal to 1.4 at sea level. The Mach number M is the ratio of the velocity to the speed of sound:

$$M = \frac{V}{a} \tag{4}$$

The research engine has fixed geometry, so the volume available for the charge is constant. Thus, decreasing air density causes the mass of each charge to decrease, leading in turn to lower power relative to that produced at lower altitude. The definition of power is located in Appendix A.2, and efficiency is also explained in that section. Anderson [6] quantifies the correction factor for power as:

$$\frac{\dot{W}}{\dot{W}_{SL}} = 1.132\frac{\rho}{\rho_{SL}} - 0.132 \tag{5}$$

where $\dot{W}_{SL}$ and ρ_{SL} represent the brake power and density at standard sea level.

Kimberlin [7] uses an equivalent equation in which $\sigma = \frac{\rho}{\rho_{SL}}$, and the result can be used to predict the change in power as altitude varies:

$$\frac{\dot{W}}{\dot{W}_{SL}} = \sigma - \frac{1-\sigma}{7.55} \tag{6}$$

Heywood cites an alternative correction factor (*CF*), non-equivalent to Equation (6), from which we also may calculate *CF* directly from air pressure and temperature:

$$CF = \frac{\dot{W}}{\dot{W}_s} = \frac{(p - p_w)}{(p - p_w)_s}\left(\frac{T_s}{T}\right)^{1/2} \tag{7}$$

where p is atmospheric pressure, p_w is the partial pressure of water vapor, and the subscript s denotes sea level standard (Heywood and Sher [8]).

Taylor's discussion of the effect of atmospheric conditions on performance focused on variability at a given altitude [3]. The approach he takes is broadly equivalent to Heywood's, but he neglects humidity and calls the correction factor R_i:

$$R_i = \frac{\dot{W}_2}{\dot{W}_1} = \frac{P_2}{P_1}\sqrt{\frac{T_1}{T_2}} = \frac{imep_2}{imep_1} \tag{8}$$

where *imep* is the indicated mean effective pressure, the subscripts *1* and *2* refer to the reference and test conditions, respectively. Normally-aspirated engines feature spark timing and compression ratio consistent with approximately sea-level atmospheric intake pressure at wide open throttle (WOT). At idle the intake manifold pressure is well below atmospheric (Taylor [9]). The delivery ratio (DR) of a 2-stroke engine is:

$$DR = \frac{q_a}{V\frac{n}{60}d_o} \tag{9}$$

where q_a is the mass flow rate of dry air at the intake in kg/s, V is engine displacement in m^3, d_o is the density of dry air at 99 kPa and 298 K, and n is engine speed in RPM (Grasas-Alsina et al. [10]).

Scavenging, which occurs as a fresh mixture of fuel and air replaces exhaust gases in a cylinder, is extremely important for the performance of a two-stroke engine. Crankcase-scavenged two-stroke engines suffer significant loss of power as altitude increases (Harari and Sher [11]) due to low air density and decreases in the delivery ratio and efficiency because the crankcase receives little air when ambient pressure is not far above that of the crankcase volume (Watanabe and Kuroda [12]). Nonetheless, crankcase-scavenged two-stroke engines are used in small RPA because of their low weight, small physical size, and relatively high power.

Aircraft engines are especially susceptible to vapor lock as the boiling temperature of fuel drops with the decreasing atmospheric pressure of rising altitude. To avoid vapor lock, designers provide vents, use fuel that allows easy starting with the smallest vapor pressure, and keep sections of low pressure and high temperature in the fuel system from coinciding. Additionally, intake pressure instead of compression ratio is usually raised for aircraft engines when detonation susceptibility can be decreased, such as through the use of high octane fuels.

Aircraft use fuel-air ratios up to $F_R = 1.8$ at max power, compared to a typical maximum of $F_R = 1.3$ in automotive engines:

$$F_R = \phi = \frac{1}{\lambda} = \frac{AFR_{stoich}}{AFR} \tag{10}$$

where F_R or ϕ is the fuel-air equivalence ratio, λ is the air-fuel equivalence ratio, AFR is the air-fuel ratio on a mass basis, and the subscript *stoich* refers to stoichiometric. Aircraft engines often run exceedingly rich at high power compared to the best-power fuel-air ratio in order to decrease exhaust valve and spark plug temperatures, the probability of detonation, and heat transfer (Taylor [9]).

For a constant throttle position, intake and exhaust pressures vary together with changes in altitude. In this scenario, the residual-gas fraction is nearly fixed, and therefore flame speed changes with pressure at a lower rate than when either the intake or exhaust pressure is held fixed. Mechanical efficiency falls off and the best-economy fuel-air ratios rise with increasing altitude until, at altitudes where the brake power drops to near zero, the maximum-power mixture is best for any load.

For a normally-aspirated engine, rising altitude or exhaust pressure usually increases the necessary fuel-air ratio for some operating conditions. Accordingly, the engine needs extra mixture control such as back-suction or a variable fuel orifice in the carburetor to adjust the fuel-air ratio at high altitude. Also, due to heat transfer as fuel evaporates, some atmospheric conditions may lead to the freezing of moisture on the throttle valve or other parts of an aircraft carburetor (Taylor [9]).

Soares and Sodré [13] tested the effects of atmospheric conditions on the acceleration of a road vehicle equipped with EFI and variable intake manifold length in a SI 4-cylinder engine. Varying the intake length allows variation of the intake volume, which in turn can be used to increase performance (Ceviz [14]). They state decreasing

atmospheric pressure decreases the air density, the mass of the fuel-air charge, and the volumetric efficiency, leading to reduced power. Lower intake temperatures yield lower flame speeds and therefore decreased power.

On the other hand, higher intake temperatures are detrimental to volumetric efficiency at high engine speeds. Humid intake air decreases the flame speed but has a less significant effect on engine power than pressure and temperature. Soares and Sodré [13] found varying atmospheric pressure to have greater effect on vehicle acceleration than temperature did, but with opposite directions. As such, decreasing pressure hurt the vehicle's acceleration, while decreasing temperature helped.

Shin, Chang, and Koo [15] conducted a combination of sea level experimental research and altitude simulation to predict BMEP, power, and brake specific fuel consumption (BSFC). Based on test results with a 25 cm^3 four-stroke glow engine converted to spark ignition, they estimated around a 25% drop in peak BMEP at 3 km and 40% at 5 km, similar power losses at the two higher altitudes, and increases in BSFC of as much as 30% as altitude and engine speed increased. Shin et al. attribute the increase in BSFC to friction remaining almost fixed for a given engine speed while air density and power decrease with altitude. Altitude chamber testing of a small RPA engine will yield useful data for advancing the development of reliable heavy fuel engines at decreased air pressure and temperature.

Harari and Sher [11] researched the effect of atmospheric pressures as low as 44 kPa on the performance of a 350 cm^3 SI two-cylinder two-stroke engine. Building on correlations made in other papers, Harari and Sher included the effect of atmospheric temperature on the predicted output power. They had previously suggested a power

correction factor *CF* for engine speeds up to 6,000 RPM and ambient pressures as low as 70 kPa, or approximately the 3 km pressure altitude:

$$CF = \frac{1-\omega}{1-\omega_s}\left(\frac{P}{P_s}\right)^{9/8}\left(\frac{T_s}{T}\right)^{0.8} \tag{11}$$

where P is the atmospheric pressure, the subscript s denotes sea level standard conditions, T is the atmospheric temperature, and ω is the air humidity ratio. The air humidity ratio is defined as:

$$\omega = \frac{M_w X_w}{M_a X_a} = 0.62198\frac{X_w}{1-X_w} \tag{12}$$

where the subscripts w and a refer to water and air, M is the molecular mass, and X is the molar concentration. Along with the correction factor Equations (5) and (8), the formulations from Harari and Sher were used in analysis for this thesis.

Harari and Sher reduced the air pressure through the use of a vacuum pump for the exhaust and throttling the intake. They found maximum engine torque decreases as the inlet air pressure decreases due largely to backflows from the crankcase to the atmosphere at low engine speeds and decreased scavenging efficiency because of short-circuiting. The loss of scavenging efficiency also seemed to have led to the observed increase in BSFC at low air pressures. Harari and Sher concluded the correction factor is proportional to the atmospheric pressure raised to a power, rather than simply 9/8, ranging from 1 for low engine speed to 2 for high speed. With a better understanding of this phenomenon in conjunction with temperature effects, engineers will be able to mitigate the negative changes in performance as RPA operate at greater altitude.

Crosbie [16] studied the effects of pressure altitude on the operation of a 95cm^3, single-cylinder, two-stroke, spark-ignition engine. After characterizing the stock carbureted engine, they converted the engine to fuel injection and compared the two fuel delivery systems. Their WOT data at a nominal temperature of 295 K in Figure 2 through Figure 4 show reduced BMEP and power as altitude increases. Details of the difficulties in matching the data of Crosbie are found in Appendix B.1, and related obstacles such as electrical power issues are discussed in Appendix B.2.

As shown in Table 1, the maximum power measured by Crosbie [16] at a pressure altitude of 1.5 km was 83% of the 0.2 km maximum, and the fraction fell to 62% at 3 km. The term "multiplier" is defined in Table 1 and throughout this thesis as the decimal fraction resulting from dividing a value by its corresponding reference or baseline value. Figure 2 depicts not only the loss of power but also the shift of the peak power point on the curve to a lower engine speed with decreasing air pressure. The maximum measured BMEP at a pressure altitude of 1.5 km was 87% of the 0.2 km maximum, and the fraction fell to 66% at 3 km. The mean BSFC at 1.5 km was 110% of the 0.2 km mean, and the BSFC for 3 km was 119% of the 0.2 km mean.

Table 1. Pressure effects on performance (from Crosbie [16])

Pressure altitude, km	**Peak power multiplier**	**Peak BMEP multiplier**	**Mean BSFC multiplier**
1.5	0.83	0.87	1.10
3	0.62	0.66	1.19

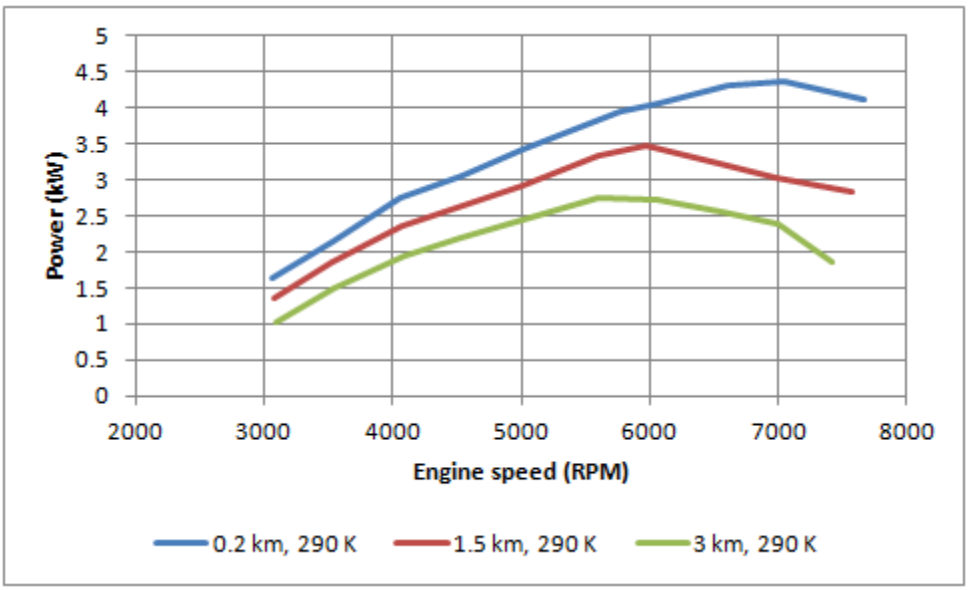

Figure 2. Power curves for pressure sweep (from Crosbie [16])

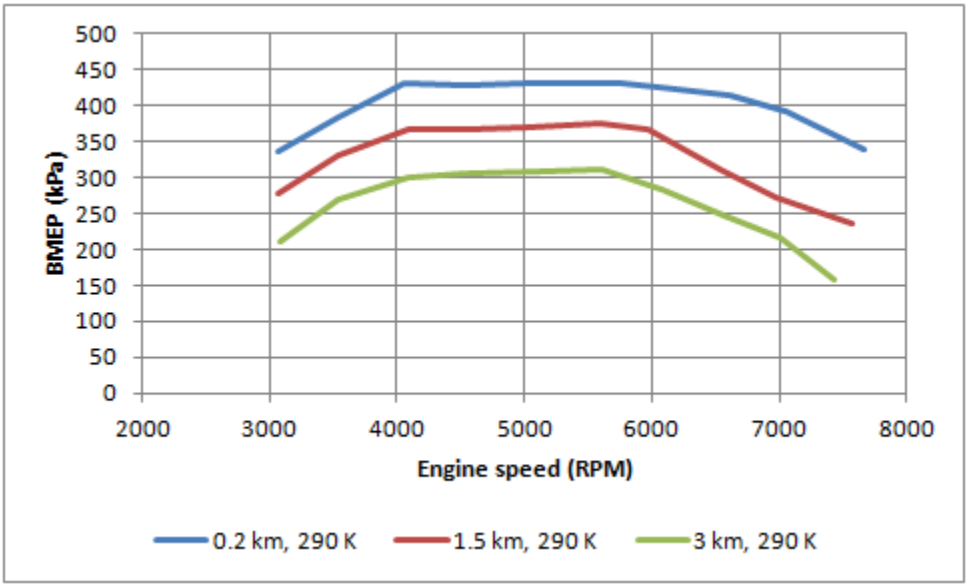

Figure 3. BMEP curves for pressure sweep (from Crosbie [16])

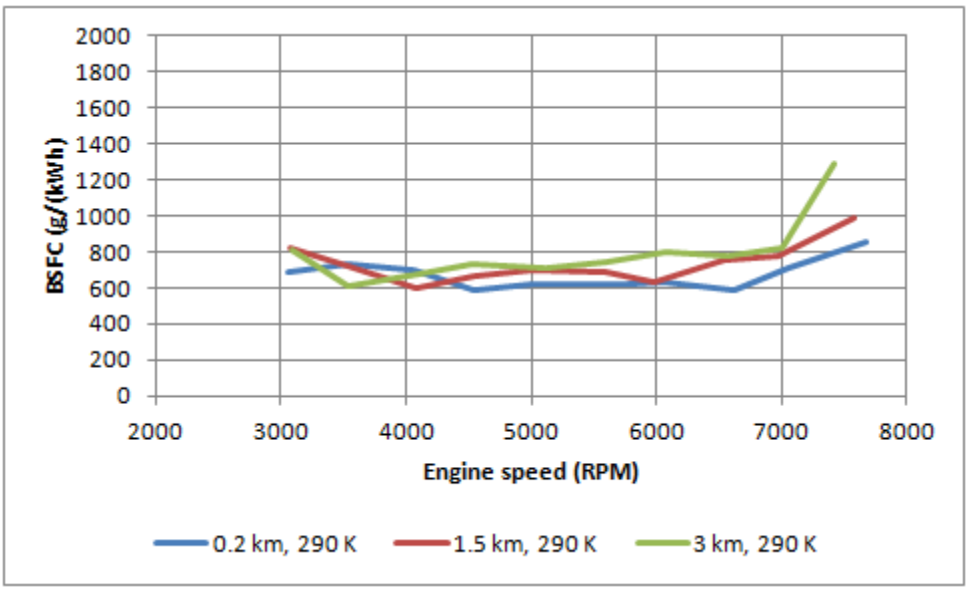

Figure 4. BSFC curves for pressure sweep (from Crosbie [16])

II.5 Temperature Effects

The effect of inlet air temperature on the power output for a 60 cm^3 two-stroke crankcase-compression gasoline engine was investigated by Watanabe and Kuroda [12]. They used a surge tank with a volume 690 times displacement of the engine and topped with a flexible diaphragm was attached to damp out pulses in the air flow pulsations. Their method of temperature control was electric heating of the intake air, and they achieved a range of 273 K to 313 K, corresponding to the standard freezing point of water at the low end and a hot day at the high end. Thus, most of their data was taken at temperatures insufficient for freezing of moisture to become an issue, while this is a common problem for aircraft.

Although the power of a 4-stroke SI engine varies inversely proportionally to the square root of the absolute intake air temperature, the data from Watanabe and Kuroda showed an inverse relationship between engine power and the temperature raised to a

power between 0.5 and 0.9, dependent on temperature and engine speed. Additionally, Watanabe and Kuroda developed an expression for this engine type's power output based on the scavenging pressure. They concluded that because of a drop in pressure ratio as the inlet temperature increases, power will also decrease.

Watanabe and Kuroda [12] also noted that their data may have been affected by the use of a constant temperature cooling airflow for the engine and that the power reduction would have been magnified had the cooling air temperature matched that of the inlet airflow. Accurately simulating both the inlet and cooling air temperatures at altitude will yield useful data for small IC engine performance characterization and improvement. Watanabe and Kuroda stated a two-stroke engine's delivery ratio decreases at low engine speeds largely because of air-fuel mixtures flowing from the crankcase back to the atmosphere. They believe scavenging efficiency decreases due to short-circuiting losses (Heywood and Sher [8]).

For multi-cylinder SI aircraft engines at fixed throttle and unaffected by detonation, the output is typically corrected for changes in air temperature by assuming indicated power varies in inverse proportion to the square root of the inlet temperature T_i. Volumetric efficiency rises with increasing T_i because of decreasing mean temperature difference between the charge and cylinder walls (Taylor [3]). Temperature has a great effect on laminar flame speed S_L, and increasing the unburned gas temperature (Turns [17]) from 300 K to 600 K will increase S_L by a factor of more than three.

Cline [18] states that when simulating altitude, air pressure and temperature are the more important parameters to control, as humidity has a lesser effect on engine performance. His test facility had 50 kW electric heaters available for heating the air to

325 K. Vacuum pumps sealed with water at 289 K provided the capability to draw a vacuum of 68 kPa, and a three-stage compressor with Freon 22 was capable of 29 kW of cooling at 217 K to allow an intake air temperature of 237 K at sea level or 241 K at a pressure altitude of 3 km. The engine is a water-cooled CI 4-stroke inline 6-cylinder of 5,654 cm^3 displacement, so it is different in several respects from the air-cooled, SI 2-stroke, single-cylinder, 95 cm^3 displacement Brison test engine.

Cline's data in Figure 5 show how the engine's power changes at a constant speed of 2400 RPM with intake air temperature varying between 286 K and 237 K, roughly corresponding to the sea level standard temperature at the high end and a cold day for 4.5 km at the low end, at a constant pressure of 100.1 kPa. The engine coolant temperature was controlled at 350 K, but the other engine and fuel temperatures varied naturally. The power climbed by over 10% as the intake air fell from 286 K to 237 K, but having reached a best value of about 365 g/(kWh), the BSFC also rose at the lowest temperatures. The exhaust gas temperature (EGT) fell from 994 K to 936 K during the test, and air-fuel ratio (AFR) varied between 18.5:1 at 261 K and 17.3:1 at 239 K.

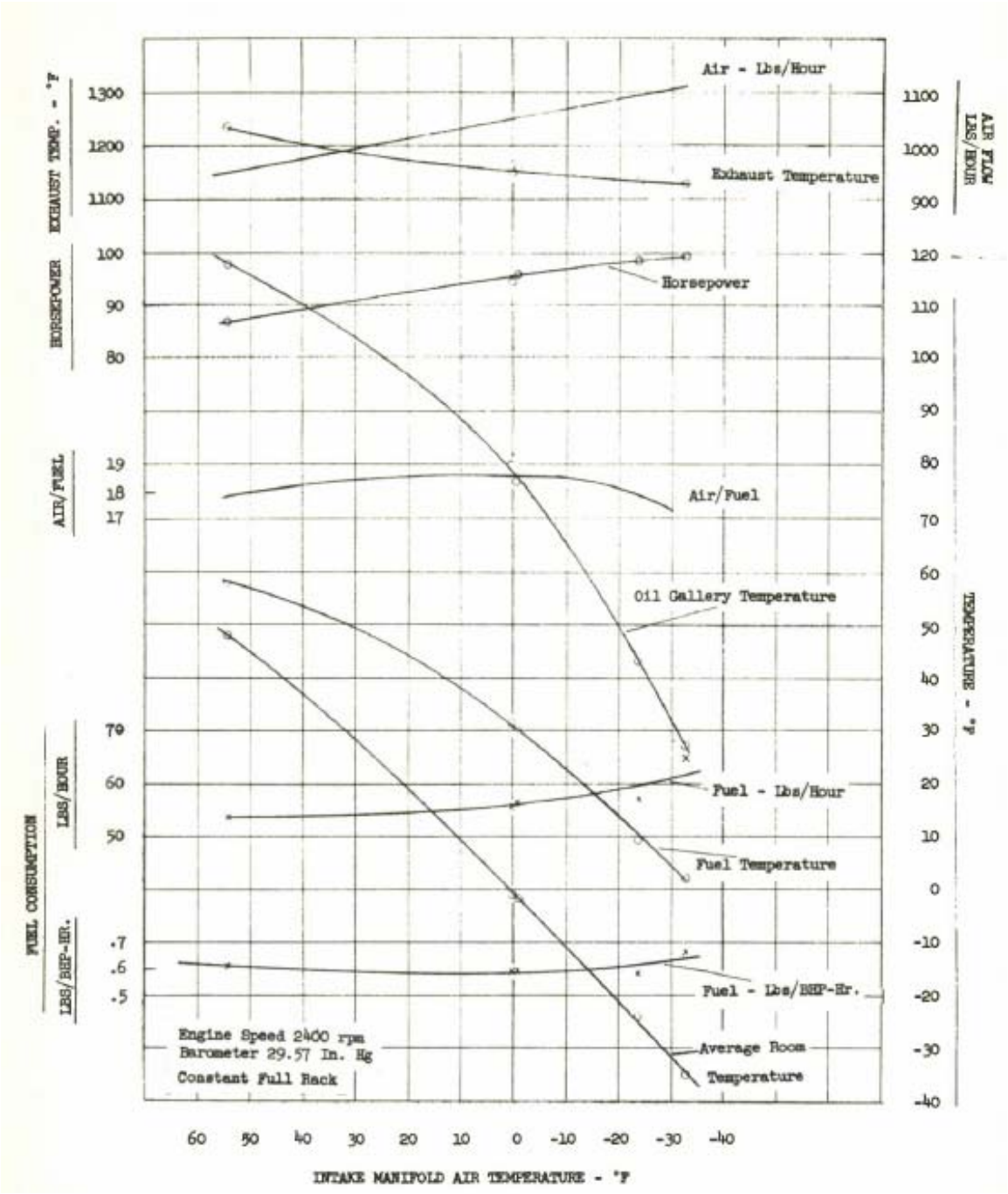

Figure 5. Effect of environment on engine performance (from Cline [18])

II.6 Air and fuel

Fire or combustion requires three essential ingredients: an oxidizer such as air, a fuel such as gasoline or kerosene, and an ignition source such as a spark or a temperature rise resulting from compression. The proportions of air and fuel must fall within limits, and the timing of the spark can have a significant effect on the efficiency and energy release of the combustion process. Furthermore, gas dynamics, fuel vaporization, and heat transfer may each profoundly affect the processes occurring within an IC engine. Maximizing the performance of an engine calls for delivering a mass of air at the most advantageous possible temperature, mixing it appropriately with the desired mass of fuel, and transferring as much of the fuel-air mixture's energy as feasible to the crankshaft.

II.6.1 Intake

Air flow is often considered incompressible for changes in density of less than 5%, and velocities corresponding to a Mach number of less than 0.3 have small pressure and density changes (Anderson [19]). Accordingly, since small RPA fly at Mach numbers below 0.3, the intake air flow may be assumed to meet the criteria for incompressible simplification. Although a ram effect results from the stagnation of air in the inlet for propeller-driven aircraft at high speeds, small RPA do not reach the velocities necessary for this pressure effect to be significant. Thus, for aircraft of the class suitable for being powered by a small engine such as the Brison 95 cm^3, power and BSFC may be assumed constant with respect to aircraft velocity. For naturally-aspirated reciprocating engines at altitudes up to around 3 km, BSFC is also assumed constant with altitude (Anderson [6]).

The inlet velocity and exhaust velocity and temperature of reciprocating engines are unsteady, and the velocities are especially variable in single-cylinder engines. In order to accurately measure air mass flow rate in single-cylinder engines, surge tanks with at least 50 times the volume of the cylinder are used between the meter and the engine to dampen the pressure oscillations due to the unsteady flow. Similarly, a single- or twin-cylinder engine with a single small intake manifold usually has pressure variations that render the measured average pressure unreliable (Taylor [3]). It is possible to measure the scavenging ratio for 2-strokes, except crankcase-scavenged ones, if the inlet air flow, pressure, and temperature and the exhaust pressure can be accurately measured. Surge tanks for both the inlet and exhaust systems are often utilized to increase the accuracy of these measurements [3].

Because the two-stroke cycle lacks individual intake and exhaust strokes, manifold tuning has a very meaningful effect on performance. The simplest two-strokes have symmetrical port timing with respect to TDC, and as such, the transfer port closes before the exhaust port. Thus, tuning can greatly alter the pressure waves in engines like the Brison (Winterbone and Pearson [20]). Intake manifold pressure is variable during intake because the piston speed and open area of the intake port vary, resulting in unsteady flow.

In crankcase-scavenged engines, the mass of charge taken into the crankcase drives the crankcase pressure at the start of scavenging, which in turn determines the delivery ratio (Heywood and Sher [8]). Ramming increases with engine speed because the intake gas momentum increases the pressure in the intake port, particularly as the port is closing. Thus, the mass in the crankcase will be greater. The unsteady intake flow to

the crankcase results in weak expansion waves moving back into the intake manifold and being reflected as compression waves. For a tuned intake, a compression wave reaches the intake port as it closes, the pressure rises, and extra air flows into the crankcase [8]. With extra air in the crankcase, extra fuel may be burned, leading to increased power.

II.6.2 Air-Fuel Ratio

For a simple 2-stroke engine such as the Brison 95 cm^3, operation at the stoichiometric air-fuel ratio (AFR) of about 14.7:1 will yield minimum BSFC and brake specific unburned hydrocarbons (BSHC) emissions. However, the maximum power AFR of around 13:1 is approximately 13% rich of stoichiometric. With the exception of HC emissions, simple 2-stroke engines can match or defeat 4-strokes in virtually any category. Thus, in terms of specific power, physical size, weight, cost of manufacture, maintenance, durability, BSFC, or emissions of CO and NO, a well-designed 2-stroke offers numerous benefits when compared to 4-strokes. Small 4-strokes have low thermal efficiency because of additional friction due to components absent from a 2-stroke such as an oil pump and camshaft (Blair [2]).

Quenching results when heat transfer by conduction from a flame occurs at a greater rate than combustion is able to generate within the flame. Flame quenching may lead to the emission of unburned hydrocarbons (HC). Flammability has upper and lower limits, where the upper limit is richest mixture that leads to smooth flame progression, and the lower limit is the leanest mixture (Turns [17]). Due to increasing time losses, spark timing other than optimum usually increases the best-economy fuel-air ratio, and throttling also increases those AFRs.

Similarly, for a fixed intake pressure, higher exhaust pressure usually lowers the flame speed and increases best-economy fuel-air ratios. On the other hand, for a fixed exhaust pressure, higher intake pressure usually increases flame speed (Taylor [9]). Directly measuring the air flow rate in two-stroke engines can affect the flow of air through the engine, but because of short-circuiting, measuring exhaust species may be complicated by the relatively high proportions of oxygen and fuel found in the exhaust (Heywood and Sher [8]). Although crankcase-compression 2-stroke engines have lower cylinder pressures, they require approximately the same octane fuel as 4-strokes with equivalent cylinder volume [9].

The stoichiometric AFR of around 14.7:1 for gasoline gives peak exhaust gas temperatures (EGT), but for best performance at WOT and with lower EGT, the 4-stroke AFR range is 11.5 to 13.0:1. Hartman [21] recommends a safe best power AFR of 12:1 to 12.5:1 for a naturally aspirated 4-stroke SI automotive engine that needs no extra gasoline for combustion cooling or controlling detonation. Retarding ignition timing with other parameters fixed will raise EGT because the mixture continues combusting at a later point in the cycle. Altitude, corrected atmospheric pressure, and air temperature can each affect the most advantageous EGT [21].

Best torque is not a point but rather a range of air-fuel ratios from rich best torque (RBT) to lean best torque (LBT) wherein power is essentially constant for a given engine speed. The difference between RBT and LBT becomes smaller at high engine speeds because the maximum flame speed limits the available time for a combustion event [21]. Hartman states that flame speeds in gasoline-air mixtures vary from 6 meters per second (m/s) to more than 45 m/s, with the speed highest at an AFR near 11:1 and falling off

drastically as the mixture becomes leaner or, even more so, as it becomes richer. He also indicates the probability of abnormal combustion rises as the flame front speed falls [21].

Hartman relates that a good goal for a naturally-aspirated 4-stroke SI engine's safe best power AFR at WOT is 12 to 12.5:1, assuming the engine does not require surplus fuel for combustion cooling and knock control. Table 2 lists several notable operating conditions and their associated approximate AFRs for a 4-stroke engine. As indicated, EFI may enable a rather wide range of AFRs between the rich and lean limits when the engine is warmed up, and the mixture may require only 50% more air than fuel when starting a cold engine in cold weather [21].

Table 2. Common air-fuel ratios for automotive operation (from Hartman [21])

Condition	**AFR**
Rich burn limit at normal operating temperature	6.0
Approximate Rich best torque at WOT	11.5
Safe best power at WOT	12.2
Approximate Lean best torque	13.3
Usual best economy	16.5
EFI lean burn limit	22+
Ambient temperatures below 255 K	4.0
Cold cranking	1.5

Griffin et al. [22] measured exhaust gas temperatures (EGT) for a 500 cm^3 4-stroke SI engine and used correlated AFR data from a wideband lambda sensor to develop a method for calculating AFR from EGT. Griffin et al. note small engines usually operate rich of stoichiometric for maximum power and cooling and because manufacturers provide a safety margin since AFR drifts higher as an engine wears.

Inexpensive lambda sensors are useful in indicating the fact, but not the degree, that the engine is running either rich or lean of a stoichiometric mixture of 14.7:1.

Small engines in some cases make use of exhaust systems short enough to permit atmospheric air to flow into the exhaust due to pressure pulsations, and this effect may render the measurements of an oxygen-concentration-type lambda sensor inaccurate. On the other hand, wideband sensors are relatively expensive. Griffin et al. found AFR and EGT are nearly linearly related for AFRs of 11 to 14.0 with three variants of gasoline, but they also report application-specific empirical data are required for calculating AFR from measured EGT. Speed, load, and ignition timing must also be known [22].

Smither et al. [23] designed a fuel injection system for small engines and note most single-cylinder engines have low-cost carburetors and fixed ignition timing via a magneto, so they often have AFRs and spark timing chosen to keep the engine in a safe operating zone. As such, the ignition angle is fixed at a value meant to protect the engine at high speeds and temperatures as well as engine start. Because of this fact, the engine's power and efficiency are lower than they could be at operating conditions compatible with greater spark advance. Smither et al. also explain that for single-cylinder engines and those with small inlet plenum volume, MAP is quite variable between a partial vacuum during the intake process in each cycle and atmospheric pressure when the intake valve or port is closed [23].

Allen and Drake [24] experimented with a digital port fuel injection system on a 4-stroke, 190 cm^3, single-cylinder SI 4.8 kW. Utilizing a low-pressure, 600 Hz EFI system with a fixed volume of fuel per pulse, Allen and Drake varied the number of pulses per engine cycle. They found that due to wall-wetting, a volume of liquid fuel

equivalent to around 40% of a cycle's total is available in the inlet port while the engine is running. The excess fuel helps to reduce cycle-to-cycle changes in AFR, as multiple engine cycles may pass before the fuel enters the cylinder [24].

II.6.3 Scavenging and port timing

Two-stroke engines require the unburned fuel-air mixture to enter the cylinder at a pressure higher than that of the burned gases for the process of replacing the combustion products with fresh fluids to proceed. The efficiency of this process, known as scavenging, is of great importance to the performance of a two-stroke. Mixing of the unburned and burned gases is very undesirable except in those cases where a form of exhaust gas recirculation (EGR) is used to control noxious emissions. However, because the two mixtures come into direct physical contact, prevention of mixing is a great challenge and cannot be totally eliminated in the test engine. Scavenging in two-stroke engines is turbulent and features interdependent momentum, mass, and heat transfer. The mass of fuel that can be burned is limited by the mass of trapped air available through scavenging (Heywood and Sher [8]).

Figure 6 (a) shows loop-scavenging, in which the air (transfer) ports are located in the same vicinity of the cylinder as the exhaust ports. Cross-scavenging, depicted in Figure 6 (b) and used in the Brison 95 cm^3 test engine, has a transfer port π radians from the exhaust port within the cylinder. In uniflow-scavenging, as seen in Figure 6 (c), a valve is located at the top of the cylinder to allow the exhaust gases to exit from that end.

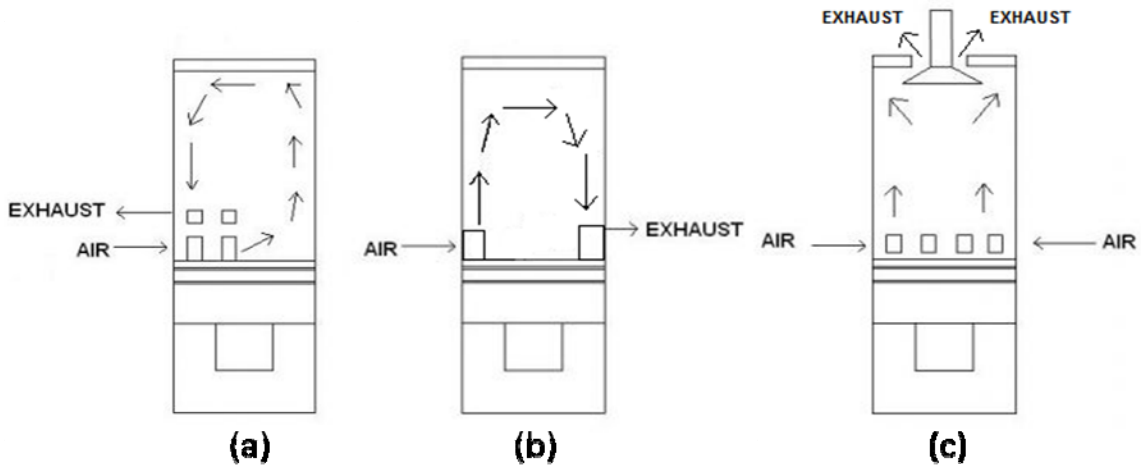

Figure 6. Scavenging types; (a) loop , (b) cross, (c) uniflow (from Schmick [25])

Fresh fuel and air enter the cylinder at higher than atmospheric pressure, but this pressure difference should be kept to a minimum so as to prevent excess pumping work. Crankcase compression is strongly influenced by the exhaust system's pressure difference (Heywood and Sher [8]). Two-stroke engines with Schnürle-type loop-scavenging are not desirable for aircraft use because of severe scavenging losses at altitude [8].

For best performance, high trapping efficiency is important, scavenging efficiency is typically high, and the delivery ratio is as low as possible. Normally, a carbureted crankcase-scavenged engine (without stratification or DI) has about 15-20% of its fuel short-circuited into the exhaust. Backflows are possible at high speed as the scavenge ports open or at low speed before the intake or scavenge ports close [8].

In a simple two-stroke engine, the opening and closing times of the piston-controlled ports are non-ideal in that they are both constant and symmetric with respect to the crankshaft at bottom center (BC), and these ports offer low resistance to both back-

flow and forward flow. On the other hand, such ports feature fast time response, no moving parts or noise, and simplicity (Heywood and Sher [8]). Piston-controlled port timing is determined by the axial dimensions and location of the ports as well as the crank-rod ratio. A loop-scavenged cylinder will necessarily have symmetric timing with respect to bottom center unless auxiliary valves are used. Exhaust ports always open before the inlet ports open and close after inlet ports close, but this allows a portion of the fresh charge to exit through the exhaust (Taylor [3]).

Supplementary literature review information is located Appendix A and includes the four-stroke cycle (Appendix A.1) and definitions of the performance measures of power and fuel efficiency (Appendix A.2). In the areas of air, fuel, and ignition, additional details regarding compression ratio, fuel injection, and spark timing are discussed in Appendix A.3. Because the line of research explored in this thesis has a long-term goal of powering small RPA with heavy fuel engines, Appendix A.3 also summarizes particular heavy fuel challenges such as knock and cold-starting.

III. Experimental Set-up

The objective of this research is to find the effects of temperature on the performance of a small internal combustion engine at altitude. The three primary performance measures are power, brake mean effective pressure (BMEP), and brake specific fuel consumption (BSFC). In order to gather the data required for accomplishing the objective, an altitude test rig for small engines built by Schmick [25] and refined by Crosbie [16] was utilized. Additional information about the experimental set-up is located in Appendix B.

Although the mobile altitude rig was originally designed and assembled for control of both pressure and temperature, the temperature control function had never been used in practice. Because standard temperatures, especially at altitude, are lower than those available for ambient air in the test cell, more realistic simulation of altitude requires air temperature control in addition to pressure control. Therefore, it was necessary to complete a design suitable for providing air at the desired pressure and temperature to the engine while maintaining matching pressure for the exhaust and matching temperature for the cooling medium.

III.1 Altitude chamber

The test set-up for these experiments is centered around a small IC engine altitude test chamber, shown schematically in Figure 7, that allows data collection at the reduced air pressures associated with altitude in lieu of flight testing. The intake flow path is broken into two separate systems, with one stream of cooling air flowing from the ambient air in the test cell through pipes of 7.6 cm diameter to the compressor and one

stream of engine intake air flowing from a compressed air source through tubes of 1.3 cm diameter. The altitude chamber is capable of achieving a 57 kPa operating environment, meaning pressure altitude conditions up to 4.5 km can be simulated with the test stand. The test facility's engine air path is represented in blue, the cooling air path in green, the fuel path in orange, and the liquid nitrogen (LN_2) paths in red.

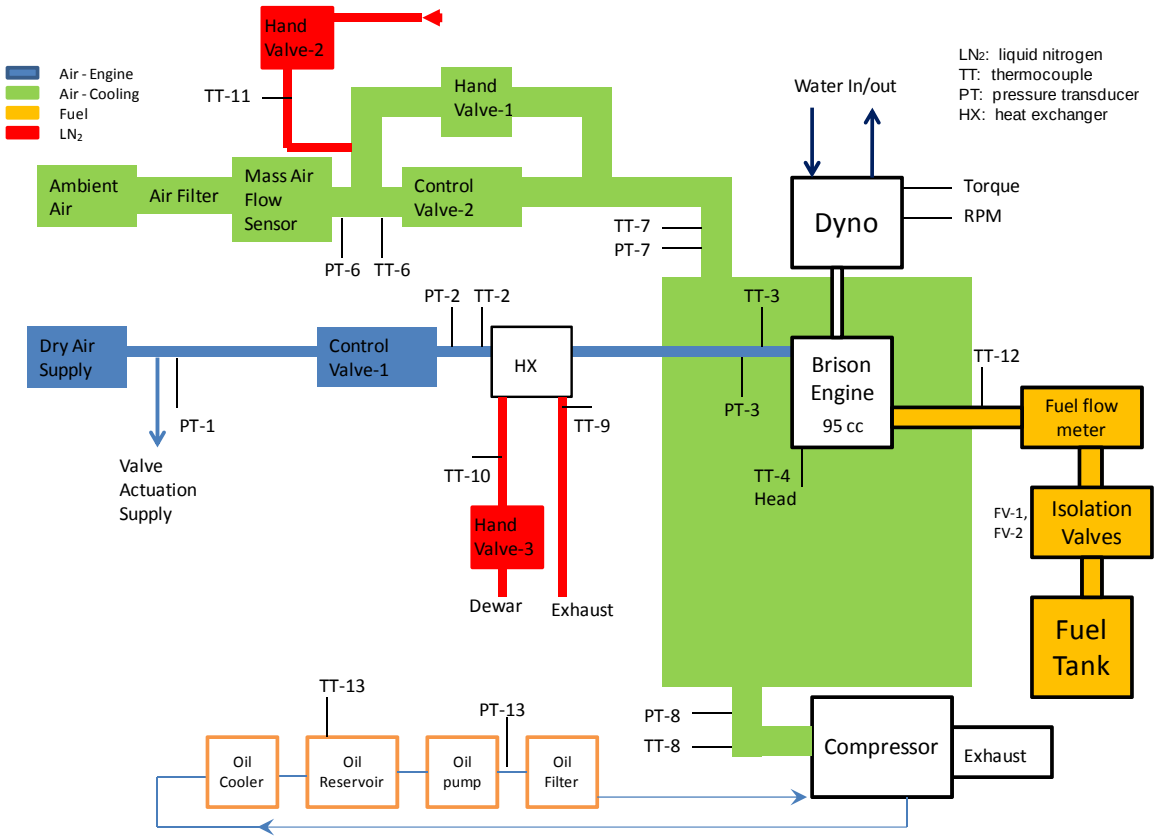

Figure 7. Experimental Set-up Diagram (from Crosbie [16])

Figure 8 is a photograph of a few of the key features of the test rig, including a screen shot from the LabView graphical user interface that provides for control. Some of the key measurements include dynamometer torque and rotational speed, from which

power and BMEP are calculated, fuel flow rate, air pressures and temperatures, and air-fuel ratio (AFR). With measured fuel flow rate and power, BSFC can be calculated.

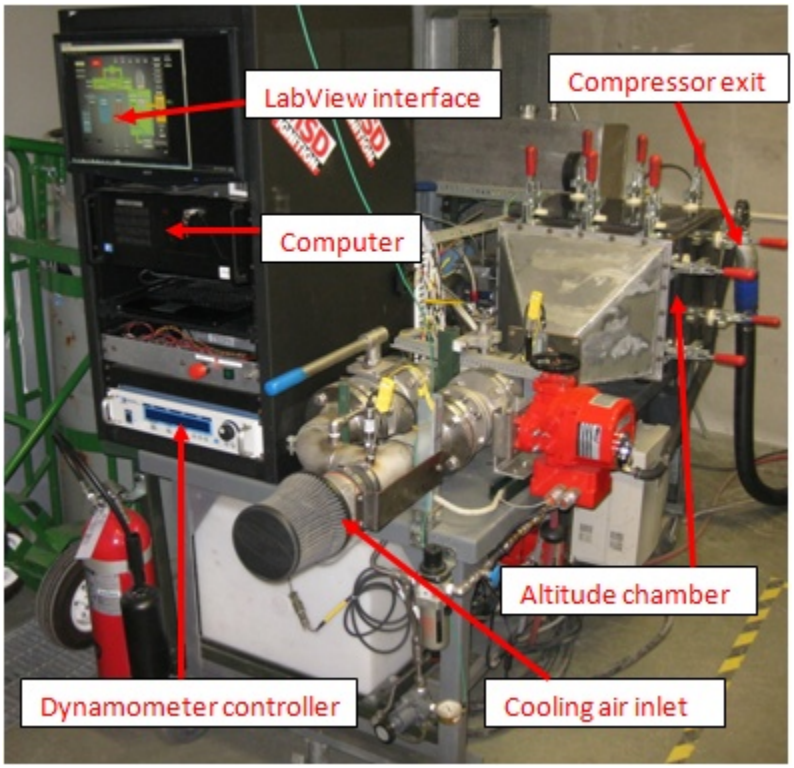

Figure 8. Test rig

The chamber is currently equipped with a 95cm^3 two-stroke engine fed by a throttle body fuel injection system. The Brison engine, shown disassembled in Figure 9, features a single-cylinder, spark-ignition, and crankcase-scavenging. Details of the difficulties in matching the performance data of Crosbie [16] for the Brison engine are found in Appendix B.1. Various advertised, measured, and calculated parameters for the test engine are found in Table 3.

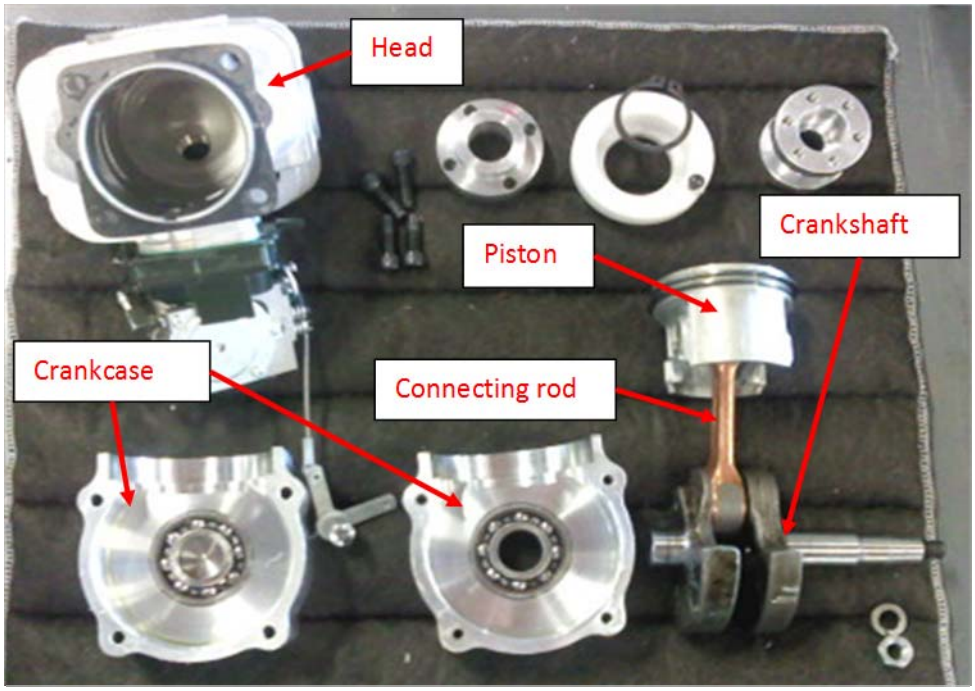

Figure 9. Brison engine components

Table 3. Brison 95 cm^3 engine properties (from Schmick [25])

Property	Value	Property	Value	Property	Value
Displacement*	95 cm^3	Type	2-stroke, crankcase-scavenged	Intake Port Arrangement	2 ports offset 180°
Bore+	5.5 cm	Intake Port Open/Close Angle	59.7° B/ATDC	Exhaust Port Open/Close Angle	81.3° B/ATDC
Stroke++	4.1 cm	Intake Port Area+	2 cm^2 / port	Exhaust Port Area+	0.626 cm^2

*Manufacturer advertised value +Measured Value ++Calculated Value

The test rig is capable of simulating standard or cold-day air pressure and temperature for local takeoff conditions up to 4.5 km MSL. Several obstacles with the rig needed to be overcome such as electrical power issues, and these are discussed in Appendix B.2. The cooling air source is the moist ambient air in the test cell. The

pressure was controlled with a Vortech V-5 K-trim automotive supercharger and air valves to enable a partial vacuum in the altitude chamber. The supercharger, a belt-driven radial compressor shown in Figure 10, is powered by a 15 kW Emerson Motor Corporation model AF18 electric motor in conjunction with a Delta VFD-F variable frequency drive. Operating parameters for the compressor including pressure ratios, mass flow rates, and speeds are summarized in Appendix B.3.

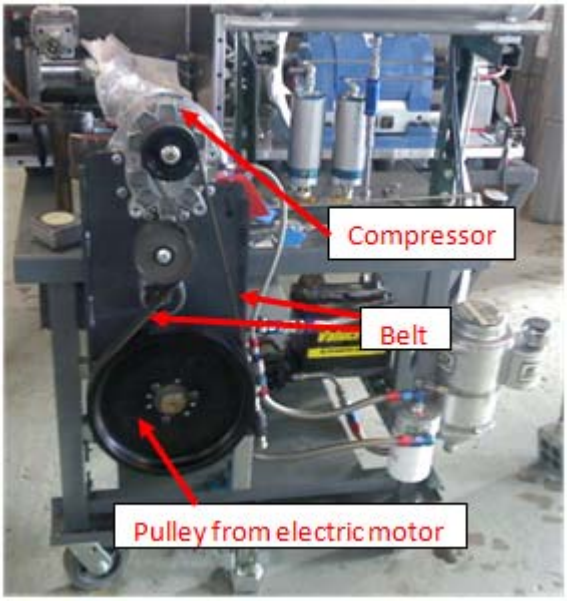

Figure 10. Belt drive from electric motor to compressor

The test fuel is 100 octane low-lead aviation gasoline (Avgas), and because the Brison 95 cm^3 is a simple two-stroke, it is necessary to mix two-stroke oil with the Avgas to provide lubrication for the engine. Both the Avgas and oil were obtained from stores located on Wright-Patterson Air Force Base (WPAFB) around 250 m from the test cell, and a graduated cylinder was used to precisely mix the gas and oil in a ratio of 80:1. The rig itself does not have a humidity control capability, but the compressed shop air used

for combustion is dry, having a dewpoint of 233 K. A few of the basic facts regarding the test rig are summarized in Table 4.

Table 4. Basic test facility facts (from Crosbie [16])

Test Engine	Brison 95 cm^3 2-stroke with spark ignition
Test Fuel	100 octane low-lead Avgas mixed 80:1 with Amsoil synthetic 2-stroke oil
Fuel Flow Meter	Max Machinery 213 rotary piston with model 294 transmitter (0.00089 cm^3/pulse)
Altitude Chamber Pressure Range	57 kPa (absolute) to ambient air pressure
Dynamometer	Magtrol 2WB65 eddy current (up to 7.5 kW)

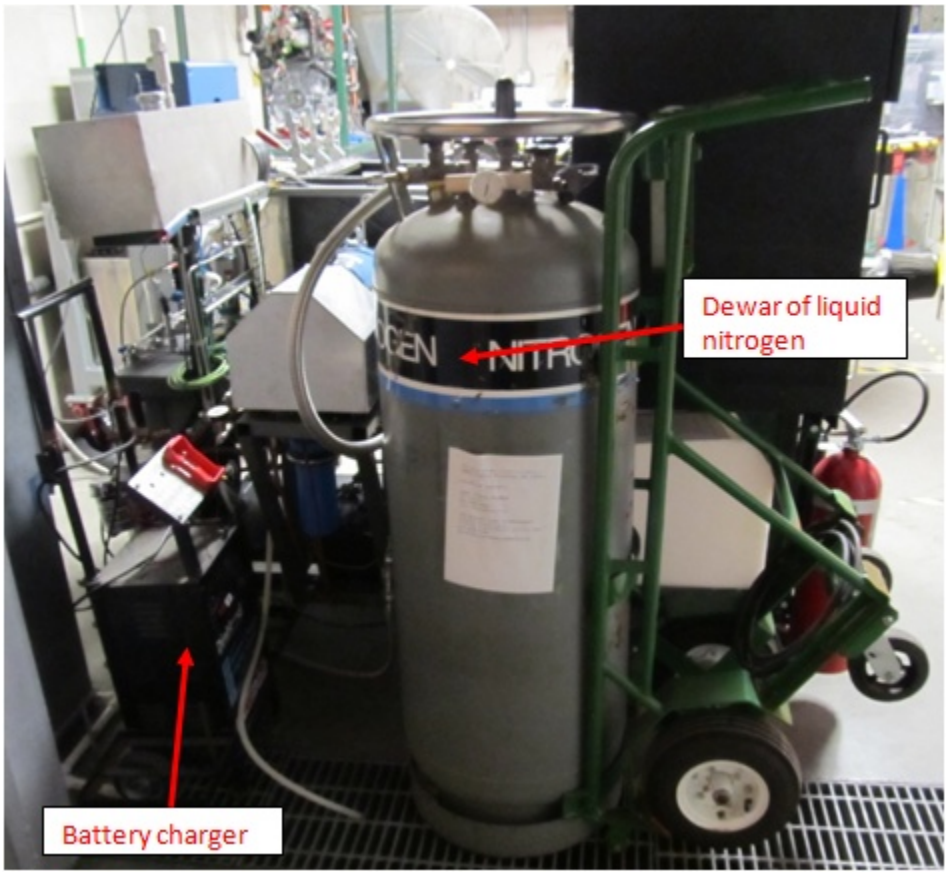

Figure 11. Dewar and battery charger

The 180 L Dewar shown with its hand truck in Figure 11 is filled with liquid nitrogen from a large pressure vessel located on WPAFB around 500 m from the test cell. The hand truck provides a human-powered transportation mechanism for the Dewar, which when full has mass in excess of 145 kg for the nitrogen alone.

The engine is started by a lawn tractor starter, itself powered by a 12-Volt automotive battery that is connected on a weekly basis to the charger shown in Figure 11. The starter drives the crankshaft by first engaging a gear at the end of the dynamometer, as shown in Figure 12.

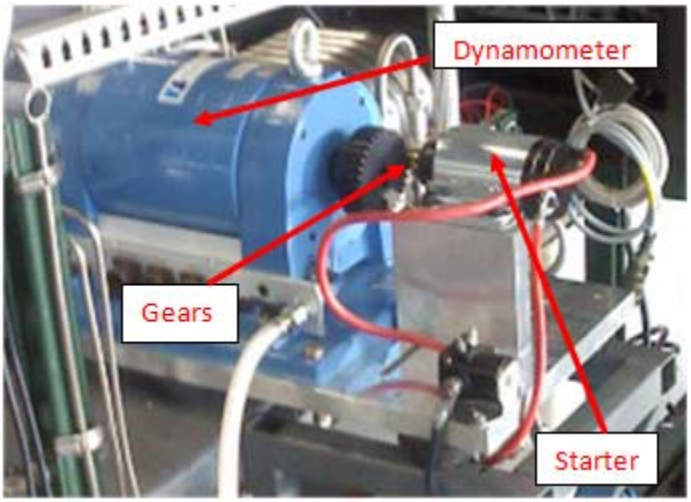

Figure 12. Dynamometer-starter interface

III.2 Fuel injection

Electronic fuel injection made it possible for the engine to operate at a wide range of simulated altitudes and to gather data regarding the effects of temperature across the range of air pressures consistent with altitudes up to 3 km. Crosbie [16] converted the fuel metering system of the Brison test engine from the stock carbureted configuration to a commercial-off-the-shelf throttle body injection (TBI) system from Ecotrons for more

precise control of the air-fuel ratio at the various operating conditions. The fuel injection kit included a 4.8 kg/hr fuel injector, fuel pump, engine computer, Pro-Cal tuning software, intake air temperature sensor, manifold absolute pressure (MAP) sensor, engine head temperature sensor, Bosch LSU4.9 oxygen sensor and CJ-125 driver chip, and 28 mm throttle body housing with attached throttle position sensor (TPS).

The fuel flow rate is a function of fuel pressure as well as the injector's opening characteristics and frequency. Because the Brison test engine is a single-cylinder two-stroke, there is one fuel injector pulse per engine revolution, and the frequency and pulsewidth are controlled by the engine control unit (ECU). The ECU also controls ignition timing. The fuel system includes a tank, filter, low pressure pump, flow meter, and a set of valves. The fuel flow meter is a Max Machinery model 213 piston flow meter with a model 294 transmitter.

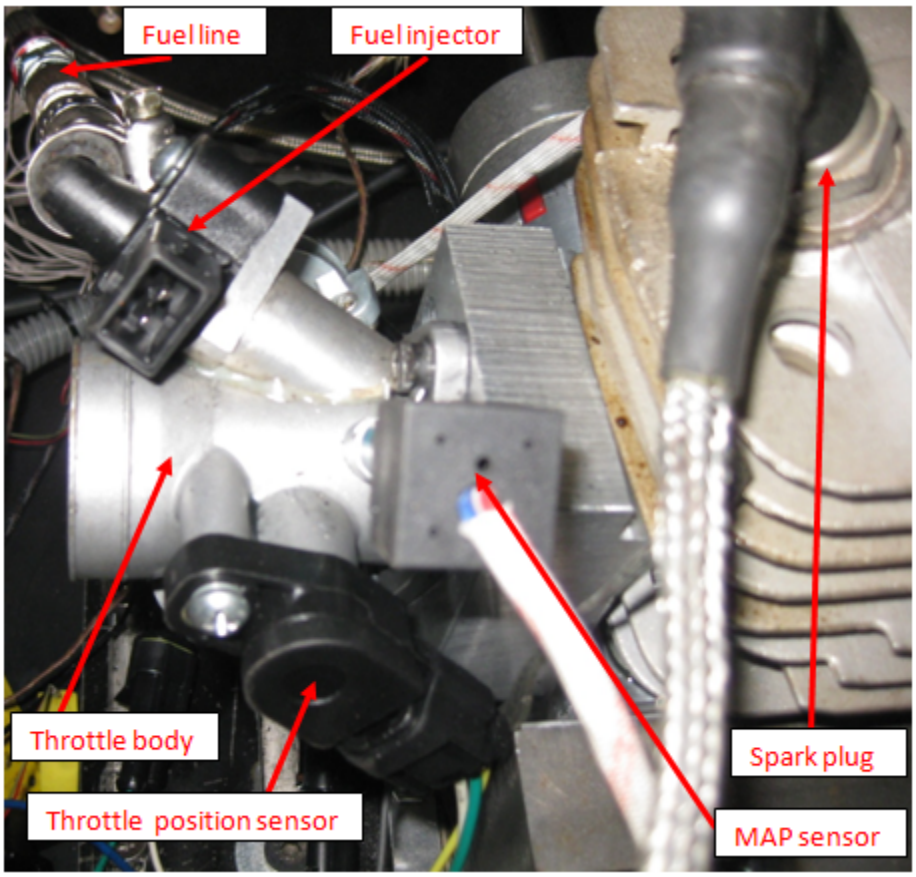

Figure 13. Throttle body and associated fuel injection parts

The ECU used a throttle position-based load table for this research, although it can also support a volumetric efficiency (VE)-based table common for four-stroke engines. The throttle position-based table, also known as a fuel map and commonly known in the fuel injection industry as "Alpha-N," features throttle angle (α) on one axis and engine rotational speed (N) on the other, whereas a "speed-density" map uses the MAP sensor to calculate air density for the fuel pulsewidth signals. A third approach is "mass air," in which a mass air flow (MAF) sensor is used to more directly measure the air flowing into the cylinder.

Single-cylinder engines have highly variable MAP, so Alpha-N systems are generally more suitable for engines such as the Brison 95 cm^3. In practice, some multi-cylinder vehicles use both approaches. In that case, the ECU uses the speed-density map for the significant vacuum at low RPM or throttle angles and switches to the Alpha-N map otherwise since it is particularly well-suited to operation with high throttle openings.

The ECU, as utilized, controls fuel flow based primarily on a 12 by 16 table of engine speeds and throttle positions, and a load value in each cell represents the fraction of the ideal air mass accommodated by the cylinder. Interpolation allows the ECU to choose a fuel injector pulsewidth for a combination of throttle position and speed not exactly corresponding to one of the 192 values in the map. The fuel flow is further tailored in open-loop according to intake air temperature (IAT) and engine head temperature. During closed-loop operation, the MAP sensor signal comes into play for the Alpha-N map, and the fuel injection system can use the oxygen sensor signal to correct for altitude as it adjust the pulsewidth to return the air-fuel ratio to that of the reference ambient pressure.

III.3 Temperature control

The objective of this research, studying the effects of temperature on the performance of a small IC engine at altitude, required introducing an operational temperature control capability to the test rig. The goals included supplying engine intake air at the desired combination of temperature and pressure to the engine. The air entering the chamber for cooling should be at the same temperature and pressure as the engine air.

The rig as delivered possessed the ability to control pressure between the limits of 57 kPa absolute and the approximately 99 kPa ambient air in the test cell, but temperature control was needed in order to simulate standard or "cold day" atmospheric conditions. Specifically, it was necessary to decrease the air temperature from around 295 K to as low as 237.7 K for the available range of altitudes. The nominal engine operating points, including air pressures and temperatures, for four altitude levels are shown in Table 5.

Table 5. Atmospheric operating points (from Mattingly et al. [26])

Point	Altitude	Pressure, kPa (std)	Temperature, K (std)	Temperature, K (cold day)
1	213 m*	98.8	286.8	223.7
2	1,524 m	84.3	278.2	247.1
3	3,048 m	69.7	268.3	246.8
4	4,572 m	57.2	258.4	237.7

*Elevation of the chamber running at standard conditions

The first step to enable temperature control was bolting the heat exchanger originally purchased for the altitude rig and shown in Figure 14 onto the stand and connecting steel lines from the exchanger to the engine inlet. Next, a 180 L liquid nitrogen Dewar and fittings, hoses, and connections suitable for cryogenic use were installed, as shown in Figure 15. Compressed shop air is delivered to the rig for operating a pneumatic safety valve in the fuel line and is also used to provide cooling air for one of the couplings joining the engine crankshaft to the dynamometer via intermediate shafts.

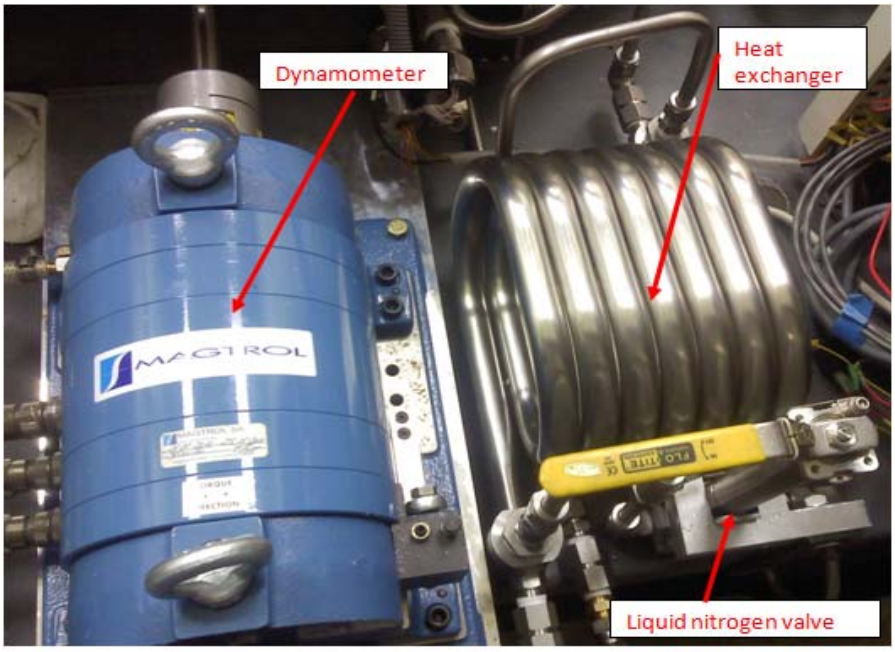

Figure 14. Heat exchanger

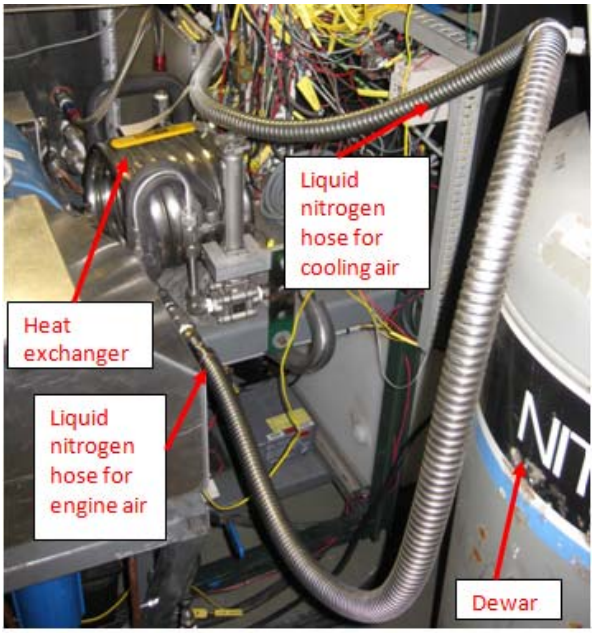

Figure 15. Both liquid nitrogen lines from Dewar

The original rig design was based on the premise of using the shop air as the source for the engine air used in combustion, while the air used for cooling the engine came from the ambient test cell air. However, because the rig came without a mechanism to decrease the shop air to sub-atmospheric pressure, the previous researcher used only one air stream, drawing the engine air from the cooling air stream and controlling the pressure through the use of an automotive supercharger. The engine air flow path had a goal maximum mass flow rate of 30 g/s.

Because the rated range of the Sierra mass flow meter that had been in the compressed air line is 0-500 standard liters per minute (SLPM), and at standard conditions air has a density of 1.2 g/L, the expected maximum mass flow rate through the meter was only 10 g/s. Therefore, the meter was viewed as a limiting component and removed from the air line. The theoretical choked flow rate (Anderson [27]) in Equation (13) is affected only by the upstream fluid conditions and with the assumed values yields a rate of 67 g/s, or more than twice the desired maximum.

$$\dot{m} = \frac{P_0 A^*}{\sqrt{T_0}} \sqrt{\frac{\gamma}{R}\left(\frac{2}{\gamma+1}\right)^{\frac{\gamma+1}{\gamma-1}}} \tag{13}$$

The engine air originates from a dry shop air supply and passes through a control valve. From that valve, the air is cooled by the seven-loop Exergy model 670 tube-in-tube counter-flow heat exchanger shown in Figure 16. The exchanger's working fluid, liquid nitrogen (LN_2), was chosen due to its low boiling point, inert qualities, abundance, availability, and relatively low cost.

Because the rig is capable of reaching a pressure altitude of 4.5 km, the lowest goal temperature was the cold day temperature at that altitude, which was 237.7 K (Mattingly et al. [26]). The rig's heat exchanger cannot handle the mass flow required for the compressor, which at 250 g/s is about an order of magnitude greater than the engine air mass flow rate. Additionally, the exchanger cannot remove enough heat to decrease the temperature of 250 g/s of air to 237.7 K.

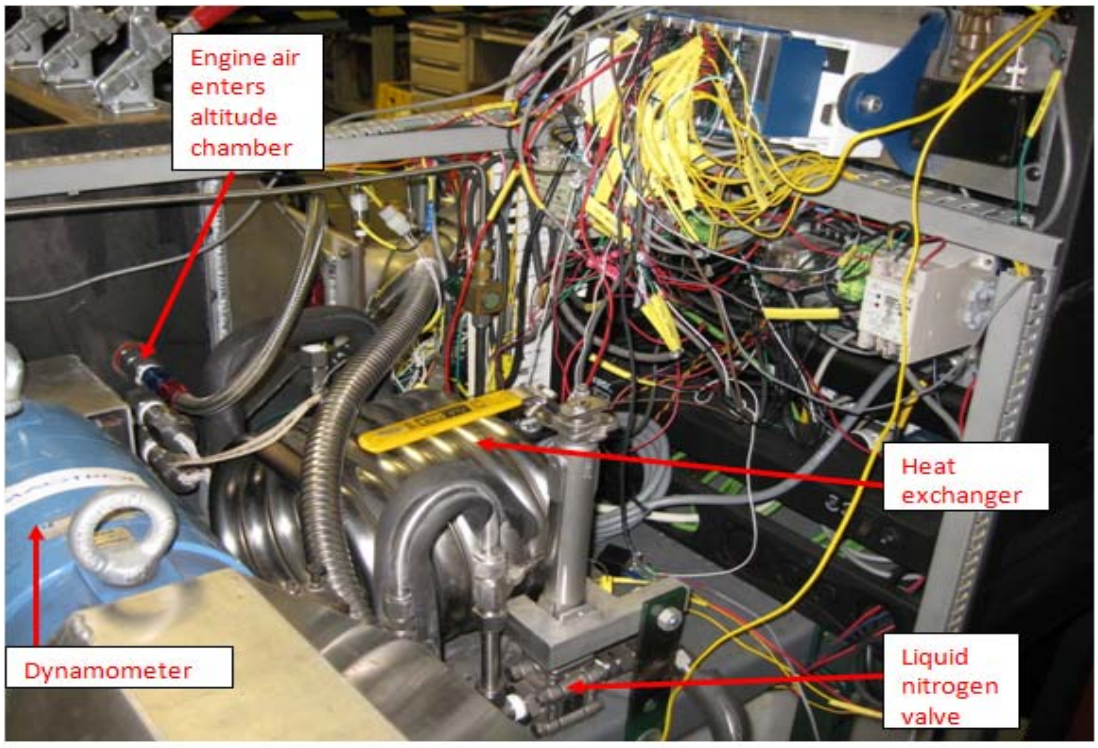

Figure 16. Engine inlet flow path heat exchanger installed on test stand

An attempt was made to use the heat exchanger to chill both air streams by simply allowing the engine air stream to mix with the cooling air and then using that mixed air for combustion. However, even with the 10 g/s engine air flow at 127 K, the air entering the throttle body dropped only from 304 to 296 K. Therefore, the decision was made to separate the air for the engine from the cooling air, and the engine air would be chilled by

liquid nitrogen (LN_2) in the heat exchanger, while cooling air would be chilled by direct injection of LN_2 (see Figure 17).

With two air streams, it would be possible to preserve the proportions of oxygen and nitrogen in the engine air while allowing the cooling air to be diluted with nitrogen. Although such a configuration has the disadvantage of requiring the pressures and temperatures of the two air streams to be matched, it does enable the greatest possible effectiveness of the heat exchange between the cooling air and nitrogen. Thus, fewer refills of the Dewar are required for a given amount of testing when compared to operating with a single chilled air stream with standard nitrogen content.

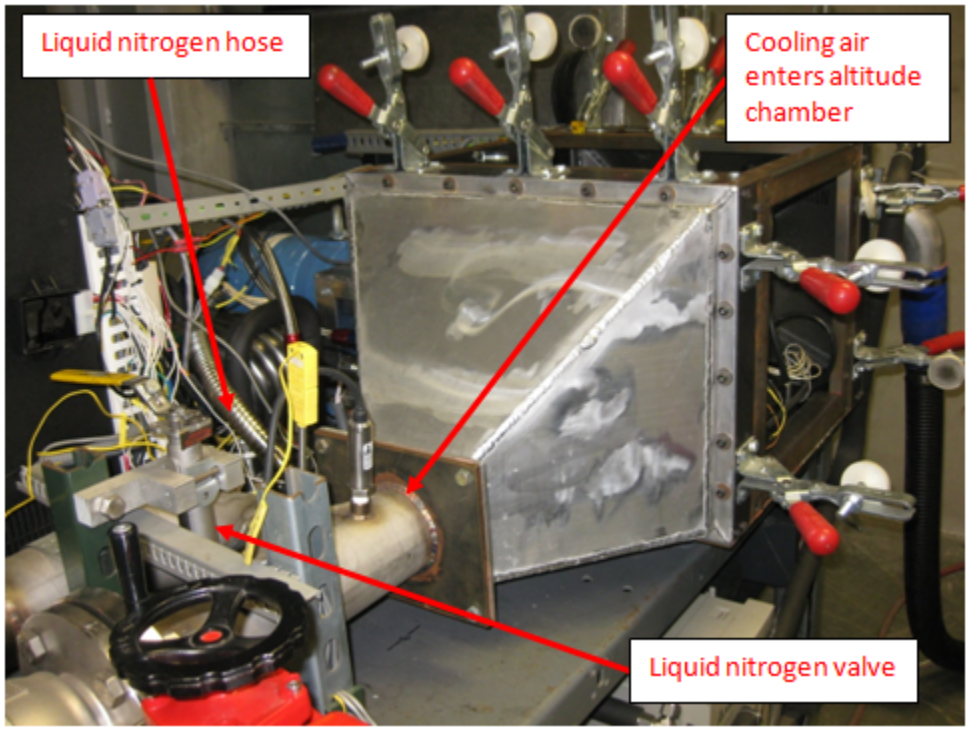

Figure 17. Direct injection of liquid nitrogen

As mentioned above, temperature control experiments showed the Exergy heat exchanger is incapable of producing the necessary ΔT for the full chamber's air stream,

although it is able to cool the air for combustion to the desired temperature. An attempt was also made to run the engine with direct mixing of LN_2 with the engine air, using the single air stream for both engine and cooling air. Due to the deleterious effect of excess nitrogen on the combustion process, drawing the engine air from the chamber and directly injecting LN_2 into the full air stream only dropped the temperature from 298 K to 280 K, even when the engine was running near its limits for N_2 concentration.

III.4 Diffuser for engine inlet

In order to accomplish the objective of studying temperature effects on the performance of a small engine at altitude, it was necessary to supply air to the engine at the desired temperature, pressure, and oxygen concentration. Beyond the discussion here in Chapter III, the diffuser design is further explained in Appendix B.4. Innovative Scientific Solutions, Inc., (ISSI) and Air Force Research Laboratory (AFRL) researchers suggested using a "free jet" approach in which the engine air stream was decoupled from the throttle body. The free jet began as a single stream of air and flowed either into the throttle body or the surrounding chamber air. The expectation was that the low-velocity free jet would expand to the appropriate pressure in the chamber.

In the chosen free jet configuration, the engine air pressure equalized with that of the cooling air in the chamber as the jet expanded in a cylindrical diffuser before entering the throttle body. The chamber air, having been chilled by the direct injection of liquid nitrogen to simulate a standard temperature at altitude, contained more nitrogen on a mass basis than is found in the atmosphere. The free jet was needed because the chamber air was not suitable for simulating the atmosphere in the combustion chamber. The free

jet approach was justified on the grounds that by flowing two to four times as much air as the engine actually needed for combustion, the engine air would remain uncontaminated by the extra nitrogen found in the cooling air. The temperatures of the two air streams were matched, and the engine air dewpoint was 233 K, but humidity was not controlled.

To limit the engine air to Mach 0.05 before it entered the throttle body, the flow diameter increased from 0.9 cm in a bulkhead fitting at the wall of the chamber to 2.5 cm in a hose looped around the diffuser and connected to the side of a cylindrical plenum, entering the plenum at a right angle to throttle body. Next, the air expanded in a 7.6 cm inner diameter chamber and passed through a 60% solid perforated plate, causing flow distribution, prior to meeting the plane of the throttle body. The engine air either enters the throttle body or freely flows into the cooling air, as shown in Figure 18. With a physical interface between the two air paths, it was necessary to avoid flow separation or a recirculation zone to prevent early mixing of the engine air with cooling air.

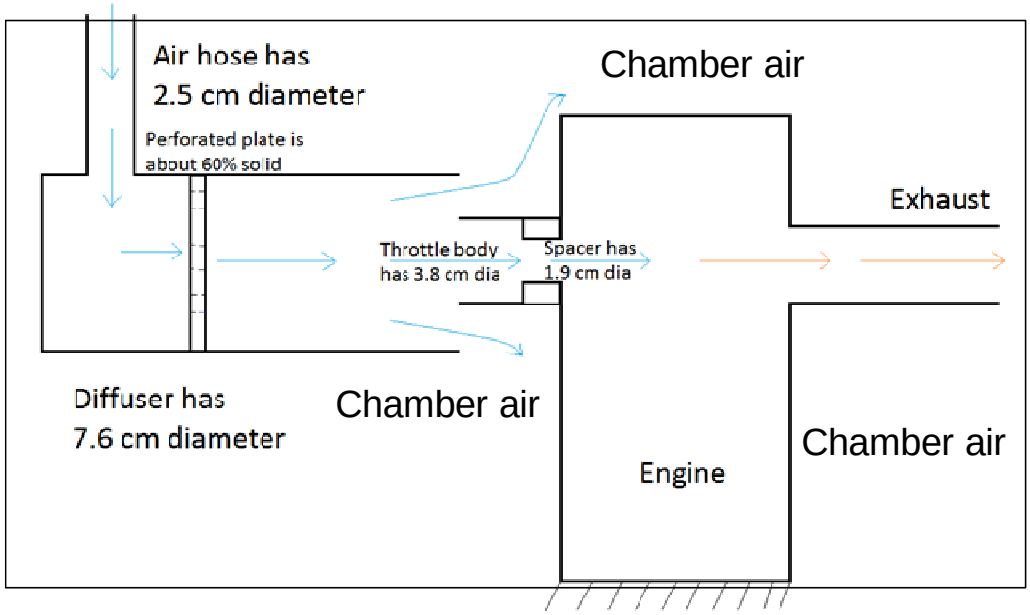

Figure 18. Diffuser air flow

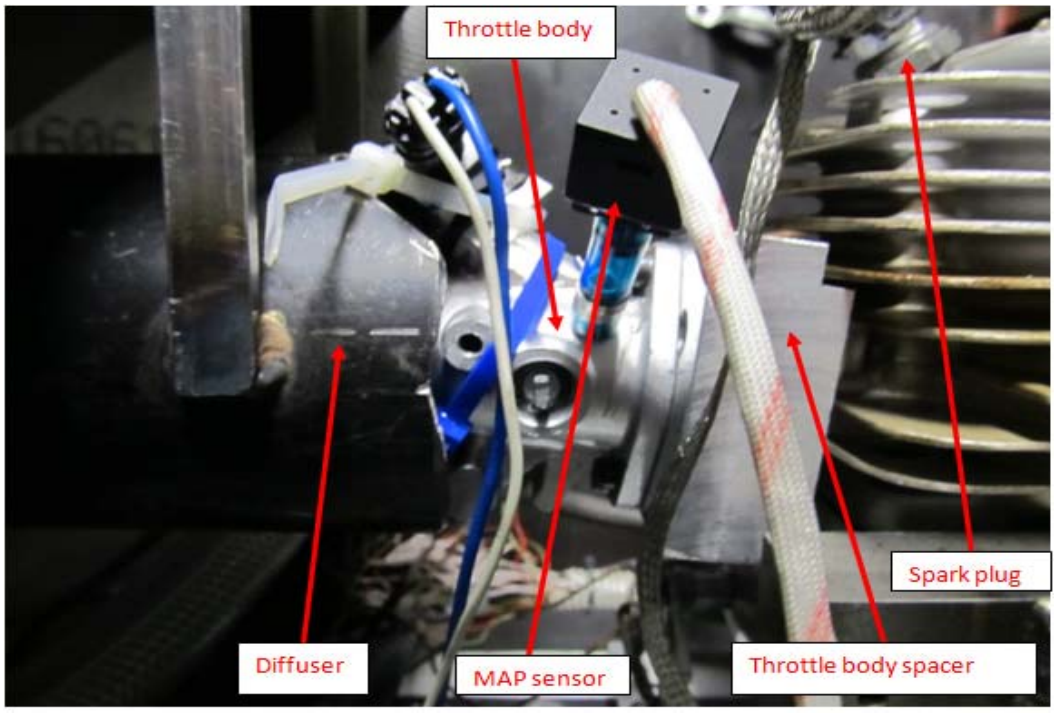

Figure 19. Diffuser, throttle body, and fuel injector

Based on the expected mass air flow, estimated flow area through the chamber, and the air density calculated from the ideal gas law with pressure and temperature in the chamber at their lowest expected values, the bulk air velocity derived from Equation (2) over the engine is approximated at 2.8 m/s. The intake air velocity at the throttle body entrance is similarly calculated at 5 m/s, or about Mach 0.02, from a mass flow rate around twice that of the peak engine demand.

The gas constant R was assumed to be 287 J/(kg*K) for this research. However, R varies from gas to gas, and the concentration of water vapor in the atmosphere varies. Therefore, R will not be absolutely constant, and its variability will have a small effect on air density for an operational RPA.

Table 6 shows the calculated mean velocity and Mach number for the engine air stream based on an assumed 30 g/s mass flow rate and standard density of 1.2 kg/m^3 with local speed of sound at 340 m/s.

The gas constant *R* was assumed to be 287 J/(kg*K) for this research. However, *R* varies from gas to gas, and the concentration of water vapor in the atmosphere varies. Therefore, *R* will not be absolutely constant, and its variability will have a small effect on air density for an operational RPA.

Table 6. Engine air flow

Section	**Area, cm^2**	**Velocity, m/s**	**Mach**
Bulkhead	0.4	197	0.58
Chamber hose	1.6	49	0.15
Diffuser inlet	1.3	61	0.18
Diffuser plenum	14.5	5	0.02
Perforated plate	5.8	14	0.04
Diffuser exit	14.5	5	0.02

A more detailed discussion of the diffuser design can be found in Appendix B.4. Appendix B.4 provides information on the initial attempts to implement a diffuser as well as providing more details of the configuration issues. Lastly, more photographs of the diffuser components are shown.

IV. Analysis and Results

Setting the stage for analyzing the experimental results to discern the effects of temperature on the Brison 2-stroke test engine's performance, the effects of pressure are isolated from those of temperature and examined as simulated altitude varies in the first portion of this section. Pressure effects were studied prior to introducing temperature control and provided a set of baseline performance curves in place of those collected by Crosbie [16]. With new baseline 295 K data at the 1.5 and 3 km pressure altitudes in addition to the local 0.2 km altitude, it was possible to investigate temperature effects at altitude on a small 2-stroke IC engine.

After pressure effects were known, temperature was varied at two pressure altitudes to study how colder air affects the engine when pressure is held approximately constant. The test engine in its current configuration has somewhat different designs for the intake and exhaust systems from those used in Crosbie's research , and it was important to compare identical versions of the engine for quantifying pressure effects. Then, temperature and pressure effects were combined, and the performance measures of power, BMEP, and BSFC were compared and contrasted at three near-standard atmospheric altitude conditions.

In all cases, the data were collected at constant WOT, as the throttle valve was held in its fully open position with a physical retainer to prevent the throttle return spring from forcing the valve toward its idle or closed position. Although the intent of the pressure and temperature control measures was to hold each of these two parameters at a constant value for a given test condition, the collected data indicate both parameters

varied from the setpoint by as much as a few percent. Two causes include random variation in settings and the heat transfer effect.

Although the systems of the altitude rig were designed with care to avoid contaminating the purity of the air used for combustion, it is conceivable some of the exhaust gases and nitrogen used for chilling the cooling air stream could have mixed with the engine air before it entered the throttle body. No measurements of the chemical contents of the engine air were made. Mixing of either exhaust or nitrogen with the engine air would be detrimental to engine performance because the proportion of oxygen in the air would decrease.

The control systems utilized were sufficient for holding a temperature or pressure setpoint to a precision within plus or minus a few percent. As configured, the dynamometer held the engine at a measured speed to within a few RPM of the maximum speed setpoint, except at the lowest and highest tested speeds where cylinder filling was poor. The mean recorded speed for a point across the speed range for a given power curve was below the setpoint by as much as 5%, with a standard deviation of 2 or 3%. The humidity of the air was not controlled on board the rig, but the shop air source provided dry compressed air with a dewpoint of 233 K. The effects of humidity were not accounted for in analyzing the data.

Based on uncertainty analysis (Kline and McClintock [28]) of three iterations of the power curve for a single low-altitude test condition, the uncertainty at a 95% confidence level is around 0.5 kW, and this translates to about a 10% uncertainty (Moffat [29]) in every value on each power curve. The Root-Sum-Square equation (Moffat [30]) yields uncertainty:

$$\delta R = \left\{ \left(\frac{\partial R}{\partial x_i} \delta x_i \right)^2 + \left(\frac{\partial R}{\partial x_2} \delta x_2 \right)^2 \ldots \left(\frac{\partial R}{\partial x_N} \delta x_N \right)^2 \right\}^{1/2} \quad (14)$$

where R is the result, x_i is the input data, and δx_i is the estimated uncertainty interval.

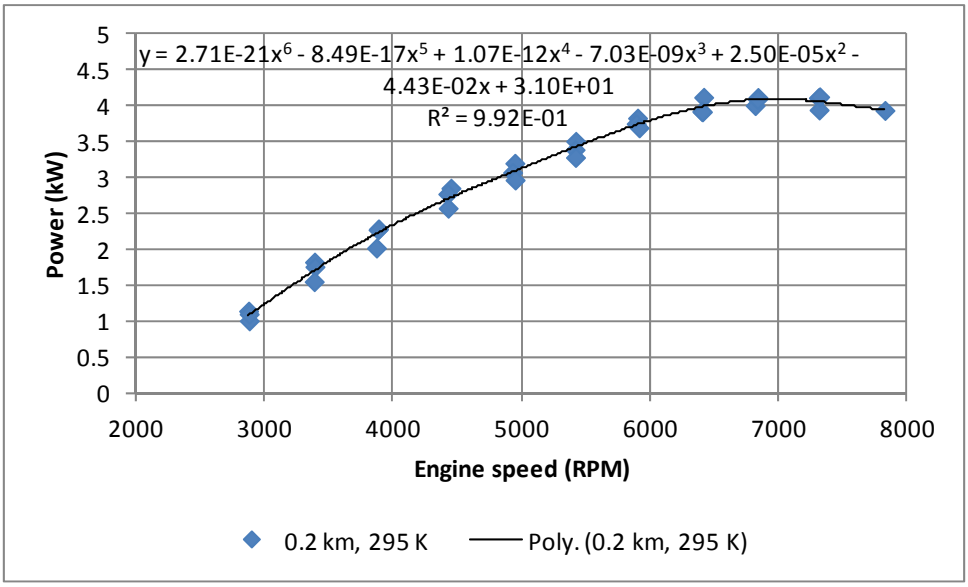

Figure 20. Uncertainty trendline for power data from low altitude

For the uncertainty analysis, the trendline for a sixth-order polynomial shown in Figure 20 was fit to the collective data from 3 iterations at 0.2 km and 295 K, and an expected value for the data point was calculated. The observed power was subtracted from the curvefit expected value, and double the square root of the sum of the squared differences for each data set provided the uncertainty value. At the 95% confidence level, the calculated uncertainty is 0.6 kW for the first data set, 0.4 kW for the second, and 0.7 kW for the third. Compared to a maximum observed power value of 4.1 kW, the 0.7 kW uncertainty translates to +/- 17%. Crosbie et. al [16] reported uncertainty values for the experimental test set-up of 0.7% for power, BMEP, and BSFC, 9% for temperature, and 1% for pressure.

The performance curves reported from this experiment are for single-sample data. The preferred approach would be to sample each parameter multiple times at every test condition and average the data. Multiple-sample curves likely would be smoother and more representative of the true quantities being measured by averaging out some of the uncertainty. Multiple samples would also provide insight into the repeatability of the measurements.

IV.1 Pressure effects

Figure 21 depicts the variation of brake power at a constant temperature as the pressure is altered. Looking strictly at the peak power for each curve, the observed correction factors were 79%, 61%, and 55% for the 1.5, 3, and 4.5 km altitudes, as shown in Table 7. Peak power occurred at the 6,500 RPM setpoint for 0.2 km, at 7,500 RPM for 1.5 km, at 7,000 RPM for 3 km, and at 8,000 RPM for the 4.5 km pressure altitude.

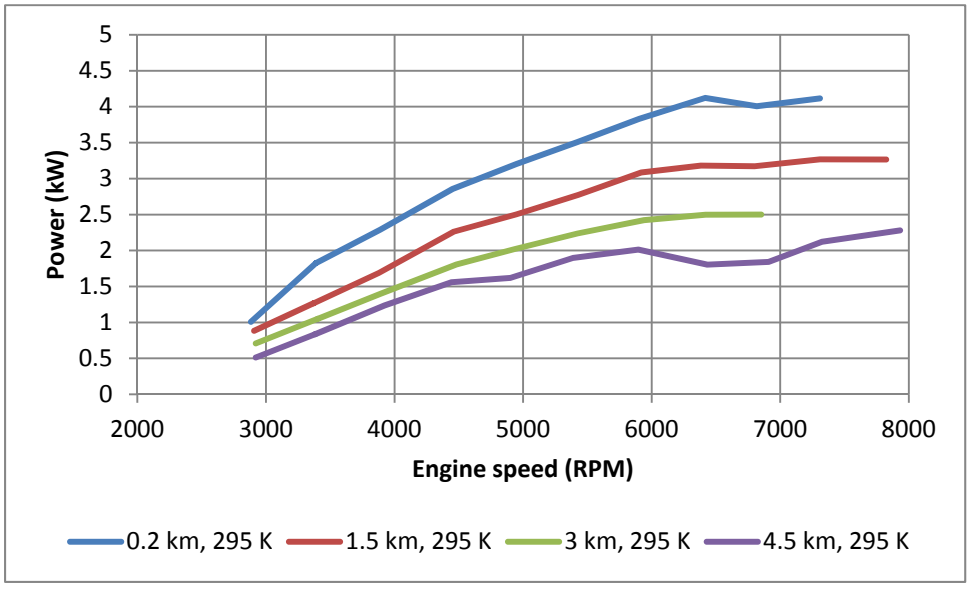

Figure 21. Power curves for pressure sweep at constant temperature

Table 7. Pressure effects on power

Pressure altitude, km	Power multiplier, expected (2-stroke at low speed; 4-stroke)	Power multiplier, observed (3,000 RPM)	Power multiplier, expected (2-stroke at high speed)	Power multiplier, observed (peak)	Pressure ratio exponent, observed (peak)
1.5	0.85	0.88	0.73	0.79	1.5
3	0.71	0.70	0.51	0.61	1.5
4.5	0.58	0.51	0.33	0.55	1.1

Air pressure P changes at constant temperature T are expected to have a proportional effect on density ρ due to the ideal gas law, as discussed in Section II.3.3

$$\rho = \frac{P}{RT} \tag{15}$$

because the gas constant R is assumed to be constant, and power and BMEP tend to follow ρ for a fixed AFR. The Brison test engine's cylinder and ports have constant geometry, so power and BMEP rise with increasing density at a constant speed, combustion efficiency, and AFR because the masses of both air and fuel per cycle increase. Increasing altitude is associated with decreasing air pressure and density, so IC engine-powered aircraft lose power and BMEP as they fly at higher altitudes.

Neglecting the effects of humidity, the literature for 4-stroke engines suggests power will vary in direct proportion to the ratio of atmospheric pressure to the reference pressure, typically taken to be the standard sea level value of 101.325 kPa. Adapting Taylor's Equation (8), the ratio of power $\dot{W}$ to the reference power $\dot{W}_{ref}$ [3] is

$$\frac{\dot{W}}{\dot{W}_{ref}} = \frac{BMEP}{BMEP_{ref}} = \frac{P}{P_{ref}}\sqrt{\frac{T_{ref}}{T}} \tag{16}$$

where the P is the air pressure, T is the air temperature, and the subscript *ref* means reference. For the standard atmosphere, T_{ref} is 288 K at sea level (Mattingly et al. [26]).

With the pressure around 98.5 kPa at the baseline test altitude, the 1.5 km power curve would then be expected to have 85% of the 0.2 km baseline value at each point. The 3 km curve multiplier would be about 70%, and the 4.5 km factor would be somewhat less than 60%. Adapting the Equation (11) relation from Harari and Sher [11] for 2-stroke engines with the assumption that humidity effects are negligible, the pressure ratio should be taken to a power x ranging from 1 at low engine speed to 2 at high speed

$$\frac{\dot{W}}{\dot{W}_{ref}} = \frac{BMEP}{BMEP_{ref}} = \left(\frac{P}{P_{ref}}\right)^{x}\left(\frac{T_{ref}}{T}\right)^{0.8} \tag{17}$$

Solving for the exponent of the three pressure ratios, the 1.5 and 3 km altitudes have an exponent of 1.5, but the exponent is 1.1 for the 4.5 km altitude. Thus, all three elevated altitude curves have a peak power pressure ratio exponent between 1 and 2, and the 4.5 km peak power exponent was approximately equal to the 9/8 reported as the 2-stroke pressure ratio exponent by Harari and Sher from their earlier research. At high speed and rounding to simple fractions, the expected multipliers of the baseline for the three higher altitude curves equate to 3/4, 1/2, and 1/3.

Figure 22 shows the BMEP curves for a pressure sweep at constant temperature. The test engine produced nearly constant BMEP of around 400 kPa between the nominal 4,500 and 6,500 RPM speeds at the baseline altitude and fell off in either direction from that range. As related in Equations (16) and (17), because BMEP at a given speed varies

in the same proportions as brake power, the same expected multipliers mentioned in the previous paragraph and shown in Table 7 also apply to the BMEP curves. For these data and as shown in Table 7, the exponents of the 1.5, 3, and 4.5 km pressure ratios are 1.4, 1.3, and 1.1.

Pressure ratio exponents greater than unity for the Brison test engine are qualitatively consistent with the literature and indicated that 2-stroke engines suffer greater losses in performance at altitude than do 4-stroke engines. The BMEP multiplier at peak matches the expected value fairly well, as the pressure ratio exponent falls for each curve between 1 and 2. Peak BMEP occurred at the 6,000 RPM setpoint for the 0.2 and 1.5 km curves, and at 5,500 RPM for the 3 and 4.5 km pressure altitudes.

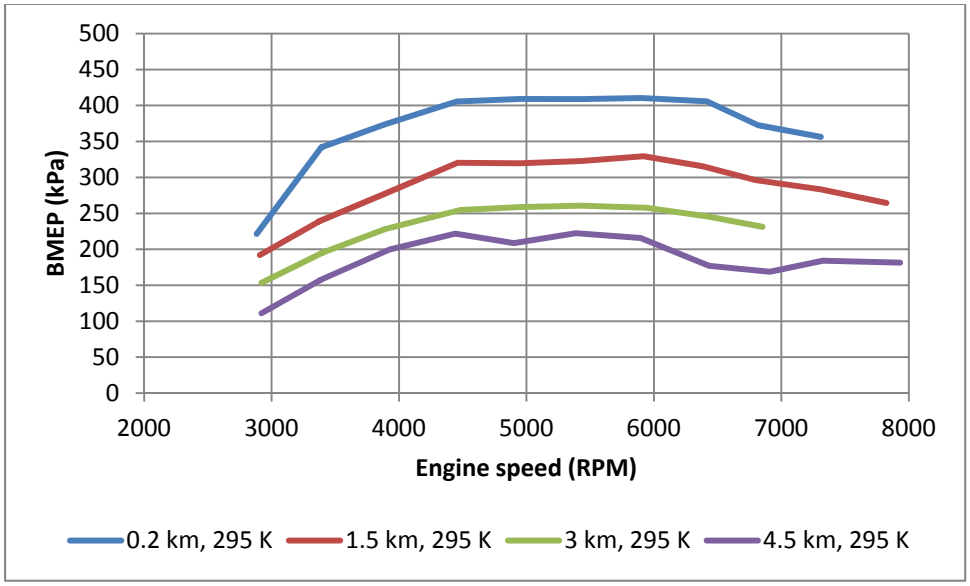

Figure 22. BMEP curves for pressure sweep at constant temperature

Table 8. Pressure effects on BMEP

Pressure altitude, km	BMEP multiplier, expected (2-stroke at low speed; 4-stroke)	BMEP multiplier, observed (3,000 RPM)	BMEP multiplier, expected (2-stroke at high speed)	BMEP multiplier, observed (peak)	Pressure ratio exponent, observed
1.5	0.85	0.87	0.73	0.80	1.4
3	0.71	0.69	0.51	0.63	1.3
4.5	0.58	0.50	0.33	0.54	1.1

The BSFC curves for a pressure sweep at constant temperature in Figure 23 demonstrate very similar BSFC performance at the 1.5 and 3 km pressures, but the 4.5 km data are much more widely distributed. In aggregate the baseline 0.2 km curve shows the most desirable performance of this group, with the BSFC falling below 750 g/kWh over most of the measured speed range. Crosbie concluded the BSFC was consistent for the fuel-injected Brison test engine between 610 and 730 g/(kWh) at the sea level standard temperature of 288 K across the range of 3,000 to 7,000 RPM, even at pressure altitudes up to 3 km. However, the performance of the engine in the current configuration never matched the characteristics observed by Crosbie [16].

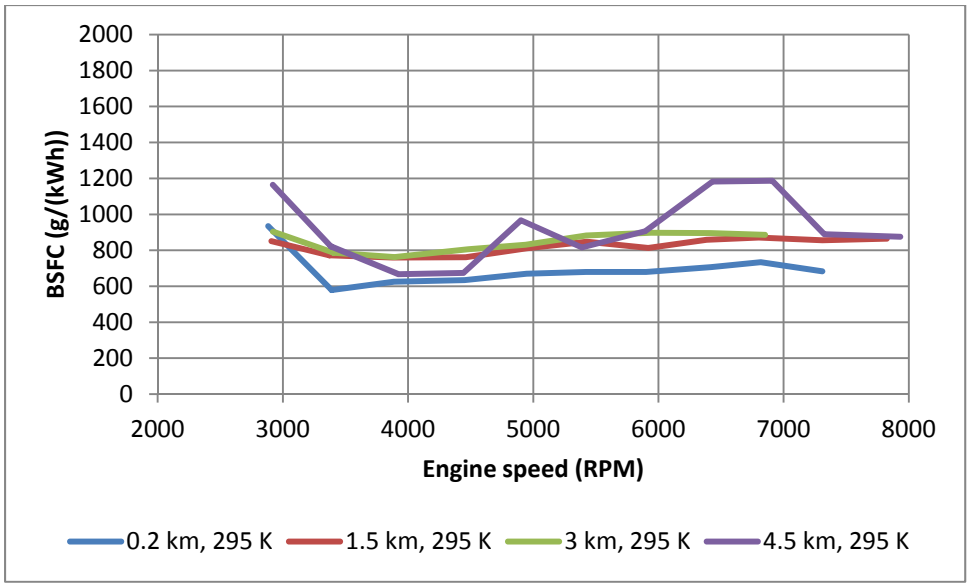

Figure 23. BSFC curves for pressure sweep at constant temperature

For low-speed general aviation aircraft, BSFC is assumed to be constant both with altitude and airplane velocity V_∞. However, general aviation engines are typically of the multi-cylinder 4-stroke SI variety and have at least an order of magnitude greater displacement and power than the Brison 95 cc. With the high surface area-to-volume ratio of the test engine and its scavenging losses at altitude, increasing BSFC with altitude is not a surprising observation.

Thermal efficiency is assumed to be simply the inverse of the product of BSFC and a lower heating value of 43.5 MJ/kg for aviation gasoline in Figure 24, and the shapes of the curves reflect this fact. As such, the baseline 0.2 km curve shows the highest efficiency with a peak value of 14%, while the middle altitudes have data clustered around on either side of 10% and the 4.5 km pressure has the greatest variability in efficiency. It must be noted that a great majority of the fuel supplied to small 2-stroke

engines such as the Brison 95 cc is wasted, and the fuel conversion efficiency is much lower than can be found in larger and heavier engines.

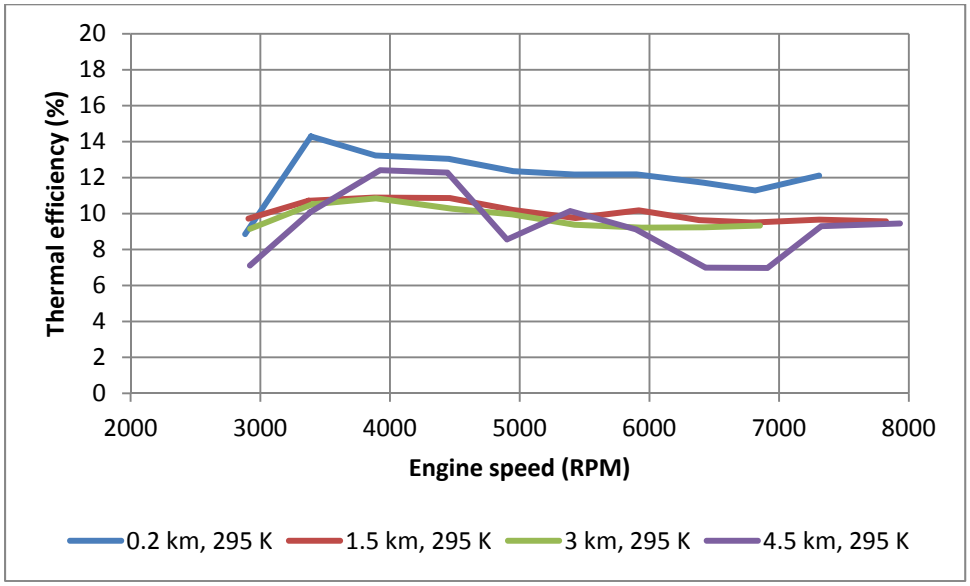

Figure 24. Thermal efficiency curves for pressure sweep at constant temperature

Crosbie [16] conducted a study of AFR effects on the Brison test engine at a constant speed of 4,000 RPM and a steady chamber condition of 98.5 kPa and 288 K. The measured AFR came not from the mass flow rates of air and fuel but rather from the Bosch LSU4.9 wide-band lambda (λ) oxygen sensor wide band. Equation 15 defines lambda as the actual air-to-fuel ratio divided by the stoichiometric air-to-fuel ratio. The BMEP and BSFC data from the AFR study are shown in Figure 25 and Figure 26.

The data indicate BMEP is maximized at an AFR of 15.5, although a local maximum occurs at an AFR of between 11.6 and 12.1, the latter value corresponding well with expected best-BMEP AFR of 12.2 cited by Blair [2]. Figure 25 indicates the BMEP was within plus or minus 3% of 400 kPa in the AFR range of 10.8 to 14.5, although Figure 26 shows a nearly linear improvement in BSFC over the same AFR

range as the mixture moves closer to the stoichiometric 14.7 AFR for gasoline. The 15.5 AFR is lean of stoichiometric and corresponds more with the best-BSFC AFR of 15.1 also suggested by Blair [2]. Crosbie observed a best BSFC of 515 g/(kWh) for his AFR study at the leanest tested AFR of 16.9, although the BSFC was relatively constant at or lean of the approximately stoichiometric 14.5 AFR test case[16].

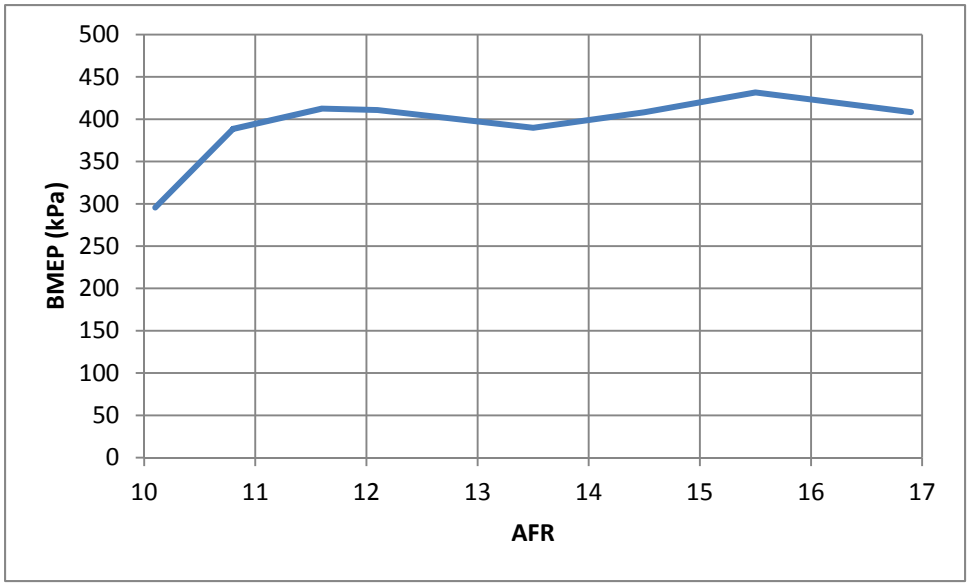

Figure 25. BMEP at a constant condition with varied AFR (from Crosbie [16])

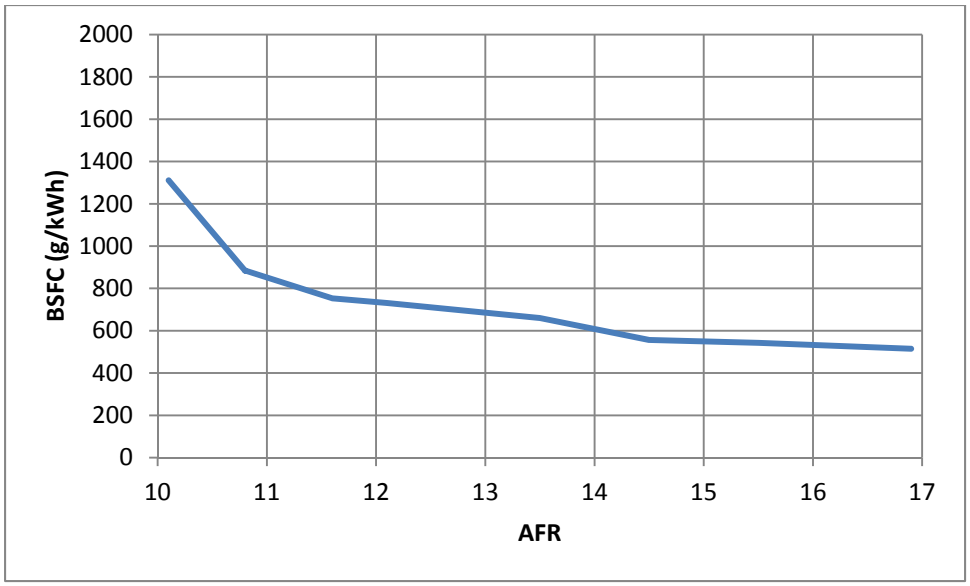

Figure 26. BSFC at a constant condition with varied AFR (from Crosbie [16])

Using the same model of Bosch LSU4.9 oxygen sensor utilized by Crosbie [16], the measured air-fuel ratio (AFR) over the tested speed range for the four altitudes are displayed in Figure 27, and the desired AFR at each point was between 13 and 14 to provide a combination of high power and adequate cylinder cooling. As mentioned in Chapter III, problems with sensors and wiring contributed to difficulty in maintaining the desired AFR, and the fuel delivery system only held the AFR in the constant desired range during some of the test cases. The AFR for the 4.5 km curve is the most variable of the four, falling below 13 at points and peaking at 15.

The points on the 4.5 km AFR curve with values below 13 correlate to the local minima on the thermal efficiency curve and local maxima for the BSFC curve associated with that pressure, suggesting that an AFR below 13 is prejudicial to fuel conversion efficiency. Furthermore, the lowest measured 4.5 km AFR values occurred at the 5,000, 6,500, and 7,000 RPM setpoints and correlated with the outlier values of low

performance seen in Figure 21 through Figure 24. The data appear to show that richer operation led to degraded engine performance at the 4.5 km pressure altitude.

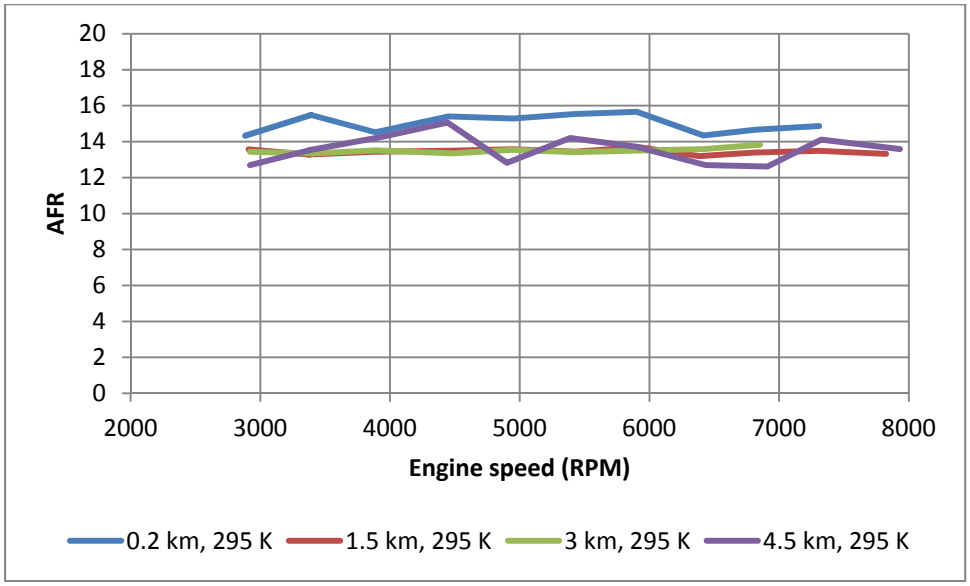

Figure 27. AFR curves for pressure sweep at constant temperature

For example , Figure 28 illustrates how the earlier baseline curve for 0.2 km and 295 K had AFR ranging from a low of 14.3 to a high of 15.7, whereas the later iterations were more consistent and fell largely in the AFR range of 13 to 14. The fuel injection system kept the AFR in that desired range for the middle altitudes, but the baseline 0.2 km curve has each AFR above 14. The trend of increasing BSFC as AFR falls numerically from a value of 14.5 is noticeable in the data from Crosbie [16]. As may be expected, since the AFR at the nominal 4,000 and 4,500 RPM setpoints for the 4.5 km curve is within a few percent of the approximate stoichiometric value of 14.7 and BMEP is also near the maximum, the BSFC and thermal efficiency for that pressure are at their observed best.

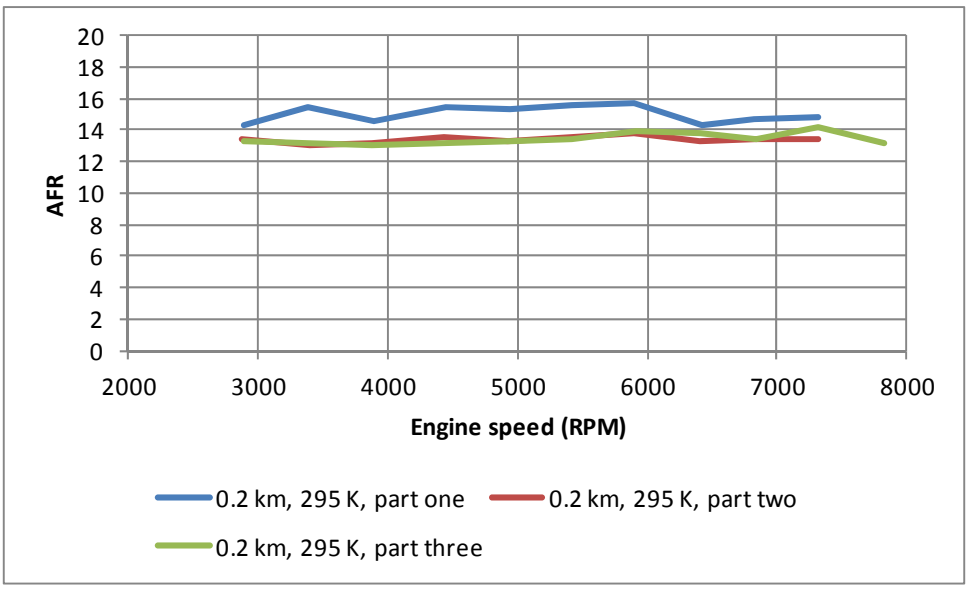

Figure 28. AFR curves for three iterations at 0.2 km and 295 K

IV.2 Temperature effects

Having captured the effects of pressure on the Brison's performance, attention is now turned to the effects of temperature at constant pressure. Comparing the standard pressure and temperature of 84 kPa and 278 K for the 1.5 km altitude with the values of 98.5 kPa and 295 K, the pressure at 1.5 km is only about 85% of the baseline, while the temperature at that pressure altitude is 94% of the baseline's value. This reveals that the pressure has a bigger effect than the temperature change as the altitude increases. However, from the ideal gas law, it is recognized that the impact of altitude on the gas density has an inverse effect.

Beyond the smaller relative change in temperature as an aircraft climbs through the standard atmosphere, the larger relative pressure change is compounded by a larger theoretical exponent, as seen in the modified forms of equations (7) and (11) reconstructed here for four-stroke engines (Heywood and Sher [8]),

$$\frac{\dot{W}}{\dot{W}_{ref}} = \frac{BMEP}{BMEP_{ref}} = \left(\frac{P}{P_{ref}}\right)^{1}\left(\frac{T_{ref}}{T}\right)^{0.5}$$

for two-stroke engines at low speed [11],

$$\frac{\dot{W}}{\dot{W}_{ref}} = \frac{BMEP}{BMEP_{ref}} = \left(\frac{P}{P_{ref}}\right)^{1}\left(\frac{T_{ref}}{T}\right)^{0.8}$$

and for two-stroke engines at high speed [11],

$$\frac{\dot{W}}{\dot{W}_{ref}} = \frac{BMEP}{BMEP_{ref}} = \left(\frac{P}{P_{ref}}\right)^{2}\left(\frac{T_{ref}}{T}\right)^{0.8}$$

Even when comparing ratios of the same magnitude, theory indicates pressure changes have a greater relative effect on power and BMEP than do temperature changes.

Figure 29 shows the variation in brake power vs. engine speed for three different temperatures. The observed power ratios range from 103 to 109% for the 278 K curve, with a mean of 106%, while the range is from 102 to 112% for the 268 K curve, with a mean of 107%.

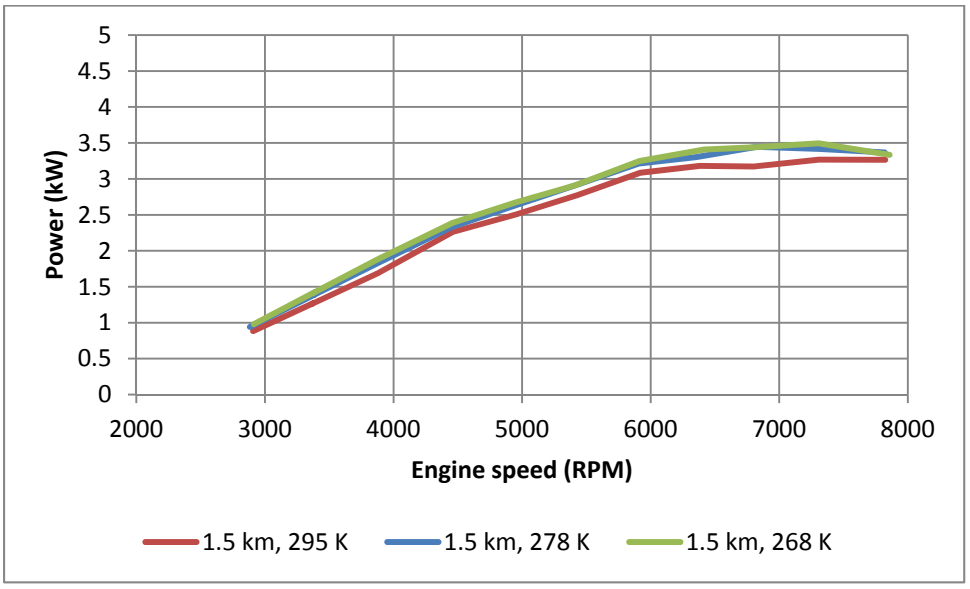

Figure 29. Power curves for temperature sweep at altitude of 1.5 km

Returning to Equation (16), the literature for 4-stroke engines suggests power will vary in proportion to the square root of the ratio of the reference temperature, typically taken to be the standard sea level value of 288 K, to the test temperature.

$$\frac{\dot{W}}{\dot{W}_{ref}} = \frac{BMEP}{BMEP_{ref}} = \frac{P}{P_{ref}}\sqrt{\frac{T_{ref}}{T}}$$

With a nominal temperature of 295 K at the baseline test condition used as the reference here and a constant pressure of 84 kPa at an altitude of 1.5 km, the power curves for 278 and 268 K would then be expected to have values of around 103 and 105% of the 295 K baseline at each point. Harari and Sher found that for 2-stroke engines [11], the temperature ratio should be taken to a power of 0.8, with Equation (17) repeated here:

$$\frac{\dot{W}}{\dot{W}_{ref}} = \frac{BMEP}{BMEP_{ref}} = \left(\frac{P}{P_{ref}}\right)^{x}\left(\frac{T_{ref}}{T}\right)^{0.8}$$

Consequently, temperature is expected to have a greater relative effect on 2-stroke engines than on their 4-stroke counterparts. Using an exponent of 0.8, the power curves for 278 and 268 K would then be expected to have values of around 105 and 108% of the 295 K baseline at each point.

Table 9. Temperature effects on power at 1.5 km

Temperature, K	**Power multiplier, expected (4-stroke)**	**Power multiplier, expected (2-stroke)**	**Power multiplier, observed (mean)**	**Temperature ratio exponent, observed**
278	1.03	1.05	1.06	0.7
268	1.05	1.08	1.07	0.9

For temperatures at or above 268 K, it does not appear from the data that the test engine, having 95 cc per cylinder, has appreciably different performance characteristics with varied temperature than those of the engine studied by Harari and Sher, with 175 cc per cylinder [11]. The surface area-to-volume ratio for each cylinder of these two engines does not appear to have led to a heat transfer rate difference great enough to substantially change the Brison engine's performance with decreased temperature on a relative basis to that of the larger engine.

The effect of temperature on BMEP at a pressure altitude of 1.5 km is shown in Figure 30. As with the power curves, assuming an exponent of 0.8 for the temperature ratio, the BMEP curves at 278 and 268 K are expected to have values of around 105 and 108%, respectively, of the 295 K baseline at each point. And again, the observed BMEP ratios range from 103 to 109% for the 278 K curve, with a mean of 106%, while the range is from 102 to 112% for the 268 K curve, with a mean of 107%. Each of the three curves indicates BMEP is at a maximum and nearly constant between 4,500 and 6,000 RPM, and this fact suggests the effective volumetric efficiency of the engine is at its best in the middle third of the speed range.

Table 10. Temperature effects on BMEP at 1.5 km

Temperature, K	**BMEP multiplier, expected (4-stroke)**	**BMEP multiplier, expected (2-stroke)**	**BMEP multiplier, observed (mean)**	**Temperature ratio exponent, observed**
278	1.03	1.05	1.06	0.7
268	1.05	1.08	1.07	0.9

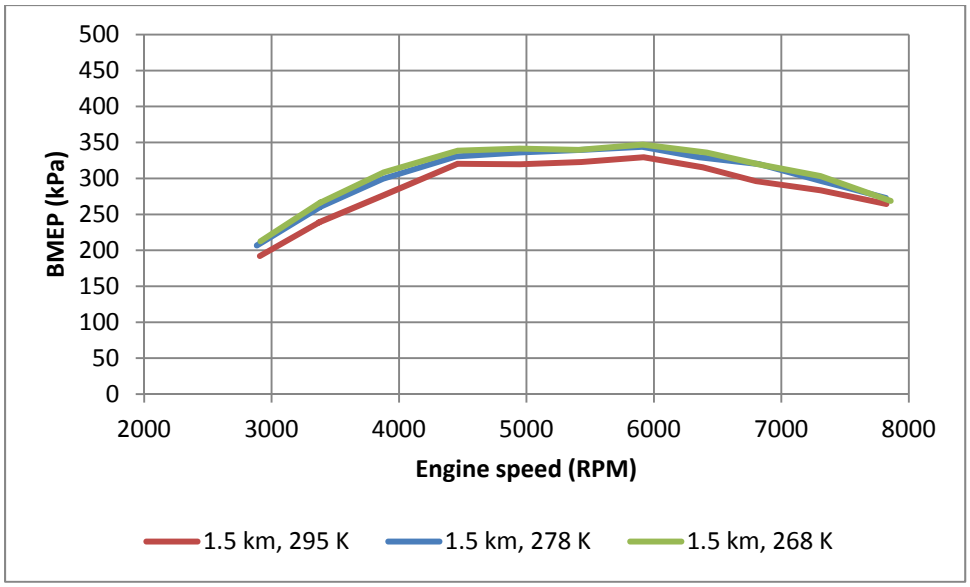

Figure 30. BMEP curves for temperature sweep at altitude of 1.5 km

The beneficial effect of decreased temperature on a fully warm engine carried over from power and BMEP to BSFC, although to a lesser degree. Figure 31 shows that the two lower temperature BSFC curves for 1.5 km have similar improvements in performance versus the 295 K baseline. The BSFC ratio ranges from 81 to 99% with a mean of 92% for the 278 and 268 K curves. The BSFC improvements with decreased temperature are primarily at low or high speeds, while the three curves are nearly coincident between the 4,500 and 6,000 RPM setpoints. The BSFC value at the 7,500 RPM setpoint in the 278 K curve correlates to greater fuel flow rate and a richer AFR.

Table 11. Temperature effects on BSFC at 1.5 km

Temperature, K	**BSFC multiplier, minimum**	**BSFC multiplier, maximum**	**BSFC multiplier, mean**
278	0.82	0.97	0.92
268	0.81	0.99	0.92

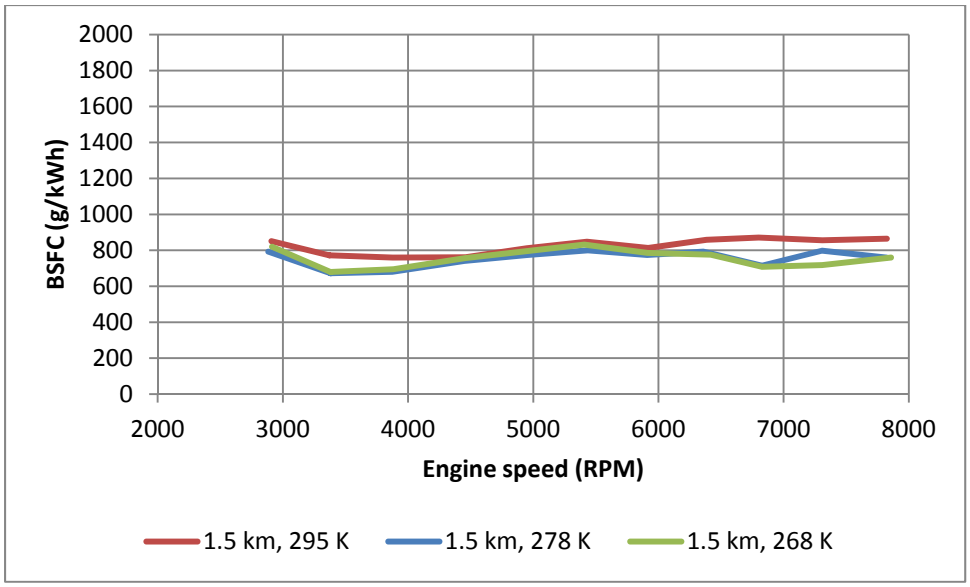

Figure 31. BSFC curves for temperature sweep at altitude of 1.5 km

The temperature effects at 3 km are similar and are discussed in Appendix C.

IV.3 Altitude effects for the near-standard atmosphere

Figure 32 is intended to show how power varies for the Brison test engine at three different altitudes corresponding to the approximately standard atmosphere. The three altitudes tested were 0.2 km where the temperature was 295K, 1.5 km with a temperature of 278K, and at 3 km with a temperature of 268K. The overall decline in power as the altitude increased is obvious. The benefits achieved with decreasing temperature were overwhelmed by the power decrease that results from reduced pressure at altitude.

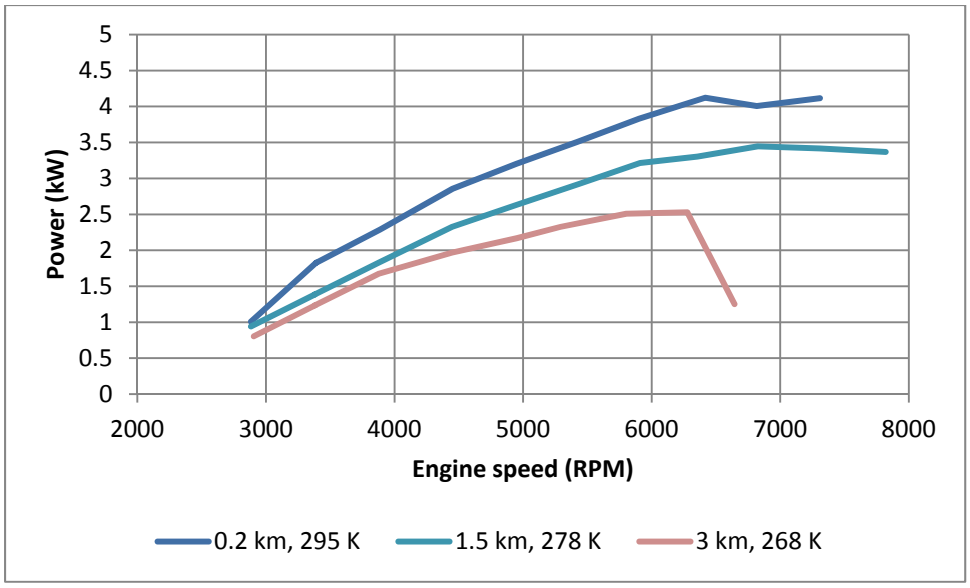

Figure 32. Power curves for near-standard temperature and pressure

As one would expect due to the loss of air density, and therefore of oxygen mass per cycle, with increasing altitude, the lowest altitude curve of Figure 32 consistently has power performance equal to or greater than that of the two higher altitudes. The pressure loss with rising altitude dominates the accompanying power boost associated with the decrease in standard temperature and results in a net loss of power. Comparing the 1.5 km curve to that of 0.2 km up to the 7,500 RPM setpoint, the power ratio has a mean value of 83% and varies from 76 to 93%, with the two extreme values coming in successive setpoints at the two lowest measured speeds.

Using the same approach to compare the 3 km curve to that of 0.2 km up to the 7,000 RPM setpoint, the power ratio has a mean value of 65% and varies from 31 to 80%, with the two extreme values coming at the two ends of the measured speed range. In the middle speed band of 4,500 to 6,000 RPM, the ratio is nearly steady at around 67%, and if the 7,000 RPM setpoint values are ignored because of the outlier point at the highest

speed for the 3 km curve, the mean ratio is 69%. The engine's peak observed power is 4.1 kW at the 6,500 RPM setpoint for 0.2 km, around 3.5 kW at 7,000 RPM for 1.5 km, and 2.5 kW at 6,500 RPM for 3 km.

Table 12. Altitude effects on power

Altitude, km	**Expected peak power, kW ([6] and [7])**	**Expected peak power, kW (adapted from [11])**	**Observed peak power, kW**	**Power correction factor, observed (mean)**	**Peak power correction factor, observed**
0.2	(4.1)	(4.1)	4.1	(1)	(1)
1.5	3.7	3.4	3.5	0.83	0.85
3	3.1	2.7	2.5	0.65	0.61

Anderson [6] and Kimberlin [7] each used an algebraically equivalent correction factor for power $\dot{W}$ as IC engines fly at increasing altitude, reprinted as Equation (5) here:

$$\frac{\dot{W}}{\dot{W}_{SL}} = 1.132\frac{\rho}{\rho_{SL}} - 0.132$$

For comparative purposes, a version of the two-stroke power and BMEP correction factor of Harari and Sher with a pressure ratio exponent of 1.5 will be used [11]:

$$\frac{\dot{W}}{\dot{W}_{ref}} = \frac{BMEP}{BMEP_{ref}} = \left(\frac{P}{P_{ref}}\right)^{1.5}\left(\frac{T_{ref}}{T}\right)^{0.8} \tag{18}$$

The 0.2 km, 295 K condition provided the power curve of choice as the baseline or reference in lieu of precisely sea level data for visually comparing the observed near-standard 1.5 km curve to calculated power values derived from models found in the literature. In this section, the sea level power $\dot{W}_{SL}$ and density ρ_{SL} will be approximated by the observed power and calculated density at the baseline condition of 98.5 kPa and 295 K. From the ideal gas law and R = 287 J/(kg*K), the baseline air density was around

1.16 kg/m^3, as shown in Table 13. Similarly, using 84 kPa and 278 K results in 1.05 kg/m^3 at 1.5 km altitude, and the 3 km density at 70 kPa and 268 K is 0.91 kg/m^3.

Table 13. Altitude effects on density and power

Altitude, km	**Pressure, kPa**	**Temperature, K**	**Density, kg/m^3**	**Power correction factor ([6] and [7])**	**Power correction factor (adapted from [11])**
0.2	98.5	295	1.16	1	1
1.5	84	278	1.05	0.89	0.83
3	70	268	0.91	0.75	0.65

Harari and Sher [11] plotted engine power against air pressure on a logarithmic coordinate system to examine the pressure ratio exponent for their power correction factor model. Following their approach, Figure 33 shows the relationships between power, ambient pressure, and engine speed for the Brison test engine at altitude. The lines on the plot correspond to pressure ratio exponents of 1, 9/8, 1.5, and 2, respectively, starting from the uppermost line. By definition all the 98.5 kPa, 295 K data points coincide at the upper right corner of the figure. Each of the other three pressures has its data points for various rotational speeds (listed in units of RPM) in a vertical cluster, and all the data are for 295 K. Reading from right to left, the three pressures at increased simulated altitude are 84, 70, and 57 kPa, respectively. From the figure, it may be noted the data points for 84 and 70 kPa have reasonably good fit with the 1.5 exponent line, while the 57 kPa points fall mainly between the 9/8 and 1.5 exponent lines.

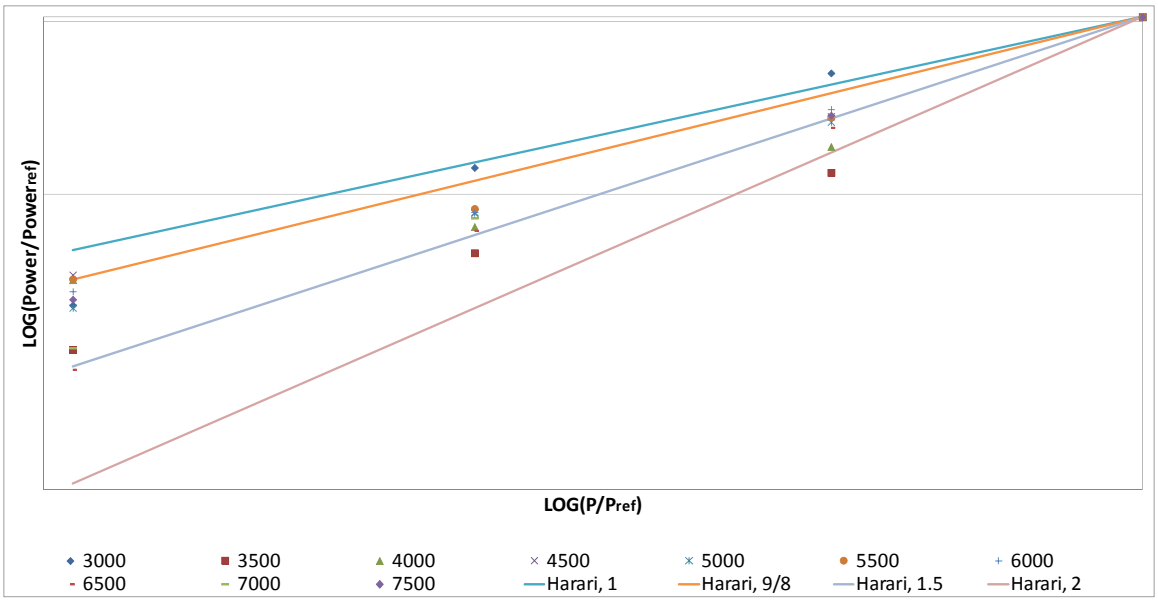

Figure 33. Engine power vs. ambient pressure on logarithmic scale

In Figure 34, the 1.5 km, 278 K power curve is plotted with curves based on the models of Harari and Sher [11] with a pressure ratio exponent of 9/8 in Equation (11),

$$\frac{\dot{W}}{\dot{W}_{ref}} = \frac{BMEP}{BMEP_{ref}} = \left(\frac{P}{P_{ref}}\right)^{9/8} \left(\frac{T_{ref}}{T}\right)^{0.8}$$

of Harari and Sher [11] in Equation (17) with pressure ratio exponent x equal to 1 or 2,

$$\frac{\dot{W}}{\dot{W}_{ref}} = \frac{BMEP}{BMEP_{ref}} = \left(\frac{P}{P_{ref}}\right)^{x} \left(\frac{T_{ref}}{T}\right)^{0.8}$$

and adapted from Harari and Sher [11] with a pressure ratio exponent x of 1.5 in a re-print of Equation (18),

$$\frac{\dot{W}}{\dot{W}_{ref}} = \frac{BMEP}{BMEP_{ref}} = \left(\frac{P}{P_{ref}}\right)^{1.5} \left(\frac{T_{ref}}{T}\right)^{0.8}$$

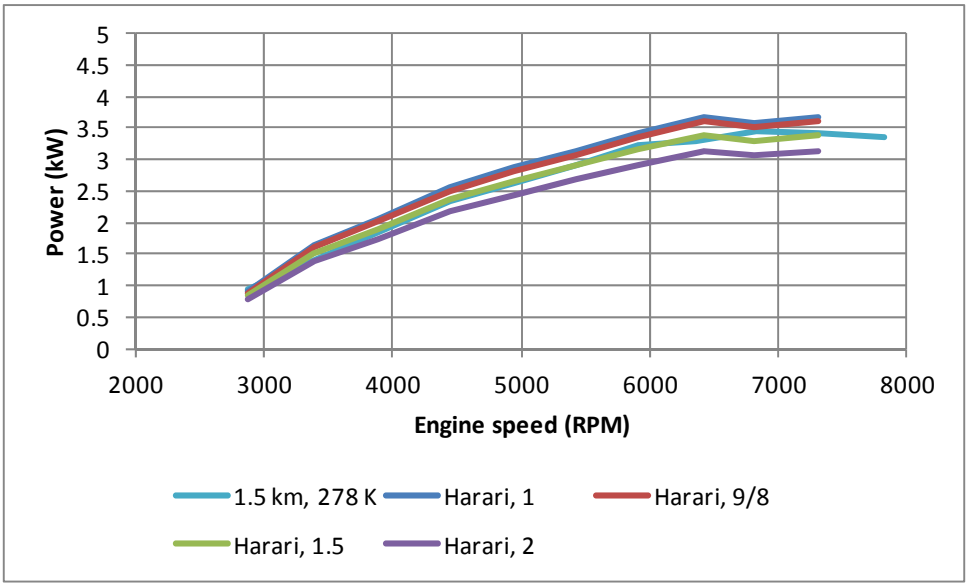

Figure 34. Observed 1.5 km power curve and literature models

Selecting Equation (18) as the closest fit to the 1.5 km power curve and re-plotting the observed data with the model curve in Figure 35, there is agreement of +/- 5% at a confidence level of 95% and relative to the peak power value.

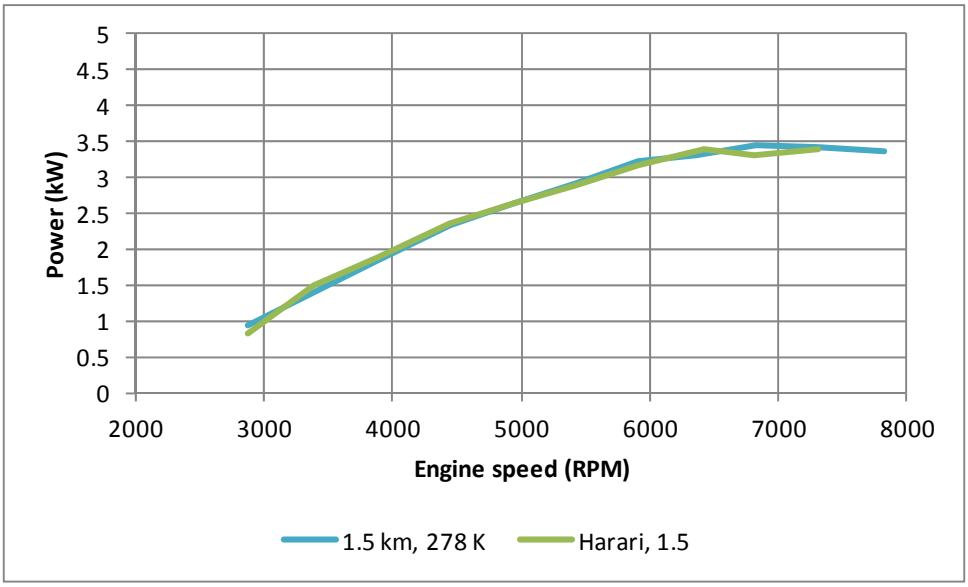

Figure 35. Observed 1.5 km power curve and adapted model

Repeating the approach of Figure 34 and Figure 35 for the 3 km, 268 K condition, Figure 36 and Figure 37 show how four models compare to empirical data.

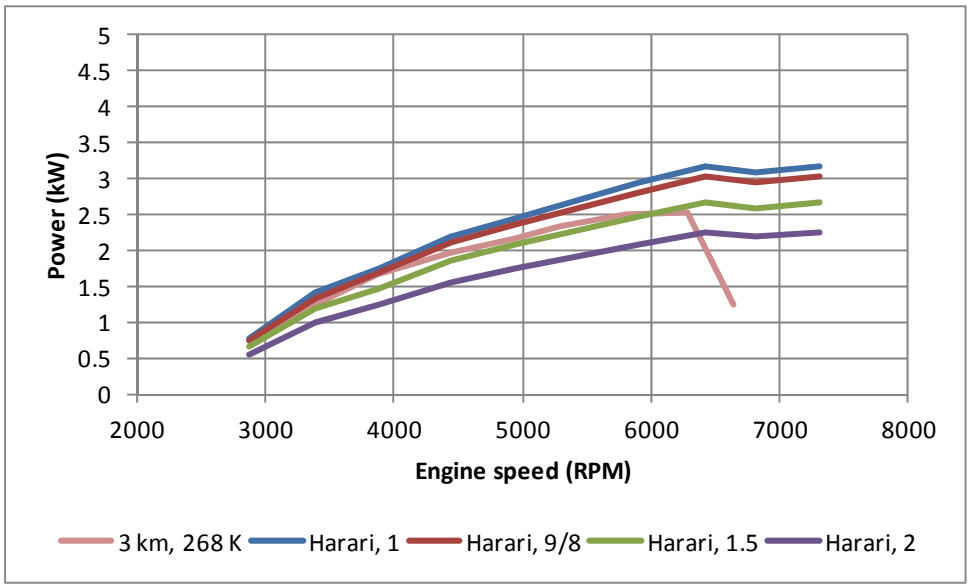

Figure 36. Observed 3 km power curve and literature models

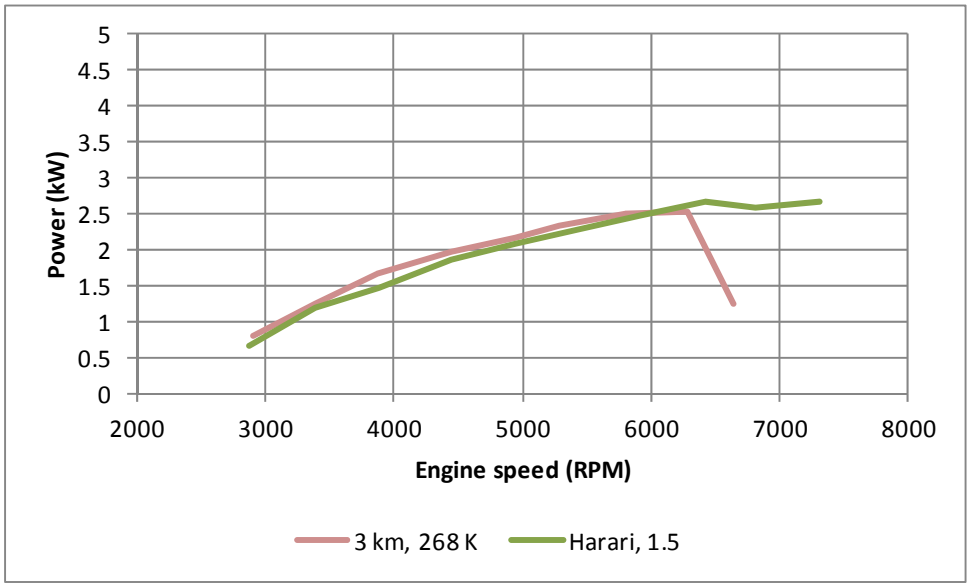

Figure 37. Observed 3 km power curve and adapted model

At a confidence level of 95% and relative to the peak power value, the 3 km data fall within +/- 8% of the Figure 37 model up to the 6,500 RPM setpoint.

The Equation (18) model adapted from Harari and Sher [11] was formed from single-sample data, and repeated measurements may lead to a revised model. Also, all data were taken with the Brison test engine fuel injected, whereas Crosbie [16] found the stock carburetor had considerably different performance characteristics at conditions for which the carburetor had not been tuned. Furthermore, a tuned exhaust could offer appreciable performance benefits in the range of rotational engine speeds for which is it optimized. Tuning the exhaust or intake systems or testing the engine with a carburetor may change the exponents in the Equation (18) model and indicate a stronger dependence on rotational speed.

Figure 38 shows how BMEP varies for the Brison test engine at three different altitudes at the approximately standard atmosphere. As with Figure 32, the lowest altitude of 0.2 km has the advantage at each measured speed setpoint over the two higher altitudes, and the middle altitude of 1.5 km gives better performance than operation at 3 km. The engine's peak observed BMEP occurred at the 6,000 RPM setpoint for 0.2 and 1.5 km and at 4,500 RPM for 3 km. The 0.2 km BMEP is approximately at its maximum of 410 kPa between the 4,500 and 6,500 RPM setpoints, and the BMEP curve at 1.5 km also has a reasonably flat plateau of around 335 kPa in a similar speed range. The 3 km curve, however, has its plateau at a somewhat lower speed setpoint range, at around 275 kPa from 4,000 to 6,000 RPM. As previously noted, the engine performance worsened badly above 6,500 RPM at the 268 K temperature for 3 km.

Table 14. Altitude effects on BMEP

Altitude, km	**Expected peak BMEP, kPa ([6] and [7])**	**Expected peak BMEP, kPa (adapted from [11])**	**Observed peak BMEP, kPa**	**Peak BMEP correction factor, observed**
0.2	(410)	(410)	410	(1)
1.5	366	339	344	0.84
3	309	265	280	0.68

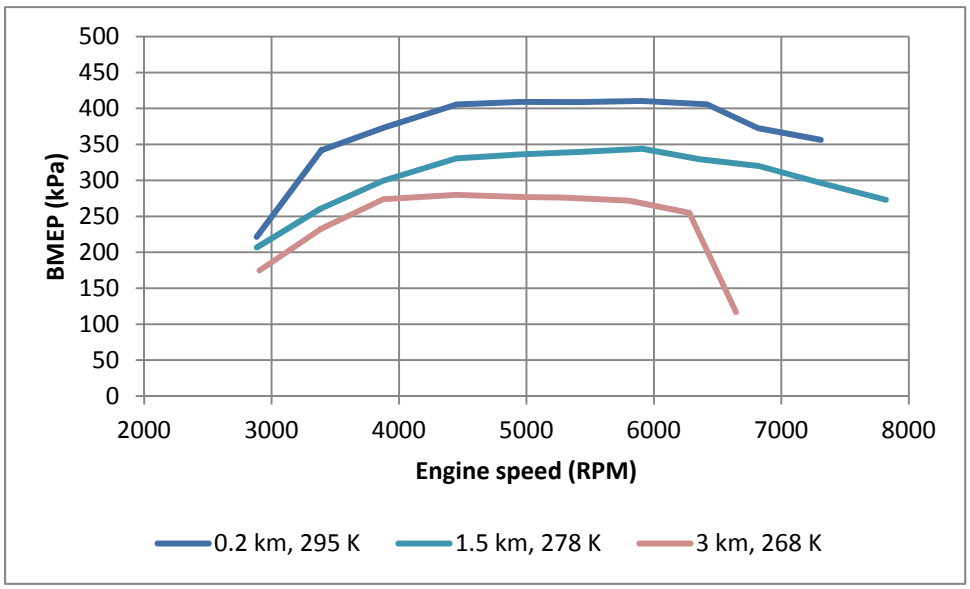

Figure 38. BMEP curves for near-standard temperature and pressure

The analysis technique utilized for creating Figure 34 is now replicated for the 1.5 km, 278 K BMEP curve in Figure 39. The data from this experiment fall below two of the model curves but generally agree with the model adapted from Harari and Sher [11].

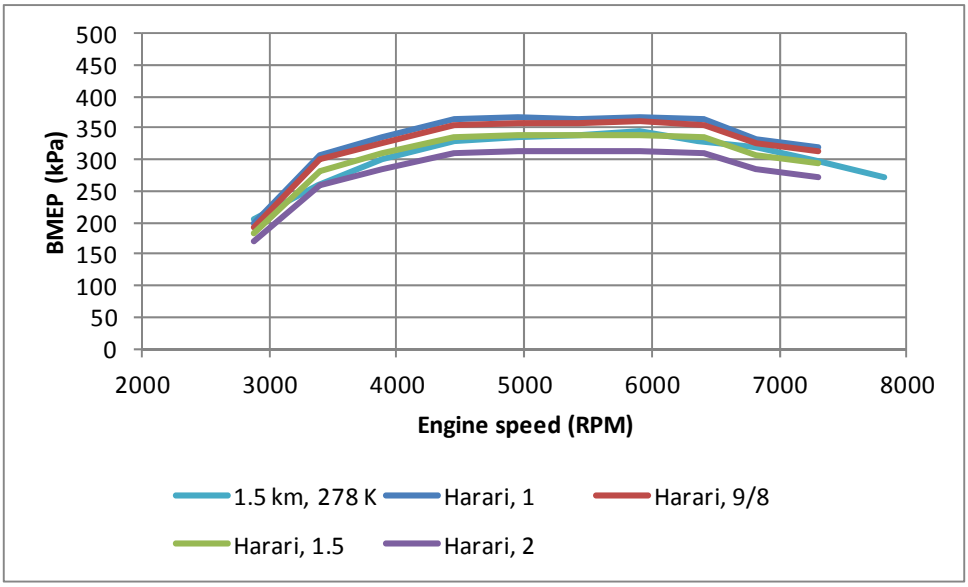

Figure 39. Observed 1.5 km BMEP curve and literature models

For visual clarity, the 1.5 km, 278 K BMEP curve and the adapted model curve are shown again in Figure 40. As with the analogous power curves, the two curves of Figure 40 agree well in the heart of the tested speed range, but here the agreement extends from 4,000 RPM out to the 7,500 RPM setpoint. The two curves fall within +/- 5% of each other at a confidence level of 95% and relative to the peak power value.

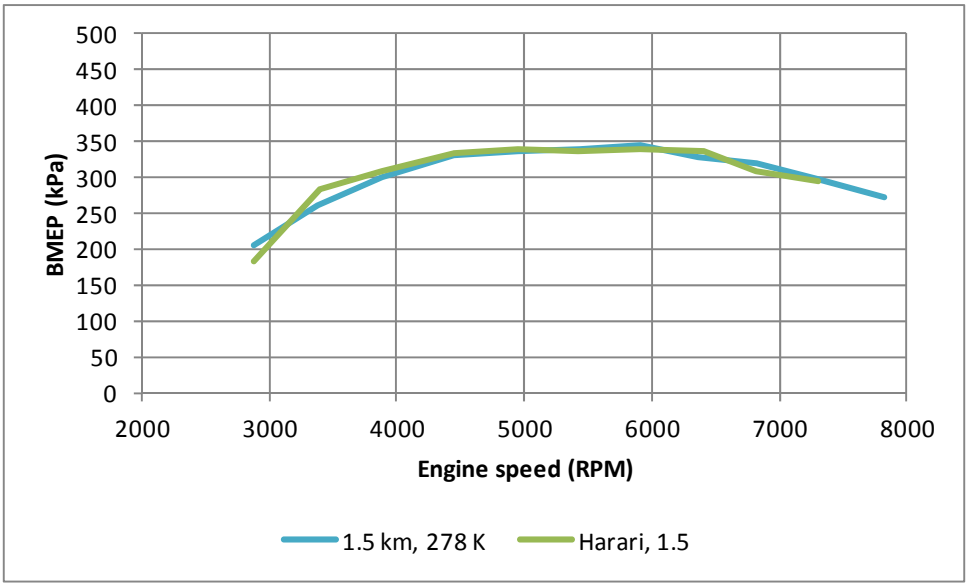

Figure 40. Observed 1.5 km BMEP curve and adapted model

The consistency of three of the models applied to the 3 km, 268 K condition is visible in the upper BMEP curves of Figure 41. Again, the data gathered in the current research fall closer to the adapted Harari and Sher model [11] than to the three others.

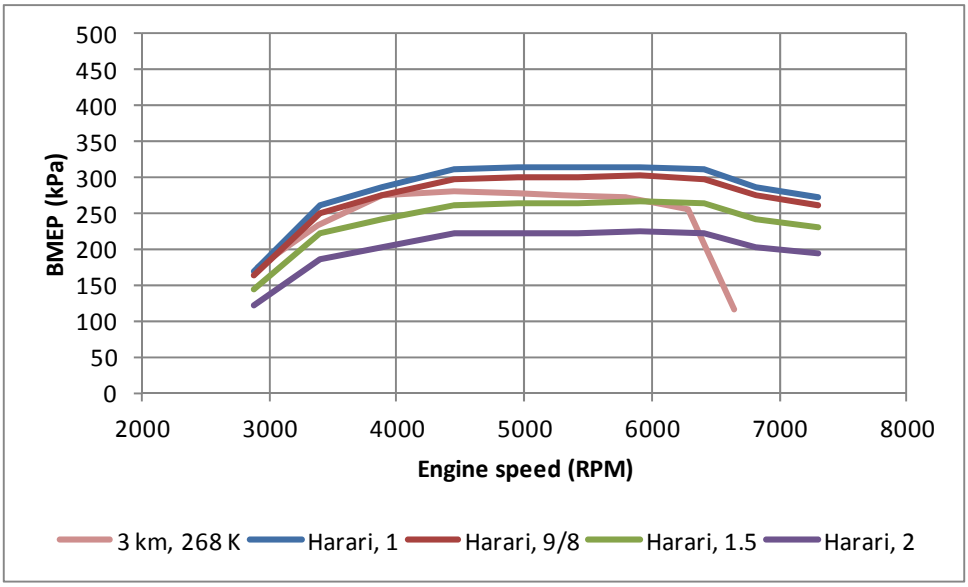

Figure 41. Observed 3 km BMEP curve and literature models

Viewing the BMEP curves for 3 km, 268 K and the adapted Harari and Sher model alone in Figure 42, the two sets of BMEP values are within +/- 8% of each other at a confidence level of 95% for speeds up to the 6,500 RPM setpoint and relative to the peak power value.

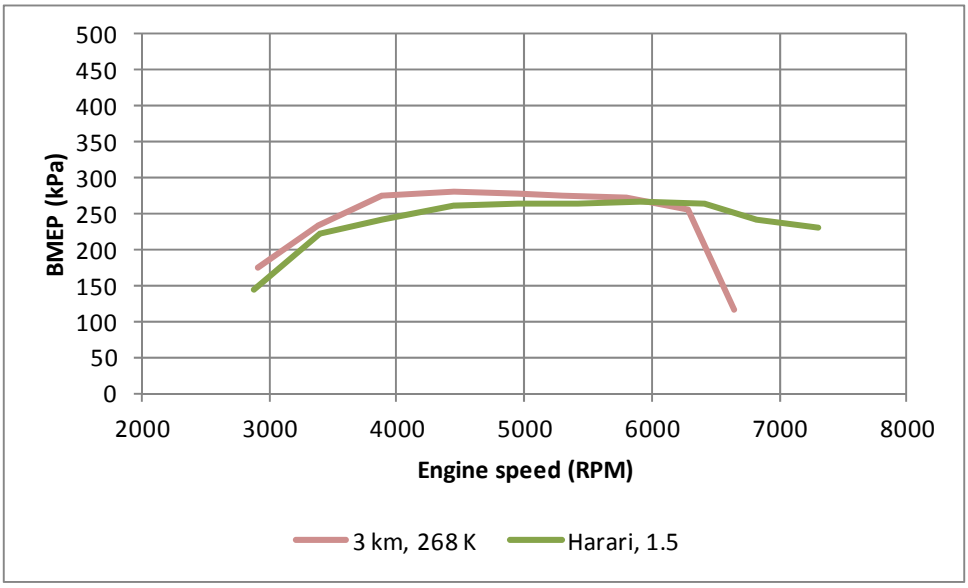

Figure 42. Observed 3 km BMEP curve and adapted model

The BSFC curves at three near-standard altitude conditions are displayed in Figure 43, and the 0.2 km efficiency of the engine is better than that of the 1.5 km condition over the majority of the measured speed range. Although the 0.2 km efficiency does not exceed those of the higher altitudes across the board, it has a great advantage over the 3 km efficiency in the upper half of the speed range. Except at the lowest speed setpoint of 3,000 RPM, the 0.2 km BSFC curve is consistently below 750 g/(kWh).

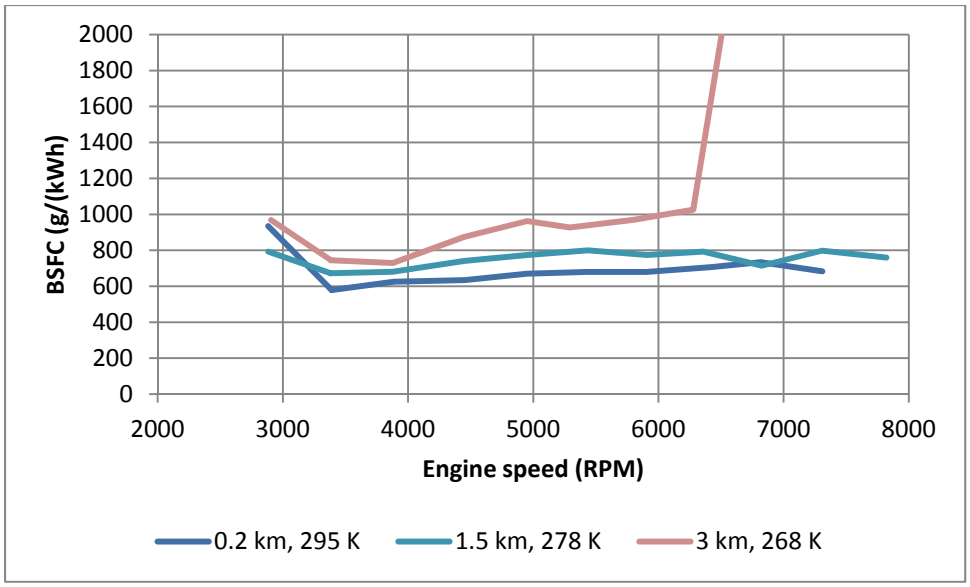

Figure 43. BSFC curves for near-standard temperature and pressure

For all observed speeds, the 1.5 km curve is at or below 800 g/(kWh). The 3 km curve, on the other hand, is in the vicinity of 1000 g/(kWh) from 5,000 to 6,500 RPM before it rises off the chart at the 7,000 RPM setpoint. In terms of BSFC ratio, the 3 km curve has values on the order of 140% the 0.2 km curve from 4,500 to 6,500 RPM.

Table 15. Altitude effects on BSFC

Altitude, km	**BSFC, g/(kWh) (minimum)**	**BSFC, g/(kWh) (mean, 3,500 to 6,500 RPM)**	**Thermal efficiency, % (mean, 3,500 to 6,500 RPM)**
0.2	580	650	13
1.5	670	750	11
3	730	890	9

Converting BSFC to thermal efficiency in the heart of the measured speed range, the 0.2 km curve equates to converting 12 to 13% of the energy in the delivered fuel into useful work, the 1.5 km corresponds to 10 to 11% efficiency, and the 3 km curve reflects

8 to 9% efficiency. In any of these cases, there is ample room for improvement of the fuel efficiency of small engines such as the Brison 95 cc, and all the more at increased altitude. The relatively higher BSFC values for these curves at low speed and for the 3 km at high speed are not unexpected.

Heywood and Sher [8] noted backflows are possible in crankcase-scavenged 2-stroke engines such as the Brison test engine at high speed as the scavenge ports open or at low speed before the intake or scavenge ports close. Backflows appear to lead to scavenging efficiency losses due to short-circuiting [8]. Furthermore, Harari and Sher [11] attributed increases in BSFC at low air pressures to decreasing scavenging efficiency.

V. Conclusions and Recommendations

The primary objective of this research was to study the effects of temperature on the performance of a small IC engine at altitude. In order to gather data for the performance measures of power, BMEP, and BSFC, a temperature control capability was introduced to an existing altitude chamber test rig. The temperature-dependent performance data were taken at pressure altitudes of 1.5 and 3 km, and baseline temperature data were also taken at altitudes of 0.2 and 4.5 km for comparison.

In the future, the altitude rig used here can be utilized for characterizing the performance of other small RPA engines as well as for facilitating research into improving the reliability, efficiency, and logistics supportability of compact engines with 1 to 8 kW of peak power. Considering that each US ground unit could benefit from having an organic intelligence, surveillance, and reconnaissance (ISR) capability in the form of a small RPA, research leading to engines that are more dependable and easily supported and maintained would offer significant advantages to the DoD. Naval and air units also operate small aircraft and would benefit from RPA engines that reliably run on the same heavy fuels used in F/A-18s, B-52s, and C-17s, particularly when deployed.

V.1 Conclusions of Research

Relative to sea level performance for the Brison test engine, peak power and BMEP each dropped about 4% per 300 m increase in altitude up to 3 km due to the effect of pressure. At a pressure altitude of either 1.5 or 3 km, BSFC increased by approximately 30% when compared to sea level. A 30% growth in BSFC translates to 2 percentage points of lost thermal efficiency.

Power and BMEP generally increased around 7% for a temperature decrease from 295 K to either 278 or 268 K, and the performance increase may be approximated as 1% per 300 m of increased altitude. Because torque and BMEP fell off at the higher engine speeds, the peak power at 268 K was approximately equal to that of 295 K for the 3 km pressure altitude. Decreased temperature to either 278 or 268 K led to an 8% drop in BSFC at 1.5 km, but the effects of lower temperature at 3 km were mixed.

The combined effects of standard temperature and pressure resulted in around a 3.5% loss of power and BMEP per 300 m increase in altitude. Rising standard altitude produced a 3% increase in BSFC per 300 m. In terms of thermal efficiency, there was a drop of about 0.4 percentage points per 300 m of increased altitude.

The results of this experiment are not general to all RPA and may not be general to all two-stroke spark ignition RPA. Extensive further testing of a wide variety of two- and four-stroke RPA engines would be necessary before firm conclusions about the effects of temperature on small IC engine performance at altitude could be drawn. Testing should include carbureted and fuel-injected engines to aid understanding of the effects of a fuel delivery system on power, BMEP, and BSFC.

Because the results indicate the negative performance impact on the 2-stroke test engine is compounded with rising altitude, an RPA designer may instead consider a 4-stroke powerplant. The 4-stroke literature suggests the degradation of performance is proportional to the percentage loss of pressure, and 4-stroke engines require no mixing of fuel and oil. However, weight or physical space constraints in combination with power requirements may render a 2-stroke engine the only viable option for some airframes.

Although standard temperature and pressure both fall with rising altitude, pressure effects dominated those of temperature and resulted in a net loss of performance as the altitude increased. In round numbers, air pressure changes for simulating the standard atmosphere caused four times the change in magnitude of performance as did temperature changes. The performance loss tied to decreasing pressure and oxygen mass per cycle simply overwhelmed the gains in air density associated with decreasing temperature. Summarizing, an altitude increase of 300 m leads to a 3 to 4% decrease in performance for the Brison 95 cc test engine.

V.2 Significance of Research

Very little data regarding the performance at altitude of small RPA engines with up to 8 kW is available from either flight testing or laboratory research. This experiment contributed data with air temperature and pressure varied according to the standard atmosphere for a 2-stroke SI IC engine of the general sort common in early 21st century RPA. The combined effects of temperature and pressure were quantified and can be used to guide decision-making with regard to powerplant selection for military RPA.

Having the capability to simulate altitudes up to 4.5 km for performance testing of small IC engines will simplify the characterization and improvement of performance for candidate engines. Controlling temperature to 238 K or lower at the reduced air pressure of high altitude would facilitate testing new applications of technology to overcome the difficulty of cold-starting and operating small IC engine-powered RPA with heavy fuel. Ultimately, success in this line of research would result in a single-fuel logistics chain for

DoD aircraft and eliminate the need for separate, inconvenient, and costly fuel supplies for small engines in deployed locations.

V.3 Recommendations for Action

The first order of business for improving the experimental set-up is re-wiring the altitude rig and repairing or replacing the starter system. Electrical problems plagued the fuel injection system and some of the other sensors and systems on board the rig throughout this research effort. Having a robust, well-executed, and vibration-resistant wiring configuration will enhance the effectiveness of testing and ease troubleshooting. It may very well also solve some of the reliability and performance problems with the fuel injection system. The starter and components with which it interfaces are in need of repair, replacement, or improvement prior to any additional engine testing.

Purchasing and integrating the larger heat exchanger for which the Super Radiator Coils company supplied a quote would be a positive step. Replacing the current direction-injection of liquid nitrogen for chilling the cooling air would eliminate the possibility of unwanted nitrogen being mixed with the engine air. Although more frequent re-fills of the Dewar would be required for a given set of tests, guaranteeing the chemical make-up of both the altitude chamber's inlet air streams would enhance confidence in the integrity of the data.

Hardware and expertise are available at the AFRL Small Engine Research Laboratory for adding variable ignition timing to the rig. Introducing variable spark timing would yield useful data and likely allow for better performance, especially when testing non-standard fuels for a given engine. The rig was originally designed to

accommodate in-cylinder pressure measurements, and such a capability should be re-visited. With modifications to the engine mounting hardware and perhaps the shafts leading to the dynamometer, other small IC engines can be studied with the rig.

V.4 Recommendations for Future Research

Future research with the altitude rig should focus on first characterizing and then improving the performance of small RPA engines that show particular promise or are being considered for operational use in current or developmental DoD aircraft. A greater range and variety of temperatures should be used for future efforts to more completely replicate the possible operating conditions small RPA engines will face in the atmosphere. Along with lower temperatures, cold starting studies of candidate engines should be accomplished. Such testing will be particularly important once testing with heavy fuel has commenced. Reliable starting and operating at altitude is a key goal.

Engine selection is based upon the determination of required thrust for an aircraft. Through the analysis of an aircraft's mission and other requirements, one will be able to find the weight, wing loading, thrust-to-weight ratio, and thrust at take-off. Thrust lapse and Thrust Specific Fuel Consumption (TSFC) models are key inputs for this process, and a drag polar model based on Mach number along with an estimated maximum lift coefficient are necessary to find the drag and lift forces encountered at various phases of flight for the chosen wing area. Future researchers can use the data gathered from testing engines in the altitude rig to translate power losses at altitude and BSFC information into thrust lapse and TSFC models. In this way, the entire aircraft system can be analyzed.

Direct injection (DI) should be introduced for whatever engine is installed in the rig and the data and conclusions collected thereafter used to aid in integrating this promising technology with small SI IC engines. DI may be a key to success along the road to starting and running small RPA engines on heavy fuel at the low temperatures associated with aviation. Cold-starting an IC engine on heavy fuel is no trivial matter, and fuel injection in general and DI in particular may be difficult to introduce to an operational small RPA engine with its attendant mass and physical space constraints. Research with heavy fuel DI in the small RPA field may lead to breakthroughs that make a single-fuel logistics concept for DoD vehicles more than a dream.

Appendix A: Additional literature review information

The topics of the literature review portions found in Chapter II and this appendix include internal combustion engines, the types of cycles and ignition used in these engines, the power and efficiency of their operation, and the three fundamental ingredients required for them to produce power: air, fuel, and ignition. Because the test engine studied in this research is of the two-stroke type and uses spark ignition, the processes involved are discussed and contrasted with alternative cycles and ignition methods. Notwithstanding the vitality of reliability to aircraft engines, the two most important parameters of this research are power and fuel efficiency, so both will be explained. Because the research engine, like others of its kind, only produces power when a suitable mixture of fuel and air (or other oxidizer) is ignited at an appropriate time during a cycle, each of the three primary combustion components is summarized.

A.1 Four-Stroke Cycle

The theoretical air-standard Otto cycle includes four processes: constant-volume energy addition, isentropic expansion, constant-volume energy removal, and isentropic compression (Turns [31]). Citing the first law of thermodynamics in analyzing the ideal Otto cycle for a 4-stroke SI engine, Turns notes that specific enthalpy h for an ideal gas is a function of temperature T only. With the subscripts *reac*, *prod*, and *init* referring to the reactants, products, and initial condition, respectively, universal gas constant R_u, and molecular weight MW,

$$0 = h_{reac} - h_{prod} - R_u\left(\frac{T_{init}}{MW_{reac}} - \frac{T_{ad}}{MW_{prod}}\right) \quad (19)$$

where T_{ad} is the constant-volume adiabatic flame temperature (Turns [17]). An actual Otto cycle consists of two revolutions and four strokes: intake, compression, expansion or power, and exhaust. The two-stroke cycle has an advantage over the Otto cycle in that power is produced twice as often for a given engine speed.

Figure 2 shows an actual four-stroke SI cycle, with TDC labeled as TC and BDC as BC. The cylinder is shown with one inlet poppet valve and one exhaust poppet valve, but four-stroke engines may use two or more of either type of valve per cylinder. Multi-valve engines, with three, four, or five valves per cylinder, have a greater flow area than is possible with only two valves, and this aids in maximizing the mass of gases admitted during intake or exhaust. The test engine has a throttle valve but no inlet, transfer, or exhaust valves, relying instead on simple piston-controlled ports for flows into and out of the cylinder.

In part (A) of Figure 2, the inlet valve is open during the intake stroke. The downward motion of the piston allows the higher pressure fuel-air mixture in the intake manifold to flow into the combustion chamber. In part (B) of the figure, both valves are closed and compression of the mixture occurs as the piston moves upward. In part (C), both valves are still closed and expansion of the gases occurs after a spark causes ignition, thus producing power as the piston descends and forces the crankshaft to rotate. Finally, the exhaust stroke is depicted in part (D), as the exhaust valve is open and the upward motion of the piston pushes the burned gases out of the cylinder for the energy removal.

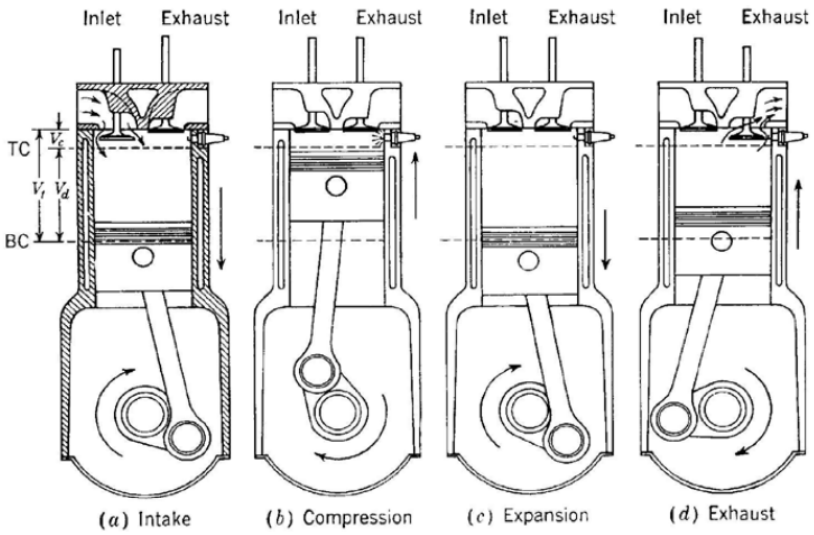

Figure 44. Four-Stroke cycle for IC engine (from Heywood [1])

The theoretical air-standard Diesel cycle includes four processes: constant-pressure energy addition, isentropic expansion, constant-volume energy removal, and isentropic compression (Moran and Shapiro [32]). The constant-pressure and constant-volume processes are adiabatic (Bose [33]). While the Otto cycle assumes combustion occurs at constant-volume, the Diesel cycle has combustion at constant-pressure. An actual four-stroke CI engine operates on the same basic cycle as the one depicted in Figure 2, but ignition is accomplished via compression rather than a spark. Turns states that Diesel engine combustion involves premixed and diffusion burning after autoignition, with fuel and oxidizer molecules diffusing from different directions toward the flame (Turns [17]).

A.2 Power and Efficiency

Power is the rate at which work is done and has the same units as a rate of heat transfer. Work and heat are each forms of energy, meaning power is energy transfer per

unit time (Cengel and Boles [34]). Power is also the product of force and velocity. Thrust is a force resulting from the rate of momentum change of a gas (Anderson [6]), and when thrust is multiplied by an aircraft's velocity, we find the useful power the propulsion device is producing. Excepting gliders, which themselves must be lifted to altitude, aircraft rely on heat engines or electric motors to generate thrust and enable flight.

Efficiency, or as Cengel and Boles [34] alternatively call it, performance, is the ratio of desired output to required input. Thermal efficiency, the ratio of net work output to total heat input, is of great interest to aeronautical engineers and to the Air Force because an engine with high efficiency produces more power for a given flow rate of fuel. Higher thermal efficiency leads to both lower fuel cost for a given sortie and to a smaller necessary fuel load to accomplish a mission. Thus, high efficiency tends to increase cost effectiveness and simplify logistics.

Heywood [1] prefers the phrase fuel conversion efficiency, η_f, in place of thermal efficiency. The efficiency data provided in the results section of this document are fuel conversion efficiency values calculated from Equation (20) in terms of brake specific fuel consumption, $BSFC$, and the lower heating value at constant pressure of the fuel, Q_{LHV}

$$\eta_f = \frac{1}{BSFC \cdot Q_{LHV}} \tag{20}$$

In this context, the term *brake* refers to the device used to absorb torque and apply a load in a power-measuring dynamometer. The BSFC is the ratio of fuel mass flow rate, $\dot{m}_f$, per unit of brake power, $\dot{W}$, measured with a dynamometer:

$$BSFC = \frac{\dot{m}_f}{\dot{W}} \tag{21}$$

Because it is desirable to minimize the mass of fuel used to produce a given amount of power, engineers work to keep BSFC as low as possible. Lower heating value represents the energy per unit mass contained in a fuel that may be released during combustion and assumes the combustion products are in the gaseous phase, that is, the water in the exhaust has not been condensed. Higher values of Q_{LHV} are better, as more energy is available for conversion to work for a given mass. This research provided efficiency in the results section using the definition of η_f from Equation (20).

The torque τ generated by an IC engine is a variable moment resulting from the force acting on a piston and transmitted through a connecting rod to a crankshaft. Torque, with units of distance multiplied by force, is dimensionally equivalent to work, heat, or energy. Torque is calculated from brake mean effective pressure, $BMEP$, the swept volume or displacement, V_d, and the number of strokes per cycle, n_R. Because higher displacement tends to result in an engine with greater physical volume and mass, aeronautical engineers prefer to minimize V_d. For a given BMEP and displacement, a two-stroke engine has twice the torque of one with four strokes.

$$\tau = \frac{BMEP \cdot V_d}{2\pi \cdot n_R} \tag{22}$$

Engine power, $\dot{W}$, is the product of torque and angular velocity. Engineers desire torque, and therefore power, to be maximized for a given engine speed. The rotational engine speed N is directly related to the angular velocity (Heywood [1]). Torque is multiplied

by the rotational speed of the engine to yield power and increasing torque at a given engine speed leads directly to increased power at that point:

$$\dot{W} = \frac{BMEP \cdot N \cdot V_d}{n_R} \tag{23}$$

Brake mean effective pressure is a useful parameter for comparing the work output of an engine per cycle to that of any other IC engine, regardless of displacement. BMEP may be found from η_f, Q_{LHV}, volumetric efficiency η_v, air density ρ_∞, and the air-fuel ratio (AFR).

$$BMEP = \frac{\dot{W} \cdot n_R}{V_d N} = \eta_f \eta_v Q_{LHV} \rho_\infty \left(\frac{1}{AFR}\right) \tag{24}$$

In practice, two-stroke engines have lower BMEP than their four-stroke counterparts, but they still tend to have higher power density on either a mass or displacement basis.

The thermal efficiency η_{th} of a device may be calculated from

$$\eta_{th} = \frac{W_{net,out}}{Q_H} = 1 - \frac{Q_L}{Q_H} \tag{25}$$

where $W_{net,out}$ is the net work output, Q is a magnitude of heat transferred, and subscripts L and H refer to the low- and high-temperature media with which the device exchanges heat (Cengel and Boles [34]). The Carnot cycle is a theoretical cycle that could be used for refrigeration or an engine, and it has four reversible processes: two are isothermal, and two are adiabatic; two are expansion, and two are compression. The Carnot thermal efficiency $\eta_{th,rev}$ represents the maximum possible efficiency for a device and is calculated from the temperature T of the low- and high-temperature media, respectively:

$$\eta_{th,rev} = 1 - \frac{T_L}{T_H} \tag{26}$$

The theoretical thermal efficiency of a four-stroke SI engine $\eta_{th,Otto}$ is driven by its geometric compression ratio:

$$\eta_{th,Otto} = 1 - \frac{1}{r^{k-1}} \tag{27}$$

where r is the compression ratio and k is a constant equal to 1.4 for ambient air [32]. Bose [33] reports that Rudolf Diesel originally intended to design a Carnot cycle-based engine, but the two isothermal processes must run very slowly, whereas a practical engine requires very fast adiabatic processes. Diesel also noted the Carnot cycle has low specific power and the Otto cycle has low efficiency due to the premixing of air and fuel, which leads to a low compression ratio [33]. Using the cold air-standard cycle, meaning air has constant specific heats, we calculate the theoretical thermal efficiency of a Diesel cycle:

$$\eta_{th,Diesel,cold} = 1 - \frac{1}{r^{k-1}} \left[\frac{r_c^k - 1}{k(r_c - 1)} \right] \tag{28}$$

where r_c is the cutoff ratio and equivalent to the volume ratio of the ending and beginning of the constant-pressure portion of the power stroke (Moran and Shapiro [32]).

The maximum temperatures allowed during engine operation are driven by the limitations imposed by the materials with which it is constructed, and excessive cooling of the engine will lead to decreased power and efficiency, and higher rates of carbon, varnish, and sludge accumulation. An air-cooled engine such as the Brison 95 cc, relative to a typical water-cooled one, has the advantages of lightweight, quick warm-up

to operating temperature, and zero cooling system maintenance, leaks, or freezing (Bonnick [35]).

A.3 Air, Fuel, Ignition

In this section, additional information regarding the three necessary ingredients for combustion are discussed. The ingredients are air, fuel, and ignition. With air and fuel at an appropriate ratio and adequate ignition energy, fire can result.

A.3.1 Compression Ratio

The commonly quoted compression ratio (CR) for an engine of the 4-stroke type is known as a geometric CR, but 2-stroke engines are more properly compared through the use of the trapped CR (Blair [2]). Trapped compression ratio involves the ratio of the volume swept by the piston after the exhaust port closes in place of the total swept volume

$$CR_t = \frac{V_{ts} + V_{cv}}{V_{cv}} \tag{29}$$

where V_{ts} is the trapped swept volume and V_{cv} is the clearance volume. Schmick reported the geometric CR (Schmick [25]) of the Brison 95 cm^3 as 19.4, but if the trapped CR were of such high magnitude, knock would be a very serious problem.

Attard et al. [36] analyzed gasoline combustion in a 0.43 L inline two-cylinder four-stroke engine to see if the inherently high levels of heat transfer, friction, and dissociation of small cylinders can be overcome with normal aspiration. Piston modifications allowed the CR to be varied from 9 to 13, taking advantage of greater knock resistance relative to large cylinders for a given CR. By increasing the CR, it was

possible to achieve a maximum BMEP of 1.3 MPa or a minimum BSFC on the order of 220 g/(kWh) (brake thermal efficiency of 37%). Although this research utilized a four-stroke engine, the results suggest the weaknesses of small engines in terms of performance and fuel efficiency can be overcome even without supercharging.

A.3.2 Fuel Injection

Crosbie [16] showed that fuel injection increases reliability, equalizes BSFC at flight altitudes, increases performance significantly for off-peak conditions, and simplifies the starting process. An electronic control unit (ECU) determines the pulsewidth for an injector fed by fuel at constant pressure (set by a regulator) in a speed-density system (Blair [2]) based on the primary signal of MAP as well as engine speed and intake air temperature (IAT) and engine coolant temperature (ECT) sensors (Heywood [1]). A fuel injector is an on-off device, and the pulsewidth is the time it is turned on and fuel is allowed to flow. The theoretical mass of air m_a per cycle for a single cylinder is the product of air density (a function of temperature and pressure) and displaced volume:

$$m_{a_{theoretical}} = \rho_a(T_{STP}, p_{STP})V_d \tag{30}$$

where standard temperature and pressure, *STP*, are used for the density determination. The actual mass of air per cycle is the product of volumetric efficiency (a function of speed, *N*), air density, and displaced volume:

$$m_a = \eta_v(N)\rho_a(T_i, p_i)V_d \tag{31}$$

For an EFI system with a Mass Air Flow (MAF) meter, the ECU primarily depends upon a measured air mass flow rate and engine speed signals for adjusting pulsewidth. The

concept of load yields a non-dimensional number, often thought of as a percentage of the mass of air theoretically accommodated by the cylinder:

$$Load = \frac{m_{a_{current}}}{m_{a_{theoretical}}} \tag{32}$$

The EFI cycle time in milliseconds for a 2-stroke engine, with one fuel pulse per revolution, is:

$$Cycle\ time_{2-stroke} = \frac{60{,}000}{N} \tag{33}$$

where the engine speed N is in RPM. Duty cycle is another non-dimensional term, expressed as the ratio of the pulsewidth to the cycle time when the pulsewidth is assumed to represent the time an injector is open for a single pulse at the maximum rated flow rate.

$$Duty\ cycle = \frac{pulsewidth}{cycle\ time} = \frac{required\ fuel\ flow\ rate}{fuel\ injector\ capacity} \tag{34}$$

For port-fuel-injected engines, it is desired for the pressure of the fresh air and fuel to yield flow stream stability and a relatively low delivery ratio. With a small delivery ratio, short-circuiting of fuel through the exhaust port is less of a problem. Stratified combustion offers appeal here (Heywood and Sher [8]), and when assisted by compressed air, direct- and other fuel-injection systems are able to stratify the charge.

A Mass Air Flow (MAF)-based fuel injection system is good for steady air flow (e.g., cruise or WOT conditions), but not for large pulsations in intake air flow. Because engines with an aggressive camshaft design and single-cylinder engines have large pulsations in intake air flow, speed-density is usually more accurate for fuel injection (Banish [37]). In the case of a two-stroke engine such as the Brison 95 cm^3, a throttle angle-based system is preferred over the speed-density approach.

Fuel injectors typically fall into one of two categories: saturation or "peak and hold". The two categories may be differentiated by the parameter of offset time, which is the difference between injector opening delay and closing delay. Saturation injectors have a relatively high impedance of 12 to 16 Ohms and long offset time. A long offset time is more significant at low pulsewidths and must be accounted for by adding it to target pulsewidth to prevent lean running (Banish [37]). Recalling Ohm's Law, the potential difference of an injector in Volts is:

$$V = IR \tag{35}$$

where I is the electric current in Amperes and R is the resistance or impedance in Ohms.

A peak and hold injector has low internal impedance of 2 to 6 Ohms and therefore higher operating current than a saturation injector. With low impedance, a peak and hold injector has much shorter injection offset times to more reliably control pulsewidths of short duration. The drawback of peak and hold injectors is they are more expensive than those of the saturation type (Banish [37]).

Because manifold absolute pressure (MAP) sensor signals affect air-fuel ratios and ignition timing for a speed-density engine management system, MAP accuracy is in some cases essential for proper fuel injection. It is important to note the test ECU uses throttle angle-based injection and does not use the MAP signal to modulate the pulsewidth when in open-loop. The Brison test engine is equipped with a typical MAP sensor that has three wires: one ground, a 5 V supply from the ECU, and a signal wire sending measured voltage to the ECU for calculating the associated pressure. Similarly, the throttle position sensor (TPS) should receive 5 V from the ECU as a reference, and the voltage between the signal wire and ground may range from less than 1 volt at idle to

nearly 5 volts at WOT (Hartman [21]). When in closed-loop, the ECU as configured will use the MAP signal to correct the pulsewidth and ignition timing for altitude.

Grasas-Alsina et al. [10] compared the performance of a single-cylinder 350 cm^3 crankcase-compression, Schnürle-type loop-scavenged SI 2-stroke engine with a carburetor to operation with two types of discontinuous fuel injection. One of the two fuel injection approaches was to position two injectors in the inlet tract to allow fuel to enter the crankcase, and the other was to place the injectors in the transfer tract to allow fuel to enter the cylinder more directly and thus reduce short-circuiting. Grasas-Alsina et al. used a chamber to damp pulsations in the air flow and then calculated the air mass flow rate based on differential pressure, but they also utilized a hot-wire sensor to check their flow calculations.

For the case of inlet injection, varying the timing all the way from 72° to 324° ATDC had little effect on performance. When Grasas-Alsina et al. attempted to equal with inlet injection the BMEP achieved with the stock carburetor, they found BSFC reduction to be negligible. However, for a 2% power drop at WOT, they achieved a 10% improvement in BSFC, and the fuel savings reached 30% for part-load operation with air-fuel ratios of about 16:1 when compared to an AFR of 11 to 13:1 with the carburetor. Because the transfer port opening only lasted 4.3 ms at 5,000 RPM, Grasas-Alsina et al. [10] used a special control system to enable the injection duration to be sufficiently short. Transfer injection was timing-dependent and suffered from inadequate fuel vaporization because the fuel entered the cylinder as a liquid, thus delaying the combustion event. Without high-precision transfer injection timing, inlet injection offers the better performance of the two approaches, but for both, maximum BMEP could only match that

of the stock engine, and the BSFC benefits were derived from leaner operation than occurred with the stock carburetor.

Carbureted crankcase-compression 2-strokes were known for being hard to start decades ago, and they suffer even today in many cases from low fuel economy, excessive oil consumption, and poor operation when idling or lightly loaded (Taylor [9]). For 4-stroke engines, port fuel injection often increases air capacity relative to a carburetor because of the pressure drop and heat transfer inherent as fuel passes through a carburetor, thus increasing volumetric efficiency. Furthermore, this volumetric efficiency rise compared to a carburetor can be up to 10% for direct injection (DI) (Taylor [3]). DI of 2-strokes is advantageous because the fuel is injected, vaporized, and mixed with air and high-temperature residual gas after exhaust port closure and the end of scavenging (Heywood and Sher [8]).

A.3.3 Heavy Fuels

According to Montemayor et al. [38], if the deployed US military is able to adopt a single-fuel approach and use Jet Propellant-8 (JP-8) for all its machines, the probability of pumping the wrong fuel into a vehicle's tank goes away, and the handling of fuels is simplified. JP-8 has a mass density greater than that of gasoline and is considered a heavy fuel. Using JP-8 offers better operation at low temperatures compared to #2 Diesel fuel (DF-2) in addition to lower engine wear and corrosion of fuel system parts that come into contact with fuel. JP-8's preferred low-temperature characteristics are due to a relatively low cloud and freezing points.

JP-8 also has less energy per unit of volume than DF-2, and the expected power and fuel economy are thus lower for JP-8. In practice, though, research has shown that at full-load, some engines actually have higher thermal efficiencies with JP-8 due to the complexities of fuel injection and combustion systems. To save money, the US military may eventually use Jet A in place of JP-8.

A.3.4 Conversion to Heavy Fuels

Falkowski et al. [39] examined the performance effects of using JP-5 in a SI two-stroke engine. The subject engine was a stratified combustion low pressure direct-injected prototype with variable spark and exhaust port timing and had a displacement of 1.5 L from three cylinders. Falkowski et al. used the variable timing features of the engine to combat knock at the higher fuel delivery rates (at or above 50%), but each approach also resulted in reduced brake torque relative to gasoline operation. Although stratified-charge combustion and timing controls helped the engine run with JP-5, problems with knock prevented full-power operation at elevated fuel flow rates and engine speeds.

Suhy et al. [40] studied the use of kerosene in a SI two-stroke and attempted to solve the problems of cold-starting such an engine with kerosene. The 388 cc engine featured a single cylinder, fuel injection, and loop scavenging as well as a vortex pneumatic atomizer that decreased the size of fuel droplets. Suhy et al. found that for operating with kerosene, except at the lowest throttle opening and even with the atomizer, knock was problematic and controlled via air-to-fuel ratios as low as 7.4:1 and retarded spark timing. The IMEP with kerosene was equal to or greater than that with gasoline,

but the WOT ISFC was significantly higher for kerosene due to the richness of the mixture and retarding spark timing for limiting knock.

Even with a very deliberate starting procedure involving gradually increasing fuel flow, atomizer pressures above 250 kPa, and kerosene at 298 K, an intake air temperature (IAT) of at least 388 K was required for cold starting when the engine was cooled to 287 K [40]. Suhy et al. did not discuss starting the engine on kerosene at temperatures other than 287 K. Attempts at starting with unheated air were unsuccessful with or without atomized fuel or a high-powered ignition box.

Suhy et al. attributed starting failures to inadequate fuel vaporization and cited 438 K as the minimum temperature at which kerosene begins to evaporate. They surmised starting is possible for an IAT of 388 K due to energy transferred to the fuel during compression and from high-temperature intake and chamber surfaces. The results indicate that because of problems with knock and cold starting, technological breakthroughs may be necessary to render kerosene a valid option for use in spark-ignition aircraft engines.

Hirsch [41] tested a 737 cm^3, twin-cylinder 2-stroke that originally ran on gasoline but had been converted to a compression-ignition heavy fuel engine with a 16:1 geometric compression ratio (CR). Direct injection requires high fuel pressure (e.g., 70 MPa) and variable timing for precisely controlling the start and duration of injection pulses as well as the amount of fuel input. The test direct injection system starts the engine with mechanical fuel injection but transitions to electronic control as electric power becomes available. Hirsch measured BSFC and found a best value of 152 g/(kWh) with the engine running 4,500 RPM at 18.6 kW using JP-5 fuel or 158 g/(kWh)

at the same conditions using DF-2. At maximum power of 32.8 kW per Liter of displacement, BSFC increased to about 182 g/(kWh).

Traditionally, Diesel engines have gone without a throttle valve because the AFR does not need to be controlled to the relatively narrow range near stoichiometric that a spark-ignition engine requires. However, the test engine featured a throttle to reduce maximum cylinder pressure and noise and to decrease cycle variability. This also allowed control of the scavenging volume, and therefore the fraction of residual gas in the cylinder, of the crankcase-scavenged 2-stroke engine. By increasing the residual fraction, the temperature of the mixture was still high enough with the lower compression pressure to ignite the fuel, and NOx emissions were decreased. Throttling the intake air at a given power level also allows a richer AFR.

Groenewegen [42] conducted tests of a 34cm^3, single-cylinder, four-stroke, spark-ignition engine with a variety of heavy fuels, including JP-8. His experiment demonstrated the difficulty of starting and running a small IC engine at low temperatures on JP-8, which has a low vapor pressure relative to gasoline. Accordingly, the engine was started on gasoline before switching to JP-8, and the inlet air was heated to aid fuel evaporation. However, the engine developed severe knock for the heated inlet air runs. Groenewegen found BSFC improvements of greater than 20% with injected JP-8 versus the stock carbureted 100 octane aviation gasoline system and suggested heavy fuels will present an attractive choice from a performance perspective if the cold-starting and knocking problems are solved.

Salter et al. [43] studied the differences between gasoline and kerosene operation in a 7.6 cm^3 loop-scavenged 2-stroke engine and found that spark-ignition, the power,

and BMEP are little changed from one fuel to the other, as shown in Figure 45. Running on kerosene, BSFC is higher than with gasoline, particularly at the lower or higher ends of the engine speed range. Salter et al. surmise that this higher BSFC results from inadequate evaporation of the kerosene or insufficient mixing with air. Salter et al. note that with the test engine as well as several others, glow ignition yielded degraded power, BMEP, and BSFC than did spark ignition. Salter et al. also believe that 2-stroke engines by nature produce lower BMEP and higher BSFC than 4-strokes due to the inefficiency of scavenging and lower effective expansion ratios.

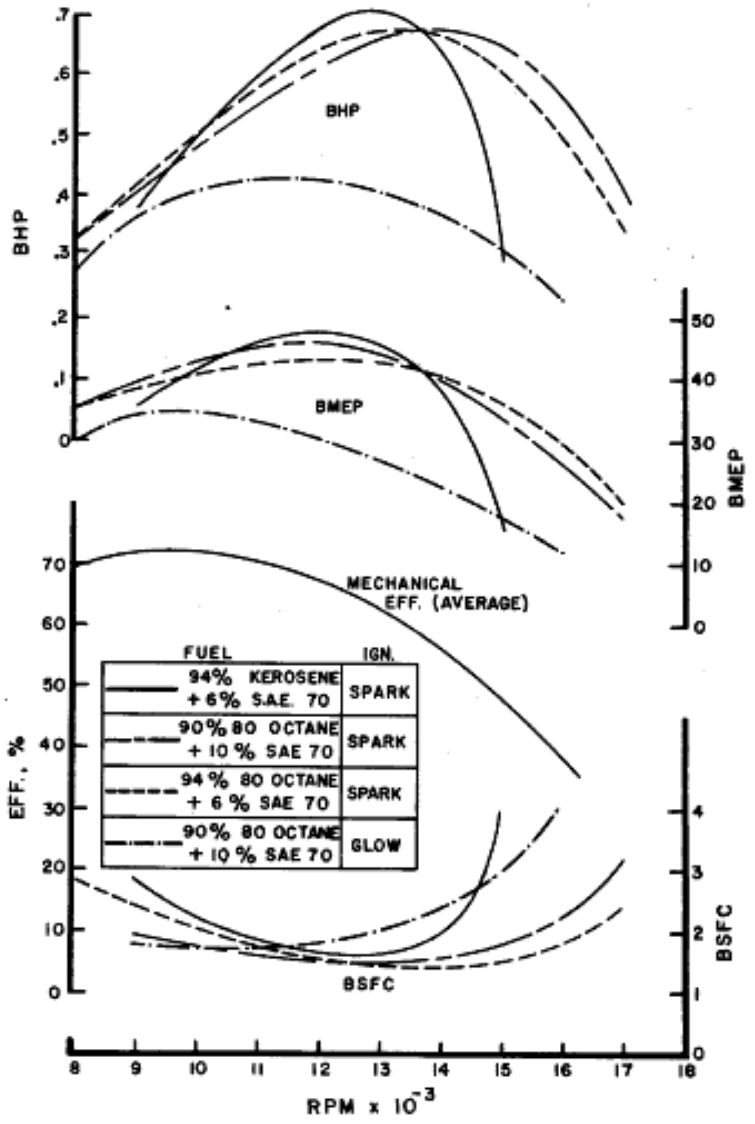

Figure 45. Loop-scavenged Performance Curves (from Salter et al. [43])

A.3.5 Knock

Knock is an undesirable phenomenon in a SI engine and is due to autoignition, that is, homogeneous reaction of the mixture in front of the flame. In contrast, autoignition is inherent in the operation of CI engines, as it provides the mechanism for beginning each combustion event. Ignition delay, a period of combustion at a low rate, is

a function of intermediate species formation [17]. A long ignition delay tends to aid to preventing knock in SI engines, while a short delay is best for a CI engine.

Wilson tested a 34 cm^3, single-cylinder, four-stroke, spark-ignition engine with both iso-Octane and n-Heptane to obtain data for brake specific fuel consumption (BSFC) and knocking [44]. He showed BSFC decreased relative to iso-Octane on average 9% with n-Heptane and spark timing advanced or retarded beyond the stock setting. Additionally, he found for this engine that knocking was not a severe problem when running on n-Heptane, which he attributed to a high cylinder surface area-to-volume ratio and low compression ratio.

Wilson further demonstrated that spark timing optimization can have significant positive effects on BSFC. He replaced the stock spark timing controller with another ignition box and used a PIC18 microprocessor chip to vary spark timing between the limits of 60 degrees before top dead center (BTDC) and 10 degrees after top dead center (ATDC) while holding the throttle position and engine speed constant. Wilson's data showed the BSFC improvement with spark timing adjusted for n-Heptane more than doubled when compared to the improvement based on stock timing. A setting of around 35 degrees BTDC resulted in the peak improvement at engine speeds above 3,500 RPM, and he surmised the optimized spark advance failed to continue increasing with speed because the AFR was varying unexpectedly [44].

A.3.6 Ignition Timing

Best-power spark advance (BPSA) results in a pressure rise that is distributed evenly with respect to top dead center. High-speed engines require little more spark

advance than normal or low-speed ones, and any difference arises primarily from the increase in combustion time prior to 10% flame travel (Taylor [9]). For a constant exhaust/intake pressure ratio, normally-aspirated aircraft engines need greater spark advance with increasing altitude because of increasing crank angles as intake and exhaust pressure decrease. Spark is advanced with increasing speed to ensure peak pressure remains in the optimum crank angle range of 15° to 20° ATDC. One benefit of higher atmospheric humidity is it makes an engine less prone to detonate [9].

SI engines use a spark plug to supply minimum ignition energy for combustion of turbulent premixed oxidizer and vaporized fuel. At low engine speeds, combustion tends to take place in the wrinkled laminar-flame regime with turbulence causing wrinkling of a mostly continuous region of burned gas surrounded by unburned gases. As the engine speed climbs, pockets or islands of unlike gas may form in either region. Combustion in SI engines in stable when the flame ignites consistently, grows at the proper rate, and reaches all portions of the chamber (Turns [17]).

Retarded ignition timing may be used in SI engines to decrease combustion temperatures for NO_x reduction by delaying the maximum pressures long past TDC. Doing so leads to decreased pressures, as the volume in the cylinder continues to rise after the point when the force acting on the piston would yield the greatest instantaneous torque. Exhaust gas recirculation (EGR) is another tactic for decreasing NO_x emissions through the reduction of temperatures. On the other hand, exhaust gases may be used to preheat the combustion air for increased flame temperatures and thermal efficiency [17].

In spark-ignition engines, combustion normally begins at an ignition point and progresses with a flame front through the charge. The elapsed time of combustion

depends on fuel type, shape and size of the combustion chamber, ignition points, and engine operating conditions such as speed (Taylor [3]). Because combustion time decreases as speed increases, the crank angle taken up by combustion is nearly constant with changing speed.

For best power and efficiency, ignition should be timed such that a point where ignition causes a steep rise in the real cycle pressure and a point where combustion is nearly finished are at almost identical crank angles from top center (TC), meaning the cylinder volumes for these two points are almost identical. In practice, later spark timing is typically chosen to decrease the likelihood of detonation [3]. An SI engine at a constant AFR with suitable spark timing tends to have almost constant ISFC even as inlet density varies. The choice of a spark timing other than for best power is for controlling detonation or to avoid the adjustment of spark with respect to the engine operating conditions (Taylor [3]).

Banish [37] provides four tips for creating ignition timing maps, and the first and most important is to avoid detonation. The second is to advance the timing with increasing engine speed because combustion must be initiated earlier in order for maximum cylinder pressure to occur at the desired time in the cycle. This desired time is in the range of 12 to 15 degrees ATDC and will provide the greatest mechanical advantage for generating torque on the crankshaft. The third tip is to retard timing with increasing cylinder load because the combustion event requires fewer crankshaft degrees. The final tip is to avoid operating at MBT at idle. By using up to 10 degrees of spark retard from MBT at idle, the ECU can increase torque when the load undergoes an abrupt change [37].

A.3.7 Exhaust

The exhaust oxygen concentration of a 2-stroke significantly higher than that of a 4-stroke and may be 10% for lean or 8% for rich operation, compared to perhaps 2% for lean or 0% for rich in a 4-stroke (Blair [2]). A tuned exhaust pipe can give a single-cylinder two-stroke racing engine a boost of 100% in power at its peak power speed by taking advantage of exhaust pressure waves to roughly double the mixture mass of fresh air and fuel trapped in the cylinder. This improvement in power production is possible when the unsteady flow is leveraged to prevent the loss of unburned fuel and air.

Ramming of the intake air results when a designer ensures a compression wave forces additional air into the cylinder or crankcase while the transfer or intake port is open. As a result, pressure waves on the intake side can increase the mass flow rate by 50% or more, or if poorly designed, these waves may drop the mass flow rate by 40%. Overall, we note pressure waves affect 2-stroke scavenging and charging to a much greater degree than they do 4-stroke engine operation. Exhaust pressure wave tuning for increasing the trapping pressure also proportionally decreases BSFC and the fraction of hydrocarbons emitted.

It is common in 4-strokes to measure the exhaust gas species for determining the air-fuel ratio. The exhaust process results in a sonic compression wave being reflected back partly as a pressure wave and partly as an expansion wave. With a tuned exhaust, an expansion wave arrives at the exhaust port during scavenging, and a compression wave arrives at the exhaust port as it is closing. The effects of tuning can double the trapped fresh charge mass and therefore double the power. Exhaust tuning can improve power to a greater degree than intake tuning for large crankcase clearance volumes. For

small crankcase volumes, intake tuning is more beneficial. With both the exhaust and intake systems tuned, the maximum delivery ratio improvement is nearly independent of crankcase clearance volume. In addition to increased power (Heywood and Sher [8]), exhaust tuning can provide a BSFC reduction of 15% and thereby make up for short-circuiting.

Pressure waves in a long exhaust pipe can be timed so that exhaust pressure is low during the initial portion of the scavenging process and high at the end of the process, so that the exhaust port essentially closes as if a valve were present. The exhaust pressure of a 2-stroke engine has a significant effect on power via the ratio of gas flow rate divided to piston area. Scavenging of a 2-stroke engine, discussed in section II.4.10 of this document, requires an exhaust pressure less than its scavenging pressure. The exhaust pressure can be calculated from the inlet pressure and, as determined by the scavenging ratio and engine flow coefficient, the exhaust/inlet pressure ratio (Taylor [3]).

A.3.8 Cold-Starting

Cold starting in automotive direct-injected Diesel engines at temperatures as low as 244 K is now enabled in most cases by glow plugs, but their operation creates a high demand for electrical energy (Hirsch [41]). Figure 46 shows the effect of intake air temperature and the rate at which a Diesel engine is cranked on the temperature in the combustion chamber at the end of the compression stroke. The “Temperature for Reliable Starting” line in Figure 46 is at around 343 °C, or 616 K. At an intake air temperature of 253 K, the subject engine required a cranking rate of 200 or more RPM in order to reach the reliable starting temperature in the cylinders.

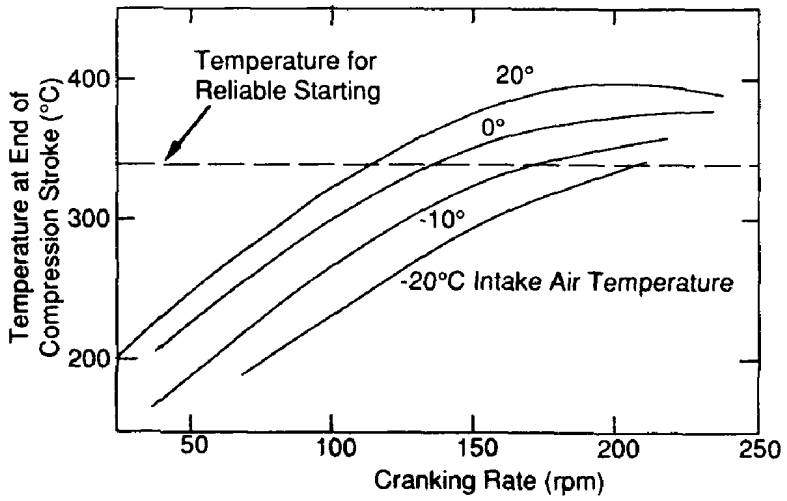

Figure 46. Diesel engine temperature at end of compression (from Diemand [45])

Ayoub and Reitz [46] modeled a Caterpillar 6-cylinder Diesel engine of 14.6 L displacement in studying the effects of fuel composition on combustion. For cold-starting, several cycles at a predictable frequency may occur without firing while sufficient fuel accumulates to allow combustion to occur. A change to 5% residual fuel from 10% carried from one cycle to the next caused a slower rate of combustion for an air temperature of 273 K, but 10% was inadequate for the delayed ignition at 254 K. The negative effect of reduced air temperature was mitigated by altering the residual fuel to contain more cetane, yielding a higher cetane number and lower ignition delay [46].

Montemayor and Owens [47] studied the effects of fuel on cold-starting a 3.48 L turbocharged uniflow-scavenged 2-stroke 4-cylinder CI engine for which starting aids were recommended at ambient temperatures below 277 K. They cite atmospheric temperature, effective compression ratio, cranking speed and time, and injection timing as the most important parameters for determining air temperature at injection but say fuel properties do have a significant effect on autoignition. Cetane number is a quantitative

measure of the physical and chemical delay periods between injection and ignition and indicates the ease with which a Diesel engine may be started for the associated fuel. Using dry ice to control temperatures and a cranking speed of 150 RPM, Montemayor and Owens found that fuel viscosity, volatility, autoignition temperature, and cetane number each have a meaningful effect on minimum unaided starting times [47].

Henein et al. [48] created a model for cold-start cranking of CI engines and report agreement with experimental data showing fuel volatility is just as important as cetane number for predicting the required number of cranking cycles for low-temperature starting. Cold-starting problems may involve white smoke, extended cranking duration, misfires or hesitation, or simple failure to start. JP-8 has higher volatility and a lower cetane number than DF-2, and the injection timing and rate for JP-8 should be adjusted from that of DF-2 to preserve power and BSFC [48].

Appendix B: Additional experimental set-up information

B.1 Low power

Replicating the previous researcher's recorded power curves (Crosbie [16]) proved to be a non-trivial task, and troubleshooting led to ineffectual replacement of the spark plug, oxygen sensor, fuel injector, and sensors for the fuel injection system. A compression check was conducted twice, and the measured pressure of 1 MPa gauge was deemed to be in the expected range. The bulk of the data was interpreted to indicate the most direct cause of the reduced power was unexpected deviation of the air-fuel ratio from the desired value of around 13, but the data collected after the AFR was controlled to the range of 13 to 14 showed no improvement in performance. Most of the early data showed the engine was running rich with an AFR of 10.5 to 12.

As the airflow through the engine was not known to have significantly changed, fuel flow rates inconsistent with those from the previous research appeared to be the main contributor to the primarily rich observed AFR. The Ecotrons fuel injection system offers an option of using a global fuel enrichment factor to coarsely adjust AFR, but adjusting the enrichment factor never gave satisfactory results in the course of this research. Beginning with a factor of 1 and changing to factors as low as 0.7 and as high as 1.5 with increments of 0.05 or 0.1 either led to the engine failing to start or running only temporarily at the desired AFR before stalling or changing to a different AFR. In any case, the enrichment multiplier was intended to adjust fuel flow rates uniformly at all conditions, but only for short-term troubleshooting.

Troubleshooting problems with the fuel injection system continued, and it was noted the MAP sensor gauge built into the fuel injection graphical user interface showed a pressure of 104 kPa when the engine and compressor were at rest. However, the local atmospheric and chamber pressure was around 99 kPa. After observing the MAP indicated by the fuel injection system did not match the pressure coming from a transducer in the same location, it was thought updating the MAP calibration would allow the air-fuel ratio (AFR) to be properly adjusted for the conditions in the throttle body.

Personnel affiliated with the Air Force Research Laboratory (AFRL) observed that an incorrectly elevated MAP should result in rich operation because the fuel injection system would assume the cylinder was being filled with a greater mass of air than existed in reality. Following the vendor's instructions for re-calibrating the MAP sensor, it was believed that an accurate indicated MAP would bring the AFR back to the desired range. Two sets of measurements using an Omegadyne pressure transducer inside the chamber at several test conditions between local atmospheric pressure and the minimum pressure attained with the compressor at full speed allowed the linear curve in Figure 47 to be constructed for the corresponding voltages from the MAP sensor.

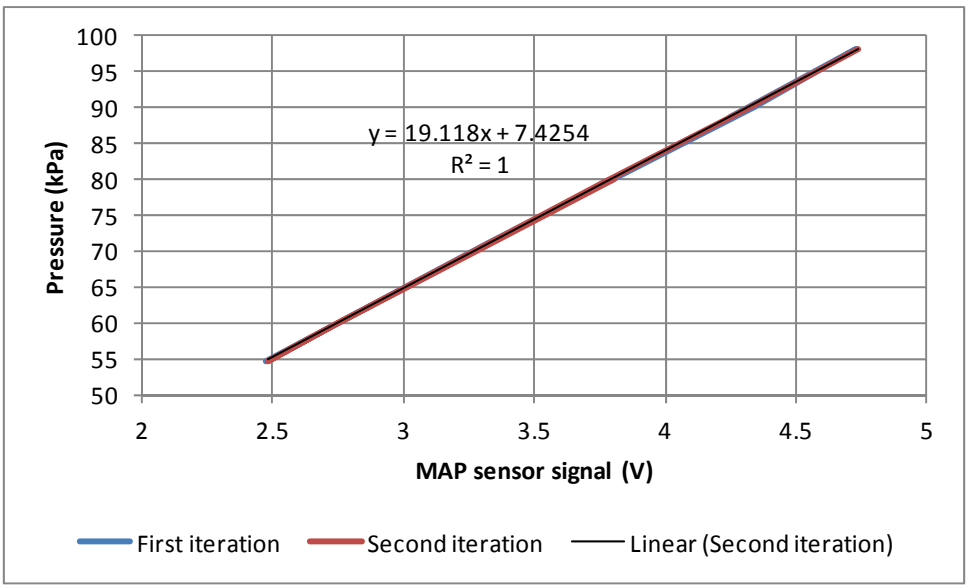

Figure 47. Pressure transducer readings vs. MAP sensor signal

Unexpectedly, after each re-calibration, the gauge continued showing a MAP around 5% higher than that calculated from the equations supplied by the fuel injection company, Ecotrons. Eventually, Ecotrons confirmed their software used a hidden multiplier of 1.05 for the MAP, and the indicated MAP was actually designed to be 5% high. Ignoring the hidden multiplier, the MAP calibration equation used for data collection was the default:

$$MAP = u_{MAP}188.6406 + 105.6641 \tag{36}$$

where u_{MAP} is the MAP sensor signal voltage and each term has final units of hPa.

Innovative Scientific Solutions, Inc., (ISSI) personnel on contract with AFRL suggested replacing the MAP sensor with a potentiometer in order to vary the indicated MAP and by extension the AFR. The potentiometer and a resistor were added to the MAP wiring to yield the desired voltage signal and send it to the ECU. Tests with constant actual air pressure showed no change in AFR even as the MAP reported by the

fuel injection system swept through a range of 50 to 110 kPa by use of the potentiometer shown in Figure 48.

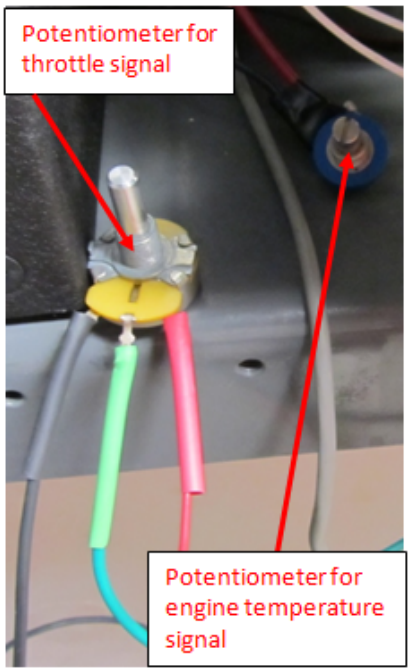

Figure 48. Potentiometers for varying throttle and engine temperature signals

The expected result was a change in AFR inversely proportional to the change in calculated MAP. For example, for constant actual air flow and an initial AFR of 12, a change in calculated MAP from 100 kPa to 50 kPa would result in a change of AFR to a very fuel-lean value of 24 because the fuel injection system would supply less fuel in response to the lower calculated air flow rate.

Follow-up queries to Ecotrons personnel revealed the MAP actually is not used for fuel pulsewidth determination while the ECU is operating in open-loop, so in that case MAP has no bearing on the fuel flow rate or AFR. All data for this experiment were taken with the fuel injection system operating in open-loop with no feedback from the oxygen sensor. Consequently, the variable MAP signal from the potentiometer was quite

useless for adjusting AFR, but the signal was instead used to control the throttle position signal and, by extension, AFR.

All test points for this thesis were at WOT, so a linearized fuel map was constructed that in tandem with the variable allowed practically linear changes in fuel flow rate and AFR at a given engine speed when the engine was warm. Data were taken in this way with the AFR controlled in the range of 13 to 14 at the three primary pressure altitudes of 0.2, 1.5, and 3 km for the research. Then, it was possible to analyze the recorded throttle position signals and correlate them to load values for building an updated WOT row for each of three pressure altitude-specific fuel maps.

In the late stages of this research, after repeated failures of the fuel injection system's engine temperature sensor due to vibration, a second potentiometer was added to the rig to provide a user-defined variable signal to prevent the system from continuously providing extra fuel for warm-up. The sensor from which LabView recorded this engine temperature measurement was used to provide indication of the warm-up state of the engine and guide adjustment of the second potentiometer (shown in Figure 48). The desired range for the second potentiometer was the actual engine temperature range 290 to 480 K. This control feature was not used for any of the data reported in this thesis, but it did allow a work-around after all the engine temperature sensors for the fuel injection system had failed.

The test engine was run at ground-level pressure to provide a baseline of performance against which the altitude data could be compared. Although existing research has shown how pressure affects operation of the Brison 95 cm^3 engine at altitude, this study investigated and characterized the combined effects of pressure and

temperature on a small IC engine. The major performance parameters studied include BSFC, BMEP (strongly related to engine torque), and brake power.

B.2 Electrical systems

Several updates were made to the rig and its LabView interface for troubleshooting, fool-proofing and introducing system protection features. The exhaust system was modified to replace a damaged threaded aluminum flange with a stainless steel bar represented in Figure 49, and vibration of the exhaust pipe was then much more controlled with the welded configuration shown in Figure 50. A screen was fabricated and added to compressor inlet to protect it from foreign object debris, and finer control of the compressor serves to prevent over-speed problems. A thermocouple for the dynamometer cooling water outlet and a fuel pressure transducer were added, and LabView now gives alerts or warnings for engine head or dynamometer water temperatures in excess of the values specified in Table 16.

The fuel pressure sensor was originally added for troubleshooting fuel flow problems, but it now provides an additional safety control, as fuel pressure is monitored continuously in LabView and fuel flow is automatically cut off by a fail-safe pneumatic valve if a leak causes the gauge pressure to fall below a specified value. The chosen value of 300 kPa for the threshold fuel pressure is also shown in Table 16. Also, because the default minimum allowable gauge pressure is 400 kPa and a regulator holds fuel pressure at a steady 304 kPa after the fuel pump is powered up, fuel will not flow unless the operator enters a minimum allowable gauge pressure of 0 kPa in the “set-up” tab of the LabView interface before attempting to start the engine.

Table 16. Threshold values for LabView safety controls

Parameter	Minimum value for alert status	Minimum value for warning status
Dynamometer cooling water temperature	355 K	366 K
Engine head temperature	450 K	478 K
Fuel pressure	300 kPa	300 kPa

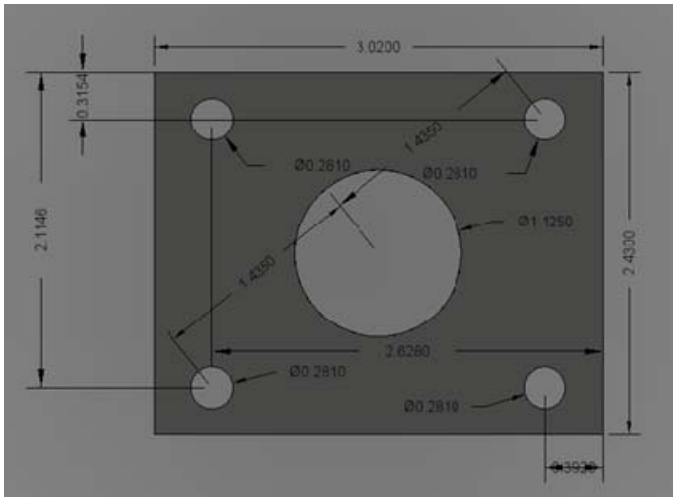

Figure 49. CAD drawing of stainless steel exhaust flange

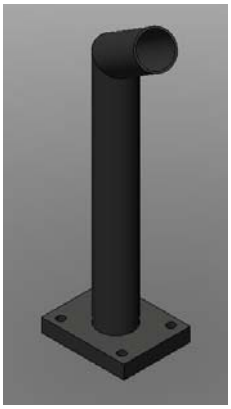

Figure 50. Stainless steel exhaust pipe and welded flange

Electrical problems were endemic throughout this research effort, due at least in part to the highly vibratory nature of the single-cylinder engine and its connection to the chamber floor and dynamometer shaft. Early troubleshooting of the fuel injection system uncovered a failed crank position signal for the ECU. Examination showed there was simply no connection from the crank position sensor to the ECU, which meant the ECU did not know the engine's rotational speed, although the signal was reaching the ignition box and allowing the engine to run in a degraded state with the desired spark once per revolution.

The previous researchers had not made use of the air mass flow meter in the compressed air line, and after noting erroneous indicated air flow rates, it was discovered the meter was simply wired incorrectly. Also, the air mass flow calculated in LabView was based on an incorrect equation, so the software was updated accordingly. However, even after the errant wiring and code were fixed, the calculated AFR values from the air and fuel mass flow meters still did not correlate with the more believable oxygen sensor measurements, presumably because pressure oscillations in the air line rendered the measured air mass flow unreliable. The fuel flow meter did appear to be reporting accurate flow rates, as the indicated volumetric flow matched the volume measured in a graduated cylinder within 1% during a verification test of the meter.

B.3 Compressor

An automotive supercharger, which is a belt-driven radial compressor, made it possible to decrease the chamber pressure below atmospheric and gather temperature effect data from a small engine operating at simulated altitude. Schmick [25] supplied a

compressor map for the Vortech supercharger installed on the rig, and mass flow rate data reflected in Figure 51 were gathered to shed light on the compressor operating line. It is possible to monitor the operating condition on the compressor map in real time during testing with one of the LabView interface tabs. The experiment started with an attempt to reach 100% compressor speed with the manual control valve closed and the electrically-actuated valve fully open.

During attempts to maximize the compressor flow rate, the VFD shut down the compressor four times due to apparent over-current failures. Next, an attempt was made to reach 100% compressor speed operating just inside the stall line with the manual valve closed and electrically-actuated valve partially closed. The recorded data for the operating parameters are shown in Table 17, and points 1 and 2 correspond to over-load conditions for the VFD. Point 3 yielded the minimum chamber pressure of 55.2 kPa (inlet 55.3 kPa, outlet 54.2 kPa).

Table 17. Compressor operating parameters

Point	Com-manded speed, %	Throttle valve position, % closed	Outlet pressure, kPa	Pressure ratio	Corrected speed, kRPM	Corrected mass flow rate, kg/s	Mass flow rate, kg/s
1	81	0	120	1.51	33	0.386	0.258
2	76	0	118	1.45	31	0.355	0.248
3	100	37	108.4	2.00	40.5	0.254	0.128
4	100	27	110.5	1.97	40.5	0.296	0.151

The 4.5 km-equivalent chamber pressure of 57.2 kPa (inlet 57.3 kPa, outlet 56.0 kPa) occurred with the parameters shown in point 4 of Table 17. During sustained operation at a pressure altitude above 4 km, the maximum observed mass flow rate was

0.232 kg/s, and the maximum corrected mass flow rate was 0.324 kg/s. A variety of observed operating points are plotted on the compressor map in Figure 51.

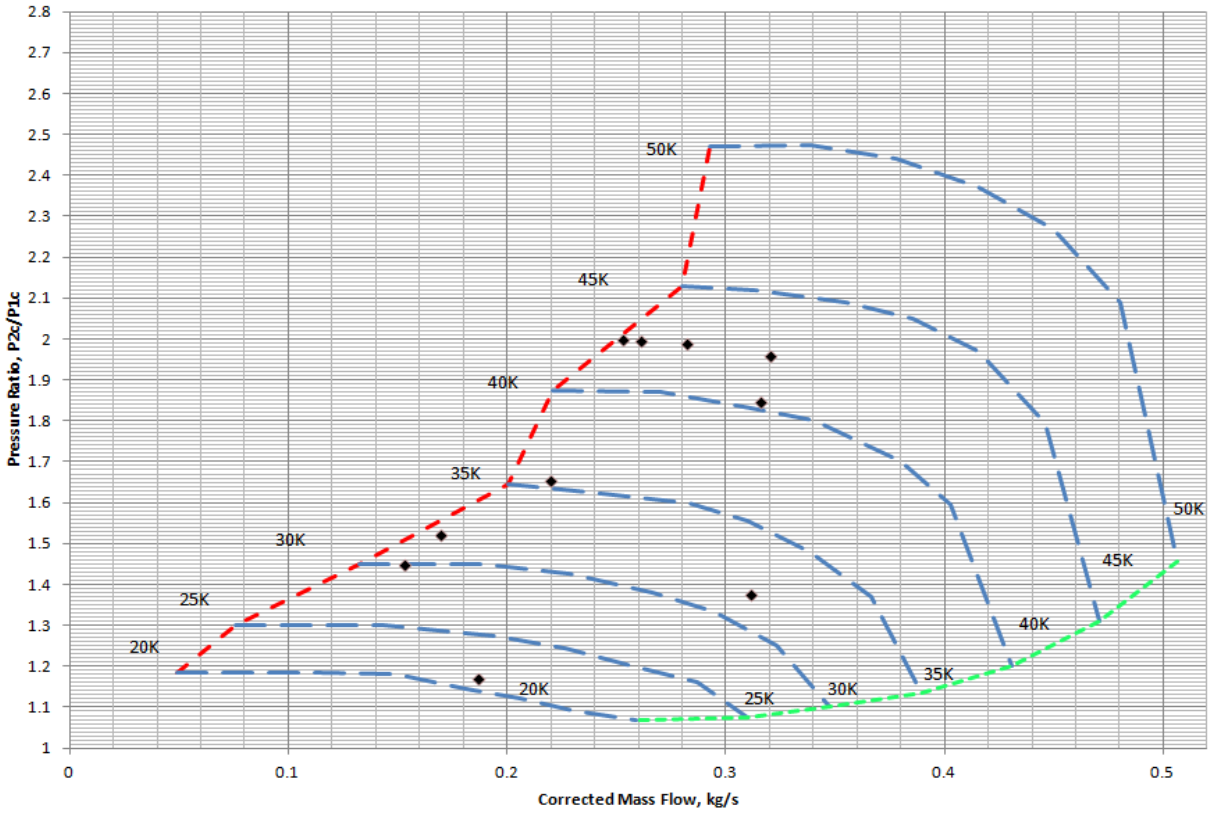

Figure 51. Compressor map with recorded operating points shown as black dots

The corrected mass flow rate $\dot{m}_c$ as recorded in LabView, with units of lbm/min, is calculated from Equation (37), where the actual measured air flow rate MAF is in lbm/s, the temperature $T_{cooling_{out}}$ of the air entering the compressor is in K, and the inlet and outlet pressures at the compressor are in kPa absolute.

$$\dot{m}_c = 60MAF\sqrt{\frac{T_{cooling_{out}}}{298.15}}\frac{P_{compressor_{out}}}{P_{cooling_{out}}} \tag{37}$$

The corrected compressor speed N_c as recorded in LabView, with units of RPM, is calculated from Equation (38), where $V_{compressor_{out}}$ is the voltage signal for controlling the compressor and $T_{cooling_{out}}$ is again the temperature of the air entering the compressor, with units of K.

$$N_c = \frac{V_{compressor_{out}} 4016.628}{\sqrt{\frac{T_{cooling_{out}}}{298.15}}} \tag{38}$$

The unit-less pressure ratio π_c as recorded in LabView is the final term of Equation (37) and is shown again in Equation (39)

$$\pi_c = \frac{P_{compressor_{out}}}{P_{cooling_{out}}} \tag{39}$$

Neglecting any air flow coming from the shop air source, the uncorrected compressor mass flow rate $\dot{m}$, with units of lbm/s, is simply the measured air mass flow rate MAF

$$\dot{m} = MAF \tag{40}$$

The uncorrected compressor speed N is the numerator of the right hand side of Equation (38), with units of RPM, and may be calculated from Equation (41)

$$N = N_c \sqrt{\frac{T_{t_{in}}}{T_{ref}}} = V_{compressor_{out}} 4{,}016.628 \tag{41}$$

Because the electric motor used to power the compressor is a rotating system, its power $\dot{W}_{motor}$ may be calculated from the voltage V and current I mentioned in Equation (35) or from its torque τ and speed N at a specific condition, as shown in Equation (42):

$$\dot{W}_{motor} = VI = \frac{N\tau_{N-m}}{9.549} = \frac{N\tau_{lbf-ft}}{5{,}252} \tag{42}$$

where the calculated power will have units of Watts if based on either Volts-amperes or Newton-meters. Alternatively, the power will have units of horsepower if based on pound-feet.

The denominators of the two torque-based portions of Equation (42) are derived from the need to reconcile N in RPM with the angular dimensions of 2π radians per revolution. The power required to drive the compressor is delivered by a belt and an electric motor (Schmick [25]). In the following power equation, ΔT is the temperature change of the gas as it flows through the compressor. Looking back at Equations (37) through (39), T_{inlet} is equal to $T_{cooling_{out}}$, P_{exit} is $P_{compressor_{out}}$, and P_{inlet} is $P_{cooling_{out}}$. For the remaining variables, $\overline{C_p}$ is the mean specific heat at constant pressure, R is the specific gas constant of the gas flowing through the compressor, and η is the compressor's efficiency

$$\dot{W}_{compressor} = \frac{\dot{m}C_p\Delta T}{\eta} = \frac{\dot{m}\overline{C_p}T_{inlet}\left(\left(\frac{P_{exit}}{P_{inlet}}\right)^{\frac{R}{\overline{C_p}}} - 1\right)}{\eta} \tag{43}$$

B.4 Diffuser

Crosbie designed an inlet manifold that is shown in Figure 52 through Figure 55 to damp out air pressure oscillations that would negatively affect the operation of the engine [16]. The previous inlet design utilized half-inch stainless tube and caused 20.7

kPa drops in pressure with a calculated inlet Mach number between 0.4 and 0.5 during engine start.

Crosbie found the manifold to be incompatible with the test engine while carbureted. The combination of high Mach number and flow oscillations caused by the reciprocating piston motion prevented smooth engine operation. The additional 549 cm^3 of inlet volume in the manifold was intended to prevent the intake line pressure from dropping more than 0.7 kPa. Crosbie did not attempt to use the manifold after converting the Brison test engine to fuel injection [16].

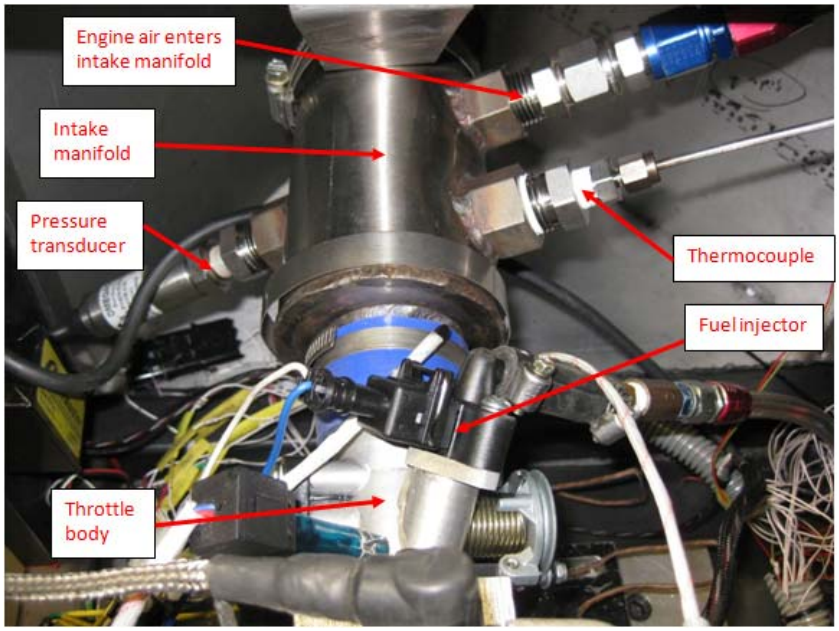

Figure 52. Diffuser and engine air sensors

The inlet manifold required modification in order to physically connect to the fuel-injected version of the Brison engine. Because the diameter of the throttle body is around 3.8 cm, a 2.5 cm length of tubular steel with a similar outer diameter was welded to the manifold in place of the carburetor fitting. Then, as neither the throttle body nor

manifold were threaded, the hose visible in Figure 53 was added to provide a physical seal between them and ensure all of the measured flow in the engine air stream was actually entering the engine.

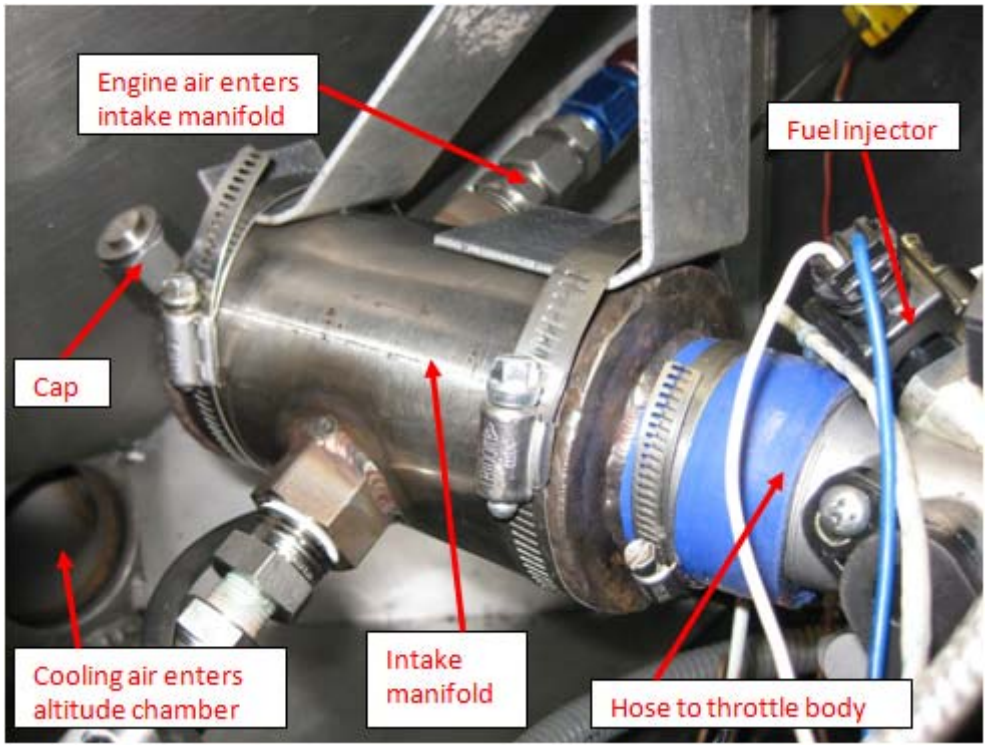

Figure 53. 7.6 cm diameter intake manifold

Of the three intake manifold configurations tested, none yielded the expected power. Initially, the manifold had no openings to the chamber, and the air flowing through the engine could be measured with a meter positioned outside the chamber. Such a set-up, in theory, allowed accurate calculation of the air-fuel ratio directly from the measured flow rates of the two fluids. Although the measured intake air pressure was above atmospheric and therefore effectively supercharged, the power output of the engine was still unacceptably low. Figure 54 illustrates how the measured wide-open throttle (WOT) power for three speeds at 155 kPa inlet pressure fell approximately on or below

the 98.5 kPa power curve of Crosbie [16], although the better than 50% increase in pressure would be expected to result in a significant boost in power.

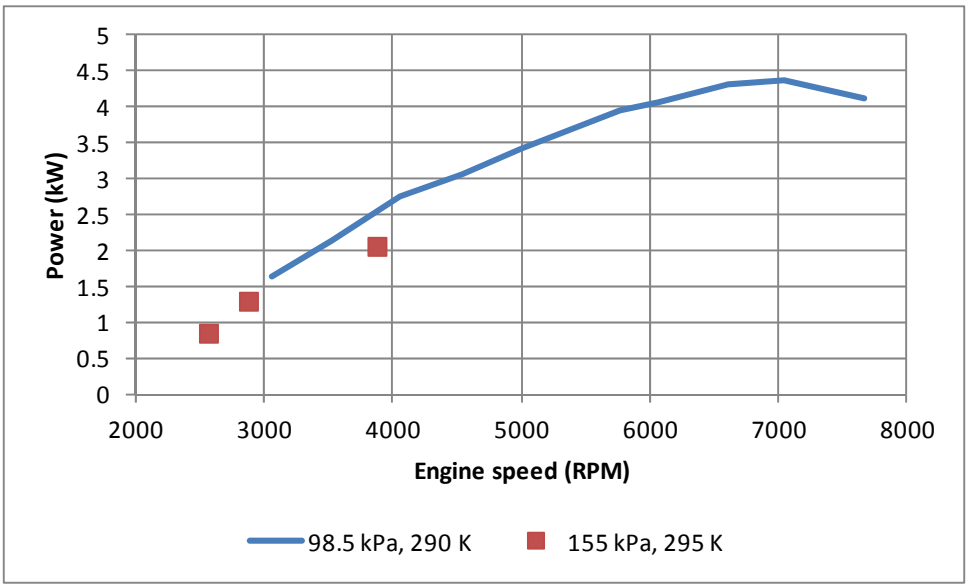

Figure 54. Power with elevated inlet pressure relative to curve from Crosbie [16]

The Crosbie manifold when paired with fuel injection allowed the engine to start and run, but the results were unsatisfactory. For example, the engine only produced 2 kW of power at a speed and condition for which Crosbie recorded around 2.5 kW [16]. The manifold was equipped with an extra port (shown capped in Figure 53), and it was thought perhaps opening that port to the chamber air would allow the pressures to equalize between the manifold and chamber. When testing with the open port failed to lead to the previously demonstrated power, a third configuration was used. Two ports were left open to the chamber and all the air for the engine was routed from the chamber through the manifold rather than coming from the compressed air line and heat exchanger.

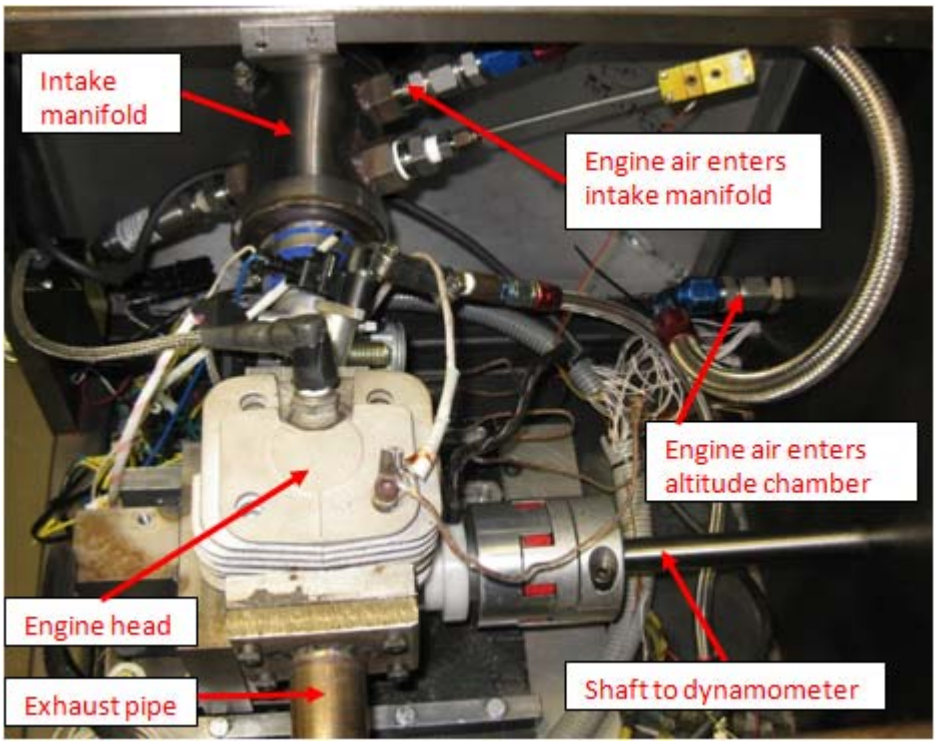

Figure 55. Intake manifold and engine

Having failed to find an acceptable iteration of the inlet manifold, which in any case had no inherent capability to allow the compressed air stream to drop below atmospheric pressure for altitude testing, it was necessary to find an alternative method to supply chilled air to the engine. A request for quote was submitted to the Super Radiator Coils company for a large heat exchanger able to chill cooling air with a water vapor proportion of 1% by mass. The assumed values for the exchange of heat from dry air to liquid nitrogen are shown in Table 18. The heat transfer rate $\dot{Q}$ is a function of the heat capacity and temperature change (Bergman et al. [49]):

$$\dot{Q} = \dot{m} C_p \Delta T \tag{44}$$

Table 18. Assumed values for heat transfer

Fluid	$\dot{m}$**, kg/s**	C_p**, kJ/(kg*K)**	$\mathbf{T_{in}}$**, K**	$\mathbf{T_{out}}$**, K**
Dry air	0.168	1.003	299.8	237.7
LN_2	0.046	2.042	81.5	--
N_2 (gas)	--	1.07	--	199.8

Assuming the change in specific enthalpy simplifies for this problem to

$$\Delta h = C_p \Delta T \tag{45}$$

and noting the desired phase change from liquid to gas for the nitrogen, we arrive at the specific enthalpy change for nitrogen:

$$\Delta h_{N_2} = C_{p_{LN_2}} \Delta T_{LN_2} + h_{fg} + C_{p_{N_2}} \Delta T_{N_2} \tag{46}$$

where h_{fg} is the specific enthalpy of vaporization and is assumed to be 200 kJ/(kg*K) for nitrogen. The calculations translate to a cooling capacity of 10.5 kW for dry air and 15 kW for nitrogen, and the manufacturer reported a capacity of 15.5 kW for the specified exchanger. However, rather than purchasing a large heat exchanger and using it to control the temperature of a single air stream, it was decided to use the two air stream approach (with liquid nitrogen lines shown in Figure 56) and find a way to control the two pressures simultaneously.

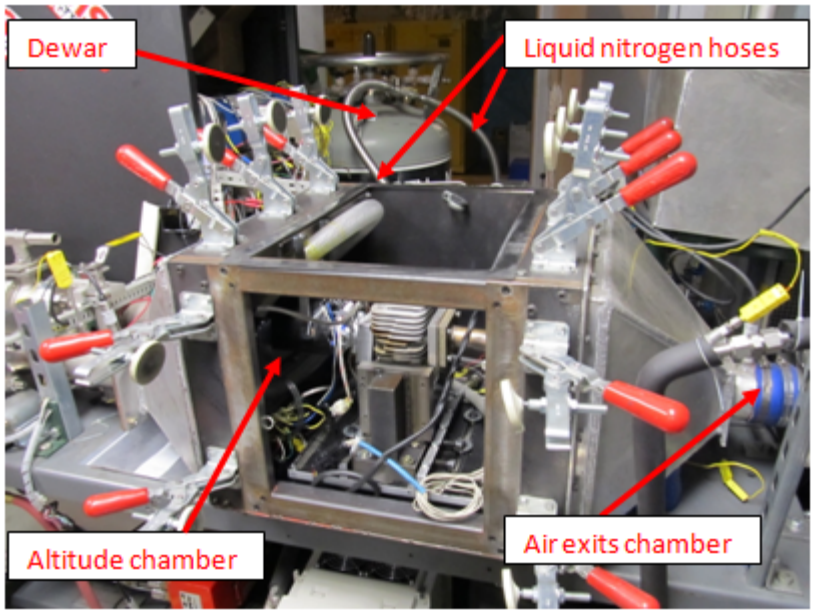

Figure 56. Dewar and chamber

For the problem of matching the pressures of two air streams, the first potential solution examined was based on using an electronic dome-load pressure regulator and control system. In conjunction with dry shop air, the system would use feedback control for the engine air pressure while retaining the existing supercharger for controlling the cooling air pressure. The electronic system called for special components to meet the specific requirements of this research, and the cost and lead time for the system were both greater than desired.

The final diffuser began as a 7.6 cm pipe and was cut to a length of 20 cm. The pipe came with threads already cut at one end, and this facilitated incorporation of a threaded cap to allow easy access to the internal portion of the pipe from either end. Starting at the threaded end, a lathe was used to increase the inner diameter of the pipe to 8.1 cm for a length of 7.6 cm. The perforated plate shown in Figure 57 was also cut to a

diameter of 8.1 cm before being press-fit into the pipe. The lip created by the lathe operation prevented the plate from moving in the downstream direction, and the press fit was sufficient to restrain the plate from moving in response to any upstream forces.

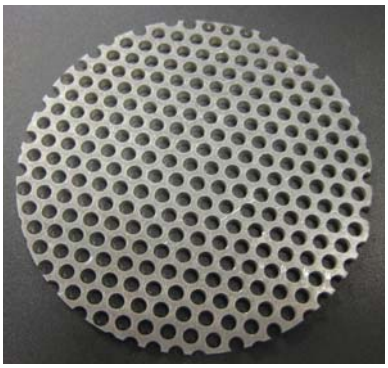

Figure 57. Perforated plate for flow distribution in diffuser

A 2.5 cm inner diameter hose barb visible in Figure 58 was cut and then welded onto a equal size hole in the wall of the pipe with a centerline located 3.8 cm from the threaded end of the pipe. Doing so provided an inlet port for air to enter a plenum section of the diffuser before flowing through the perforated plate. The plate was meant to distribute flow more evenly across the sectional area of the diffuser and prevent a high-velocity jet with a high stagnation pressure from entering the throttle body and practically creating a supercharging effect.

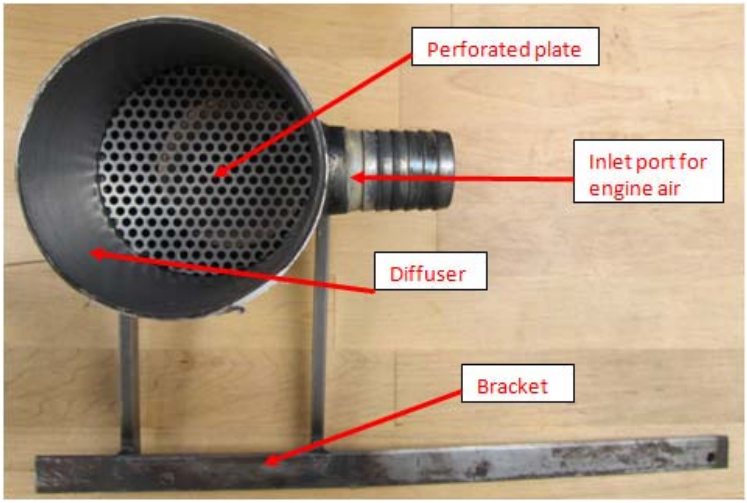

Figure 58. Diffuser viewed from upstream end

Grinding the downstream end of the diffuser was necessary to prevent physical interference with the throttle body and fuel line and injector. Fittings for pressure and temperature ports were welded onto a capped pipe downstream of the perforated plate.

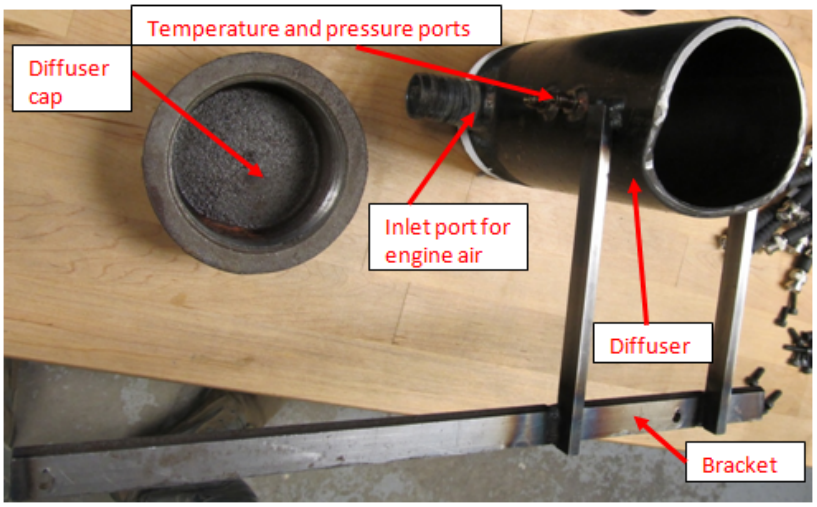

Figure 59. Diffuser with cap uninstalled

The first version of the cylindrical diffuser incorporated a straight reducer hose coupler, pictured in Figure 60, with inner diameters of 8.9 and 10.2 cm at its two ends.

The 8.9 cm end was clamped onto the downstream end of the diffuser to extend the diffuser further beyond the entrance plane of the throttle body and reduce the likelihood of mixing nitrogen-enriched cooling air with the engine air. The coupler provided a flexible, close fit around the fuel injection and throttle body components while still allowing the engine air to flow either into the throttle body or into the chamber.

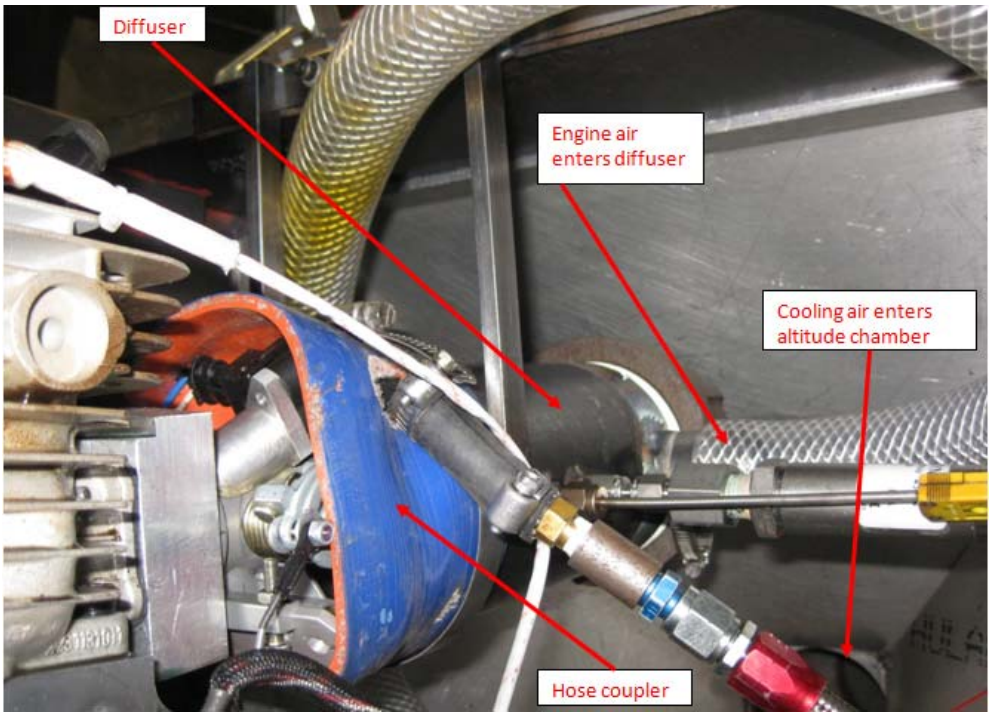

Figure 60. Hose coupler for diffuser

Whereas the intent was for the two pressures to remain virtually identical at any engine air flow rate, testing showed the coupler was significantly restricting the engine air flow. At high mass flow rates, its static pressure rose above the cooling air pressure by 20 kPa. Therefore, the coupler was removed for all further testing. The remainder of the diffuser design, shown in Figure 61, was retained.

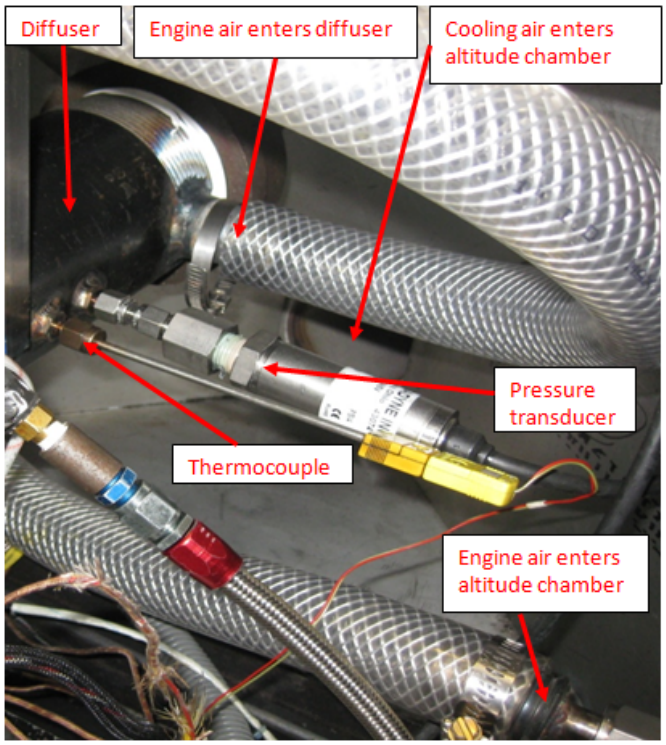

Figure 61. Diffuser from bulkhead fitting to plenum

After removing the hose coupler from the diffuser, the measured differential pressure between the diffuser and the chamber only rose by approximately 0.1 kPa at maximum mass flow rate. The air supply system was now in its final configuration (pictured in Figure 62). The close proximity of the diffuser exit to the throttle body and fuel injection components is evident in Figure 19.

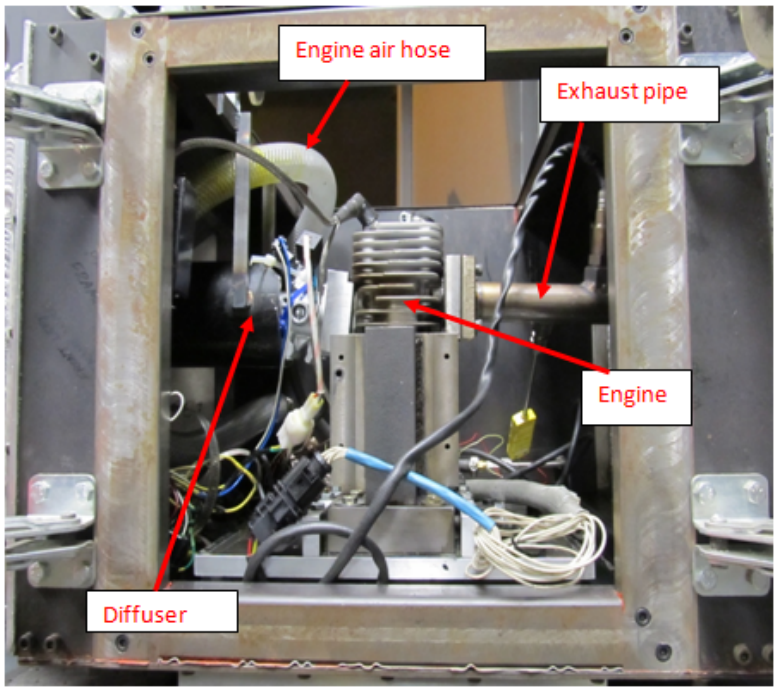

Figure 62. Diffuser and engine

The initial free jet design was based on a simple steel funnel with a half-inch tube fitting welded to its small-diameter end, and the engine air would have issued freely from the funnel's large-diameter end to either the throttle body or the chamber's cooling air mass. Personnel at ISSI and AFRL were concerned the funnel's tube fitting was too small to keep the required mass flow entering the diffuser cone at around Mach 0.05 and low stagnation pressure. Furthermore, the half-angle of the cone was greater than 7 degrees and therefore could allow separation in the transition section. Separation could in turn create a recirculation zone in which nitrogen-enriched cooling air could enter the funnel and throttle body. The two major design issues to be addressed for the diffuser were keeping the engine air's total pressure at approximately the static pressure of the

chamber's cooling air and keeping the oxygen content of the engine air at about 21%. The funnel design for the diffuser was never tested.

Previously, the engine received its intake air from the cooling air flowing through the chamber. In utilizing the heat exchanger, the chemical constituents of atmospheric air were preserved. The temperature of the cooling air stream, on the other hand, was independently controlled by direct injection of LN_2, and the concentrations of oxygen and nitrogen in the chamber air were thus no longer representative of what the engine would encounter in the atmosphere.

The decision was made to implement the "free jet" approach for supplying chilled air to the engine. Mass flow is driven by pressure difference between shop air source, compressed to up to 700 kPa gauge, and the cooling air pressure in the chamber. The mass flow rate was targeted at two to four times that demanded by the engine, and it was desired to keep the stagnation pressure nearly equal to the static pressure of both air steams by reducing the velocity of the air to no greater than Mach 0.05.

Appendix C: Additional analysis and results for temperature effects at 3 km

The effects of temperature on power at a pressure altitude of 3 km are depicted in Figure 63. The two lower temperatures led to enhanced power relative to the 295 K curve below 6,000 RPM. Recalling the assumption of an exponent of 0.8 for the temperature ratio in calculating a power correction factor, the power curves at 278 and 268 K are again expected to have values of around 105 and 108%, respectively, of the 295 K baseline at each point.

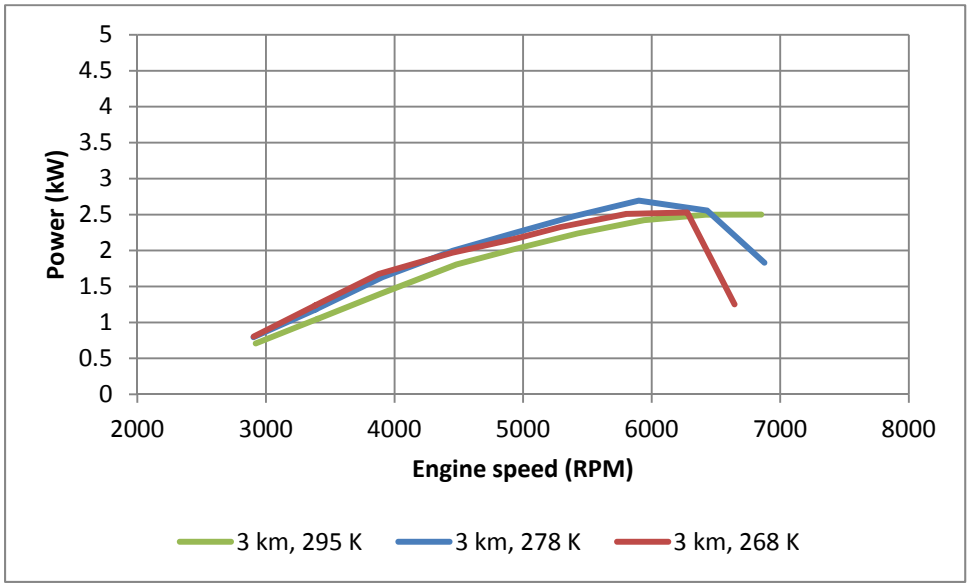

Figure 63. Power curves for temperature sweep at 3 km altitude

The power ratio ranges between 107 and 116% for the 278 K curve between 3,000 and 6,000 RPM, but it drops below 75% at the 7,000 RPM setpoint. The power ratio ranges between 104 and 120% for the 268 K curve between 3,000 and 6,000 RPM, but it drops to 50% at the 7,000 RPM setpoint. The 268 K curve shows a more noticeable degradation of the power advantage between 5,000 and 6,000 RPM than does the 278 K condition. There is a dramatic loss of power at the highest speeds for both of the lower

temperature curves, and none of the three temperatures led to tolerable engine performance above the 7,000 RPM setpoint for this altitude.

Comparing peak power values among the three curves, the 278 K curve has 108% the peak of the 295 K curve, while the 268 K has its peak at 101% the 295 K peak. The expected trend was for the 268 K condition to have a greater power advantage over the 295 K temperature than the 278 K would. It is clear from Table 19 that without considering uncertainty, the peak power data do not follow the theory (Harari and Sher [11]) for the 3 km pressure altitude.

Table 19. Temperature effects on power at 3 km

Temperature, K	**Power multiplier, expected (4-stroke)**	**Power multiplier, expected (2-stroke)**	**Peak power multiplier, observed**	**Temperature ratio exponent, observed (peak)**	**Error from calculated with 0.8 exponent, %**
278	1.03	1.05	1.08	1.6	+3
268	1.05	1.08	1.01	0.2	-6

The loss of performance advantage at 3 km for the colder temperatures at speeds above 6,000 RPM is again visible in the BMEP curves of Figure 64. While the BMEP for the 295 K condition remains fairly constant on either side of 250 kPa, BMEP falls below 200 kPa at speeds above 6,500 RPM for the 278 and 268 K curves. The curves are each approximately constant in the region of their respective maximum values between 4,500 and 6,000 RPM, so it may be concluded the engine has its greatest volumetric efficiency in approximately the middle of the speed range, even as the pressure altitude

rises to 3 km. Indeed, referring back to Figure 22, this trend holds at the highest attained pressure altitude of 4.5 km, at least for a temperature of 295 K.

The compensatory effect on power of having relatively constant torque at the higher engine speeds is evident in Figure 64, in which the BMEP curve for 295 K has a peak noticeably lower than the peaks of the 278 and 268 K curves, when compared to Figure 63. In fact, the 278 K curve in Figure 64 has 111% the maximum BMEP of the 295 K peak, and the 268 K curve has its BMEP peak at 107% of the 295 K peak. Noting the values in Table 19, the analogous multipliers for peak power were lower in each case, at 108% and 101%.

The loss of torque and BMEP at the highest speeds for the two lower temperature curves are directly tied to the lack of direct correlation between the BMEP ratio and the power ratio when comparing either the 278 or 268 K curves to those of the 295 K temperature. As with the power curves of

Figure 63, the peak BMEP curves of 278 and 268 K in Figure 64 have their roles reversed, in the sense that it is the 278 K curve rather than 268 K that has the highest peak BMEP. However, the two curves are close to each other, and the uncertainty makes it difficult to accurately distinguish between the lines.

Table 20. Temperature effects on BMEP at 3 km

Temperature, K	**BMEP multiplier, expected (4-stroke)**	**BMEP multiplier, expected (2-stroke)**	**Peak BMEP multiplier, observed**	**Temperature ratio exponent, observed (peak)**	**Error from calculated with 0.8 exponent, %**
278	1.03	1.05	1.11	1.8	+6
268	1.05	1.08	1.07	0.7	-1

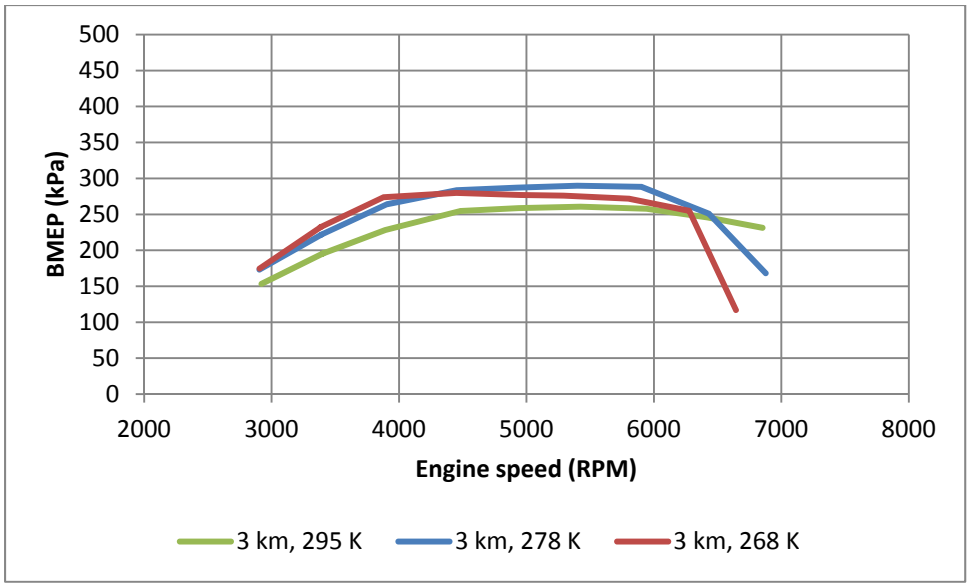

Figure 64. BMEP curves for temperature sweep at 3 km altitude

The 3 km BSFC curves shown in Figure 65 demonstrate how the Brison engine's efficiency benefits from a colder inlet temperature at the 278 K condition below 6,500 RPM. However, the 268 K curve has degraded performance relative to the 295 K condition at all points above 4,000 RPM. Additionally, the BSFC for 268 K at the 7,000 RPM setpoint is off the chart due to a combination of the 50% loss in power and nearly 50% greater fuel flow rate compared to that of the analogous point on the 295 K curve.

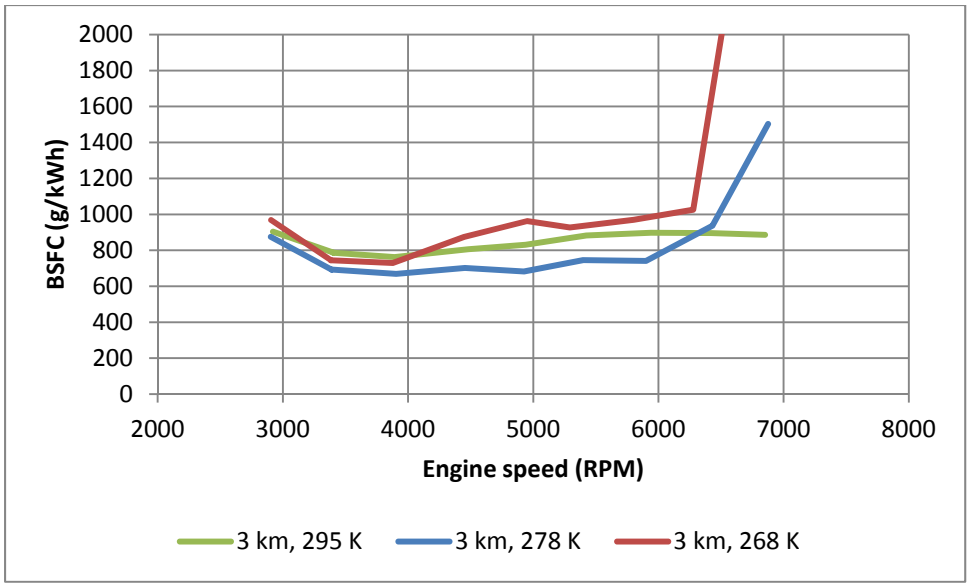

Figure 65. BSFC curves for temperature sweep at 3 km altitude

Looking more closely at the fuel flow rates for the three curves of Figure 66, the fuel flow rate for the 278 K condition is within plus or minus 10% of the 295 K curve except at the highest observed setpoint of 7,000 RPM. In contrast, the 268 K fuel flow rate exceeds that of the 295 K curve at all points and averages over 115% of the recorded room temperature condition fuel flow. Apparently, the fuel injection system was overcompensating for the lower inlet temperature by supplying more fuel than necessary.

Referring back to the power curves of Figure 63, the power advantage of the 268 K curve over the 295 K dwindles at the highest speeds. Had the 268 K efficiency remained in the league of the 295 K curve, the significantly higher observed fuel flow rates shown in Figure 66 at the coldest test temperature of 268 K would not have been necessary. In terms of thermal efficiency, the engine converted only 3% of the fuel supplied at a setpoint of 7,000 RPM into useful work at 268 K.

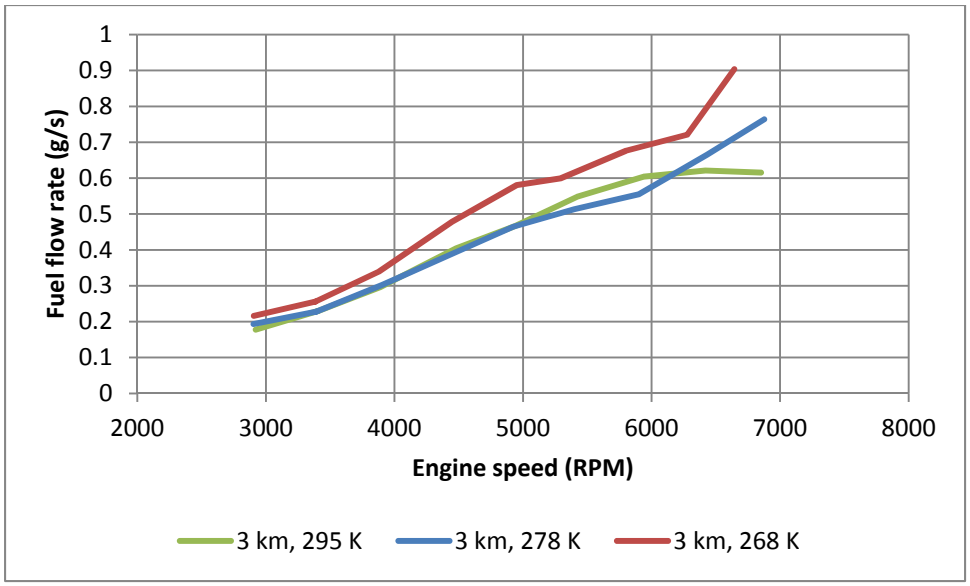

Figure 66. Fuel flow rates for temperature sweep at 3 km altitude

Appendix D: Fuel maps for four pressure altitudes

New fuel maps were created for the current configuration of the Brison test engine using the ProCAL software associated with the Ecotrons fuel injection system. Each of the four maps is for a single pressure altitude targeted for this research. The throttle position signal potentiometer shown in Figure 48 was utilized to essentially vary the AFR at a constant WOT for each of the three lower altitude conditions, and the 4.5 km pressure altitude map was extrapolated from the 3 km map. A linearized fuel map was created for the new map effort to aid in controlling the AFR between 13 and 14.

The load values for WOT were deduced from data analysis and entered into the 65% and 70% throttle position rows. The load values in each column decreased linearly from the desired WOT value at 65% throttle opening to 0 at 30% throttle. Similarly, the load values in each column increased linearly from the desired WOT value at 70% throttle opening to 1.3 times that WOT load for the 100% throttle row. With this approach, the potentiometer was adjusted to cause the throttle opening indicated by ProCAL to fall between 65% and 70% for each simulated altitude, and the AFR could be increased or decreased as desired.

The fuel maps shown in Table 21 through Table 24 were created for pressure altitudes of 0.2, 1.5, 3, and 4.5 km, respectively. The user should recall that the fuel injection system compensates for a low engine head temperature by adding extra fuel until the engine has fully warmed up to 343 K. The intake air temperature is also a variable used for calculating the fuel injection pulsewidth. Additionally, each table will need to be updated for throttle opening compensation once varied throttle testing resumes. The 4.5 km fuel map was never tested.

Table 21. Fuel map for 0.2 km pressure altitude (98.5 kPa)

MAP_LdTp_Tps_N: [%] "characteristic map; normalized load based on TPS and engine speed (Alpha/N model)"												
X: N; [Rpm] "Engine speed in Rpm"												
Y: Tps; [%] "throttle position with respect to lower mechanical stop"												
Y/X	2500	3000	3500	4000	4500	5000	5500	6000	6500	7000	7500	8000
0	0	0	0	0	0	0	0	0	0	0	0	0
30	0	0	0	0	0	0	0	0	0	0	0	0
34.99929	13.16515	13.16515	14.38571	17.19143	20.81857	22.04143	22.04143	22.04143	19.83714	18.95286	12.55143	12.55143
39.99857	26.33029	26.33029	28.77143	34.38286	41.63714	44.08286	44.08286	44.08286	39.67429	37.90571	25.10286	25.10286
44.99786	39.49544	39.49544	43.15714	51.57429	62.45571	66.12429	66.12429	66.12429	59.51143	56.85857	37.65429	37.65429
49.99714	52.66058	52.66058	57.54286	68.76571	83.27429	88.16571	88.16571	88.16571	79.34857	75.81143	50.20571	50.20571
54.99643	65.82573	65.82573	71.92857	85.95714	104.0929	110.2071	110.2071	110.2071	99.18571	94.76429	62.75714	62.75714
59.99571	78.99088	78.99088	86.31429	103.1486	124.9114	132.2486	132.2486	132.2486	119.0229	113.7171	75.30857	75.30857
64.995	92.15602	92.15602	100.7	120.34	145.73	154.29	154.29	154.29	138.86	132.67	87.86	87.86
69.99429	92.15602	92.15602	100.7	120.34	145.73	154.29	154.29	154.29	138.86	132.67	87.86	87.86
74.99357	96.76382	96.76382	105.735	126.357	153.0165	162.0045	162.0045	162.0045	145.803	139.3035	92.253	92.253
79.99286	101.3716	101.3716	110.77	132.374	160.303	169.719	169.719	169.719	152.746	145.937	96.646	96.646
84.99214	105.9794	105.9794	115.805	138.391	167.5895	177.4335	177.4335	177.4335	159.689	152.5705	101.039	101.039
89.99143	110.5872	110.5872	120.84	144.408	174.876	185.148	185.148	185.148	166.632	159.204	105.432	105.432
94.99071	115.195	115.195	125.875	150.425	182.1625	192.8625	192.8625	192.8625	173.575	165.8375	109.825	109.825
99.99	119.8028	119.8028	130.91	156.442	189.449	200.577	200.577	200.577	180.518	172.471	114.218	114.218

Table 22. Fuel map for 1.5 km pressure altitude (84 kPa)

MAP_LdTp_Tps_N: [%] "characteristic map; normalized load based on TPS and engine speed (Alpha/N model)"												
X: N; [Rpm] "Engine speed in Rpm"												
Y: Tps; [%] "throttle position with respect to lower mechanical stop"												
Y/X	2500	3000	3500	4000	4500	5000	5500	6000	6500	7000	7500	8000
0	0	0	0	0	0	0	0	0	0	0	0	0
30	0	0	0	0	0	0	0	0	0	0	0	0
34.99929	9.948571	9.948571	11.02	12.73429	15.37143	16.27286	17.26571	17.26571	16.16286	15.44286	14.54143	14.38714
39.99857	19.89714	19.89714	22.04	25.46857	30.74286	32.54571	34.53143	34.53143	32.32571	30.88571	29.08286	28.77429
44.99786	29.84571	29.84571	33.06	38.20286	46.11429	48.81857	51.79714	51.79714	48.48857	46.32857	43.62429	43.16143
49.99714	39.79429	39.79429	44.08	50.93714	61.48571	65.09143	69.06286	69.06286	64.65143	61.77143	58.16571	57.54857
54.99643	49.74286	49.74286	55.1	63.67143	76.85714	81.36429	86.32857	86.32857	80.81429	77.21429	72.70714	71.93571
59.99571	59.69143	59.69143	66.12	76.40571	92.22857	97.63714	103.5943	103.5943	96.97714	92.65714	87.24857	86.32286
64.995	69.64	69.64	77.14	89.14	107.6	113.91	120.86	120.86	113.14	108.1	101.79	100.71
69.99429	69.64	69.64	77.14	89.14	107.6	113.91	120.86	120.86	113.14	108.1	101.79	100.71
74.99357	73.122	73.122	80.997	93.597	112.98	119.6055	126.903	126.903	118.797	113.505	106.8795	105.7455
79.99286	76.604	76.604	84.854	98.054	118.36	125.301	132.946	132.946	124.454	118.91	111.969	110.781
84.99214	80.086	80.086	88.711	102.511	123.74	130.9965	138.989	138.989	130.111	124.315	117.0585	115.8165
89.99143	83.568	83.568	92.568	106.968	129.12	136.692	145.032	145.032	135.768	129.72	122.148	120.852
94.99071	87.05	87.05	96.425	111.425	134.5	142.3875	151.075	151.075	141.425	135.125	127.2375	125.8875
99.99	90.532	90.532	100.282	115.882	139.88	148.083	157.118	157.118	147.082	140.53	132.327	130.923

Table 23. Fuel map for 3 km pressure altitude (70 kPa)

MAP_LdTp_Tps_N: [%] "characteristic map; normalized load based on TPS and engine speed (Alpha/N model)"												
X: N; [Rpm] "Engine speed in Rpm"												
Y: Tps; [%] "throttle position with respect to lower mechanical stop"												
Y/X	2500	3000	3500	4000	4500	5000	5500	6000	6500	7000	7500	8000
0	0	0	0	0	0	0	0	0	0	0	0	0
30	0	0	0	0	0	0	0	0	0	0	0	0
34.99929	7.805714	7.805714	8.571429	9.647143	11.38	12.04857	13.32857	13.32857	11.02	13.16143	13.16143	13.16143
39.99857	15.61143	15.61143	17.14286	19.29429	22.76	24.09714	26.65714	26.65714	22.04	26.32286	26.32286	26.32286
44.99786	23.41714	23.41714	25.71429	28.94143	34.14	36.14571	39.98571	39.98571	33.06	39.48429	39.48429	39.48429
49.99714	31.22286	31.22286	34.28571	38.58857	45.52	48.19429	53.31429	53.31429	44.08	52.64571	52.64571	52.64571
54.99643	39.02857	39.02857	42.85714	48.23571	56.9	60.24286	66.64286	66.64286	55.1	65.80714	65.80714	65.80714
59.99571	46.83429	46.83429	51.42857	57.88286	68.28	72.29143	79.97143	79.97143	66.12	78.96857	78.96857	78.96857
64.995	54.64	54.64	60	67.53	79.66	84.34	93.3	93.3	77.14	92.13	92.13	92.13
69.99429	54.64	54.64	60	67.53	79.66	84.34	93.3	93.3	77.14	92.13	92.13	92.13
74.99357	57.372	57.372	63	70.9065	83.643	88.557	97.965	97.965	80.997	96.7365	96.7365	96.7365
79.99286	60.104	60.104	66	74.283	87.626	92.774	102.63	102.63	84.854	101.343	101.343	101.343
84.99214	62.836	62.836	69	77.6595	91.609	96.991	107.295	107.295	88.711	105.9495	105.9495	105.9495
89.99143	65.568	65.568	72	81.036	95.592	101.208	111.96	111.96	92.568	110.556	110.556	110.556
94.99071	68.3	68.3	75	84.4125	99.575	105.425	116.625	116.625	96.425	115.1625	115.1625	115.1625
99.99	71.032	71.032	78	87.789	103.558	109.642	121.29	121.29	100.282	119.769	119.769	119.769

Table 24. Fuel map for 4.5 km pressure altitude (57 kPa)

MAP_LdTp_Tps_N: [%] "characteristic map; normalized load based on TPS and engine speed (Alpha/N model)"												
X: N; [Rpm] "Engine speed in Rpm"												
Y: Tps; [%] "throttle position with respect to lower mechanical stop"												
Y/X	2500	3000	3500	4000	4500	5000	5500	6000	6500	7000	7500	8000
0	0	0	0	0	0	0	0	0	0	0	0	0
30	0	0	0	0	0	0	0	0	0	0	0	0
34.99929	6.356082	6.356082	6.979592	7.855531	9.266571	9.81098	10.85327	10.85327	8.973429	10.71716	10.71716	10.71716
39.99857	12.71216	12.71216	13.95918	15.71106	18.53314	19.62196	21.70653	21.70653	17.94686	21.43433	21.43433	21.43433
44.99786	19.06824	19.06824	20.93878	23.56659	27.79971	29.43294	32.5598	32.5598	26.92029	32.15149	32.15149	32.15149
49.99714	25.42433	25.42433	27.91837	31.42212	37.06629	39.24392	43.41306	43.41306	35.89371	42.86865	42.86865	42.86865
54.99643	31.78041	31.78041	34.89796	39.27765	46.33286	49.0549	54.26633	54.26633	44.86714	53.58582	53.58582	53.58582
59.99571	38.13649	38.13649	41.87755	47.13318	55.59943	58.86588	65.11959	65.11959	53.84057	64.30298	64.30298	64.30298
64.995	44.49257	44.49257	48.85714	54.98871	64.866	68.67686	75.97286	75.97286	62.814	75.02014	75.02014	75.02014
69.99429	44.49257	44.49257	48.85714	54.98871	64.866	68.67686	75.97286	75.97286	62.814	75.02014	75.02014	75.02014
74.99357	46.7172	46.7172	51.3	57.73815	68.1093	72.1107	79.7715	79.7715	65.9547	78.77115	78.77115	78.77115
79.99286	48.94183	48.94183	53.74286	60.48759	71.3526	75.54454	83.57014	83.57014	69.0954	82.52216	82.52216	82.52216
84.99214	51.16646	51.16646	56.18571	63.23702	74.5959	78.97839	87.36879	87.36879	72.2361	86.27316	86.27316	86.27316
89.99143	53.39109	53.39109	58.62857	65.98646	77.8392	82.41223	91.16743	91.16743	75.3768	90.02417	90.02417	90.02417
94.99071	55.61571	55.61571	61.07143	68.73589	81.0825	85.84607	94.96607	94.96607	78.5175	93.77518	93.77518	93.77518
99.99	57.84034	57.84034	63.51429	71.48533	84.3258	89.27991	98.76471	98.76471	81.6582	97.52619	97.52619	97.52619

Bibliography

[1] J. B. Heywood, Internal combustion engine fundamentals, McGraw-Hill, 1988.

[2] G. P. Blair, Design and simulation of two-stroke engines, Warrendale, PA: Society of Automotive Engineers, 1996.

[3] C. F. Taylor, The internal-combustion engine in theory and practice. Vol. 1: Thermodynamics, fluid flow, performance, Cambridge, MA: MIT Press, 1966.

[4] S. Menon, N. Moulton and C. Cadou, "Development of a dynamometer for measuring small internal-combustion engine performance," *Journal of Propulsion and Power,* vol. 23, no. 1, pp. 194-202, January-February 2007.

[5] S. Park, D. Walther, A. Pisano and A. Fernandez-Pello, "Development of liquid fuel injection system for small-scale rotary engines," in *44th AIAA Aerospace Sciences Meeting and Exhibit*, 2006.

[6] J. D. Anderson, Aircraft performance and design, McGraw-Hill, 1999.

[7] R. D. Kimberlin, Flight testing of fixed-wing aircraft, AIAA, 2003.

[8] J. B. Heywood and E. Sher, The two-stroke cycle engine: Its development, operation, and design, Warren, PA: SAE International, 1999.

[9] C. F. Taylor, Internal combustion engine in theory and practice: Vol. 2-revised: Combustion, fuels, materials, design, Cambridge, MA: MIT Press, 1985.

[10] C. Grasas-Alsina, E. Freixa, P. Esteban and J. & Masso, "Low-pressure discontinuous gasoline injection in two-stroke engines," Society of Automotive Engineers Technical Paper Series, 860168, 1986.

[11] R. Harari and E. Sher, "The Effect of Ambient Pressure on the Performance Map of a Two-Stroke SI Engine," *SAE International Congress & Exposition,* pp. 115-123, 1 March 1993.

[12] I. Watanabe and H. Kuroda, "Effect of atmospheric temperature on the power output of a two-stroke cycle crankcase compression gasoline engine," *SAE International*

Congress and Exposition, 23-27 February 1981.

[13] S. M. C. Soares and J. Sodré, "Effects of atmospheric temperature and pressure on the performance of a vehicle," *Journal of Automobile Engineering,* pp. 473-477, 2002.

[14] M. Ceviz, "Intake plenum volume and its influence on the engine performance, cyclic variability and emissions," *Energy Conversion and Management,* vol. 48, pp. 961-966, 2007.

[15] Y. Shin, S. H. Chang and S. O. Koo, "Performance test and simulation of a reciprocating engine for long endurance miniature unmanned aerial vehicles," *Journal of Automobile Engineering,* vol. 219, pp. 573-581, 6 Oct 2004.

[16] S. C. Crosbie, *Increasing reliability of a small 2-stroke internal combustion engine for dynamically changing altitudes,* Wright Patterson AFB, OH: Air Force Institute of Technology Thesis AFIT/GAE/ENY/12-M08, 2012.

[17] S. R. Turns, An introduction to combustion: Concepts and applications (3rd ed.), New York: McGraw-Hill, 2012.

[18] H. Cline, *Testing Engines in Simulated Atmospheric Environments,* 1960.

[19] J. D. Anderson, Modern compressible flow: With historical perspective, McGraw-Hill, 1990.

[20] D. Winterbone and R. Pearson, "Theory of engine manifold design," *Journal of Automobile Engineering,* 2001.

[21] J. Hartman, How to tune and modify engine management systems, Motorbooks, 2004.

[22] J. Griffin, T. Ferguson, H. Servati and M. Swanson, *Calculated A/F ratio via exhaust gas temperature measurement for small engine control,* SAE Technical Paper 01-1339, 2001.

[23] B. Smither, I. McFarlane, T. Drake and P. Ravenhill, *Engine management system for fuel injection system specifically designed for small engines,* SAE Technical

Paper 32-0052, 2008.

[24] J. Allen and T. Drake, *Experimental results of new fuelling strategies for high frequency low cost injection systems for small engines,* SAE Paper 32-0051, 2007.

[25] P. J. Schmick, *Effect of Atmospheric Pressure and Temperature on a Small Spark Ignition Internal Combustion Engine's Performance,* Wright Patterson AFB, OH: Air Force Institute of Technology Thesis AFIT/GAE/ENY/11-M28 , 2011.

[26] J. D. Mattingly, W. H. Heiser and D. T. Pratt, Aircraft engine design, AIAA, 2002.

[27] J. D. Anderson, Fundamentals of aerodynamics, New York: McGraw-Hill, 2001.

[28] S. J. Kline and F. McClintock, "Describing uncertainties in single-sample experiments," *Mechanical Engineering,* pp. 3-8, January 1953.

[29] R. J. Moffat, "Describing the uncertainties in experimental results," *Experimental Thermal and Fluid Science,* vol. 1, pp. 3-17, 1988.

[30] R. J. Moffat, "Contributions to the Theory of Single-Sample Uncertainty Analysis," *Journal of Fluids Engineering,* vol. 104, pp. 250-260, 1982.

[31] S. R. Turns, Thermodynamics: Concepts and applications, New York: Cambridge University Press, 2006.

[32] M. J. Moran and H. N. Shapiro, Fundamentals of engineering thermodynamics (5th ed.), Hoboken, NJ: John Wiley & Sons, 2006.

[33] T. Bose, Airbreathing propulsion: An introduction, New York, NY: Springer Aerospace Technology, 2012.

[34] Y. A. Cengel and M. A. Boles, Thermodynamics: An engineering approach, McGraw-Hill Higher Education, 2006.

[35] A. Bonnick, A practical approach to motor vehicle engineering and maintenance, Routledge, 2011.

[36] W. Attard, E. Toulson, F. Hamori and H. Watson, *Combustion system development and analysis of a carbureted and PFI normally aspirated small engine,* 2009.

[37] G. Banish, Designing and tuning high-performance fuel injection systems, SA Design, 2009.

[38] A. F. Montemayor, L. L. Stavinoha, S. J. Lestz and M. E. LePera, *Potential Benefits from the use of JP-8 Fuel in Military Ground Equipment,* 1989.

[39] D. Falkowski, D. Abata and P. Cho, *The performance of a spark-ignited stratified-charge two stroke engine operating on a kerosine based aviation fuel,* SAE Technical Paper 972737, 1997.

[40] J. P. J. Suhy, L. W. Evers and J. E. Wank, *The feasibility of a kerosene fueled spark ignited two-stroke engine,* SAE Technical Paper 911846 , 1991.

[41] N. R. Hirsch, *Innovative heavy fuel compression ignition engine design,* 1999.

[42] J. R. J. Groenewegen, *The Performance and Emissions Characteristics of Heavy Fuels in a Small, Spark Ignition Engine,* 2011.

[43] R. G. Salter, M. L. Smith and C. P. Roberts, *Study of Miniature Engine-Generator Sets, Part II. Investigation of Engines, Fuels, and Lubricants,* 1954.

[44] C. W. Wilson, Performance of a Small Internal Combustion Engine using N-Heptane and Iso-Octane, Wright Patterson AFB, OH: Air Force Institute of Technology Thesis, AFIT/GAE/ENY/10-M28, March 2010.

[45] D. Diemand, *Automotive and Construction Equipment for Arctic use: Heating and Cold Starting,* 1991.

[46] N. Ayoub and R. Reitz, *Multidimensional Modeling of Fuel Composition Effects on Combustion and Cold-starting in Diesel Engines,* 1995.

[47] A. F. Montemayor and E. C. Owens, *Fuel Property Effects on the Unaided Cold Starting of a Two-Cycle Diesel Engine,* 1985.

[48] N. A. Henein, D. Taraza and N. Chalhoub, *Adaptation of advanced diesel engines for military requirements under severe environmental conditions,* 2004.

[49] T. L. Bergman, A. S. Lavine, F. P. Incropera and D. P. DeWitt, Fundamentals of heat and mass transfer, Wiley, 2011.

[50] F. Zhao, M. C. Lai and D. L. Harrington, "Automotive spark-ignited direct-injection gasoline engines," *Progress in Energy and Combustion Science,* pp. 437-562, 1999.

REPORT DOCUMENTATION PAGE

Form Approved
OMB No. 074-0188

1. REPORT DATE *(DD-MM-YYYY)*	2. REPORT TYPE	3. DATES COVERED *(From – To)*
21-03-2013	Master's Thesis	August 2011 – March 2013

TITLE AND SUBTITLE

Effects of Temperature on the Performance of a Small Internal Combustion Engine at Altitude

5a. CONTRACT NUMBER

5b. GRANT NUMBER

5c. PROGRAM ELEMENT NUMBER

6. AUTHOR(S)

Husaboe, Travis Don, Captain, USAF

5d. PROJECT NUMBER

5e. TASK NUMBER

5f. WORK UNIT NUMBER

7. PERFORMING ORGANIZATION NAMES(S) AND ADDRESS(S)
Air Force Institute of Technology
Graduate School of Engineering and Management (AFIT/ENY)
2950 Hobson Way, Building 640
WPAFB OH 45433-8865

8. PERFORMING ORGANIZATION REPORT NUMBER

AFIT-ENY-13-M-17

9. SPONSORING/MONITORING AGENCY NAME(S) AND ADDRESS(ES)
Air Force Research Lab, Aerospace Systems Directorate, Combustion Branch, 1790 Loop Road, Wright-Patterson AFB, OH, Paul Litke, DSN 785-1673, paul.litke@wpafb.af.mil

10. SPONSOR/MONITOR'S ACRONYM(S)
AFRL/RQTC, SERL

11. SPONSOR/MONITOR'S REPORT NUMBER(S)

12. DISTRIBUTION/AVAILABILITY STATEMENT
APPROVED FOR PUBLIC RELEASE; DISTRIBUTION UNLIMITED.

13. SUPPLEMENTARY NOTES

14. ABSTRACT

The effects of atmospheric pressure and temperature variations on the performance of small internal combustion (IC) engines operating at altitudes significantly above sea level are not widely documented. Using an altitude chamber and fuel-injected two-stroke engine, data were collected while varying air temperature along with pressure. The peak engine power was 4.1 kW at roughly sea level standard conditions and dropped to 3.5 kW at the standard conditions for an altitude of 1.5 km. At a combination of pressure and temperature corresponding to an altitude of 3 km, peak power fell further to 2.5 kW. The combined effects of standard atmospheric conditions showed pressure dominated temperature and resulted in around a 3.5% loss of power and brake mean effective pressure (BMEP) along with a 3% increase in brake specific fuel consumption (BSFC) per 300 m increase in altitude.

15. SUBJECT TERMS

Spark Ignition, Internal Combustion Engine, Altitude, BSFC, BMEP, Two-stroke, Temperature, Pressure

16. SECURITY CLASSIFICATION OF:			17. LIMITATION OF ABSTRACT	18. NUMBER OF PAGES	19a. NAME OF RESPONSIBLE PERSON
a. REPORT	b. ABSTRACT	c. THIS PAGE			Marc Polanka, Ph.D.
U	U	U	UU	167	19b. TELEPHONE NUMBER *(Include area code)* (937) 255-6565, ext 4174 (marc.polanka@afit.edu)

Standard Form 298 (Rev. 8-98)
Prescribed by ANSI Std. Z39-18